POLITECNICO DI MILANO

School of Industrial and Information Engineering
Department of Chemistry, Materials and Chemical Engineering “Giulio Natta”
Master of Science in Materials Engineering and Nanotechnology

POLITECNICO
MILANO 1863

RUBBER COMPOUNDS WITH BIOASH FILLER: A CASE OF CIRCULAR ECONOMY

Supervisor: Prof. Stefano TURRI

Internal Co-Supervisors: Dr. Riccardo CIAPPONI

External Co-Supervisors: Dr. Veronica CANTONETTI

Elisabetta Sisti

ID 10603078

Academic Year 2018-2019

改善

Table of contents

List of figures

List of tables

Glossary

#

6PPD	N-1,3-dimethylbutyl-N'-phenyl-p-phenylenediamine

A

AO	Oleic Acid
AS	Stearic Acid
ASTM	American Society for Testing and Materials

B

BA	Bioash from trial plant
BA BM	Ball Milled bioash
BA BMM	Ball Milled bioash in metal case
BA BMW	Wet Ball Milled bioash
BA S	Sieved bioash
BA S BM	Sieved and Ball Milled bioash
BMW	Wet Ball Milling

C

c.a.	Contact angle
CE	Circular Economy
CB	Carbon Black

D

DMA	Dynamic Mechanical Analyer

E

ENR	Epoxydized Natural Rubber
ESP	Electrostatic Precipitator

F

F-F	Filler-Filler interactions
FT-IR	Fourier Transform Infra-Red spectroscopy

G

gMAH	Polyisoprene-graft-maleic anhydride

I

ISO	International Organization for Standardization

K

KPI	Key Performance Indicator

M

MES	Mild Extracted Solvate

N

NR	Natural Rubber

O

OCA	Optical Contact Angle Analyzer

P

P-F	Polymer-Filler interactions
phr	Parts for hundred parts of rubber
PM	Particulate Matter

R

RAW	Raw bioash
RPA	Rubber Process Analyser

S

SBR	Styrene Butadiene Rubber
SDGs	Sustainable Development Goals
SEM	Scanning Electron Microscope
SIR	Standard Indonesian Rubber
STD	Standard rubber compound for tyres

T

TBBS	N-tert-butyl-2-benzothiazolsulfenamide
TESPT	Bis(3-triethoxysilylpropyl) tetrasulfane
TGA	Thermogravimetric Analysis
TSR	Technically Specified Rubber
TWS	Trelleborg Wheel System S.p.a.

U

u.m.	Unit of Measure
USP	United States Pharmacopeial Convention, Incorporated

X

XRD	X-ray Diffraction Analysis

Nomenclature of the formulations

Each compound formulation is identified by an acronym, which can be generalized as **STDn-X Ym**:

- **STD** represents the standard rubber compound formulation for tyres (§ 2.3.1)
- **STDn**, n indicates the number of parts for hundred parts of rubber (phr) that are used to modified standard formulation with the addition of bioash filler. It can be:
    - **STD0**, i.e. Standard formulation without bioash
    - **STD1**, i.e. Standard formulation with the addition of 1 phr of bioash
    - **STD3**, i.e. Standard formulation with the addition of 3 phr of bioash
    - **STD5,** i.e. Standard formulation with the addition of 5 phr of bioash
    - **STD8,** i.e. Standard formulation with the addition of 8 phr of bioash
    - **STD15**, i.e. Standard formulation with the addition of 15 phr of bioash
- **X** represents the type of bioash functionalizer or of compatibilizer used to improve rubber-filler interaction. It can be:
    - **RAW Y**, i.e. treated bioash instead of raw bioash
    - **gMAH**, i.e. polyisoprene-graft-maleic anhydride
    - **ENR**, i.e. epoxidized natural rubber
- **RAW Y**, Y addresses the type of bioash modification. It can be:
    - **RAW BMW**, i.e. wet ball milled bioash
    - **RAW AS**, i.e. bioash functionalized by stearic acid
    - **RAW AO**, i.e. bioash functionalized by oleic acid
    - **RAW TESPT**, i.e. bioash functionalized by silane
- **RAW Ym**, m is the number indicating the percentage of the weight of functionalizer to the weight of bioash. It can be:
    - **RAW AS1**, i.e. bioash modified by 1% of stearic acid
    - **RAW AS3**, i.e. bioash modified by 3% of stearic acid
    - **RAW AS5**, i.e. bioash modified by 5% of stearic acid
    - **RAW AS10**, i.e. bioash modified by 10% of stearic acid
    - **RAW AO5**, i.e. bioash modified by 5% of oleic acid
    - **RAW AO10**, i.e. bioash modified by 10% of oleic acid

Abstract

A circular economy is an economic system aimed at eliminating waste and at continuous using of resources. Circular systems employ reuse, sharing, repair, refurbishment, remanufacturing and recycling to create a close-loop system, minimizing the use of resource inputs and the creation of waste, pollution and carbon emissions.

Circular economy takes part in twelfth Sustainable Development Goal of United Nations Member States: the commitment to a responsible consumption and production.

Trelleborg Wheel Systems S.p.a. is a leading global supplier of tyres and complete wheels for agricultural machines, material handling and construction vehicles, and two-wheeled vehicles. Its plant in Sri Lanka produce 3 tons per day of bioash as waste from biomass combustion for the generation of hot steam used in rubber mixing.

The bioash could have a high added value if it would be used as new filler in the rubber compounding, avoiding its disposal as waste. The problem is the high dimension of bioash grains and the low compatibility between the polar rubber compound and the apolar bioash.

In this work, the possible physical and chemical treatments to improve the compatibility between rubber and bioash are investigated.

After a preliminary characterization of the bioash, some mechanical and chemical processes are explored by using of different functionalizers and in various percentages. The resulted bioash is characterized by X-ray Diffraction (XRD), Fourier Transform Infra-Red Spectroscopy (FT-IR), Kumagawa Extraction, Thermogravimetric Analysis (TGA), Particle Size Analysis, Scanning Electron Microscope (SEM), Tap Density Testing and Optical Contact Angle (OCA).

The standard formulation of rubber compound for tyres has been modified by the addition of some parts of untreated or treated bioash per hundred rubber.

The properties of final rubber are investigated by Dynamic Mechanical Analysis (DMA), Tensile Testing and Dispersion Grade Analysis.

A comparison among the most significant results from testing of the compounds with modified bioash, is done in conclusion.

Estratto in lingua italiana

Secondo le ultime stime dell'Onu, la continua crescita demografica porterà la popolazione mondiale a passare da 6.9 a 8.6 miliardi di abitanti nel 2030, con conseguente aumento del consumo di risorse che aprirà uno scenario mondiale caratterizato da un alto tasso di povertà e rapidi cambiameti climatici.

La struttura del business attuale, basato principalmetne su un'economia lineare: produzione-consumo-smaltimento, è la maggiore causa dei pronostici negativi sovraccitati e dunque risulta inadeguata a soddisfare i fabbisogni della futura popolazione mondiale.

I paesi dell'Onu hanno presentato una lista di 17 obiettivi di sviluppo sostenibile, da raggiungere entro il 2030, per contrastare questi drammatici effetti.

Il nostro attuale concetto di creare nuova ricchezza deve cambiare drasticamente: l'obiettivo numero 12 incentiva l'implementazione di modelli sostenibili di produzione e di consumo, trasformando la struttura economica attuale in un modello sempre più circolare che tenda ad estendere il ciclo di vita dei prodotti, contribuendo a ridurre l'ammontare dei rifiuti al minimo.

Questa struttura economica permette di avere una minor impronta ambientale e anche maggiori guadagni economici, come riportato nel repost dalla Ellen MacArthur Foundation in occasione del World Economic Forum del 2012.

Trelleborg Wheel Systems S.p.a. è una società leader mondiale nella fornitura di pneumatici e ruote complete per macchinari agricoli e forestali, per carrelli elevatori e altre attrezzature per la movimentazione di materiali, per veicoli industriali, motocicli ed altri segmenti specialistici. In particolare, il settore dedicato alle ruote solide per applicazioni industriali e costruttive ha stabilimenti ubicati in Sri Lanka, Cina e Brasile.

Nello stabilimento cingalese, le alte temperature necessarie alla miscelazione delle materie prime che andranno a formare il composto di gomma finale, sono generate dalla combustione di legna che avviene in una caldaia a biomassa.

Questo processo produce in media tre tonnellate di cenere al giorno che vengono smaltite dal fornitore della biomassa.

Questo enorme quantitativo disponibile giornalmente nell'impianto può acquistare un alto valore aggiunto se re-introdotto nel ciclo produttivo come agente di

riempimento del composto di gomma, un ottimo caso di economia circolare che minimizza gli sprechi, aumentando il valore del prodotto finito.

Lo scopo di questa tesi è studiare la fattibilità di questo caso di economia circolare mantenendo le proprietà meccaniche del prodotto finale.

Lo studio inizia dalla caratterizzazione preliminare delle ceneri, per poi passare a misurare gli effetti che l'aggiunta delle cenere al composto di gomma ha sulle proprietà del prodotto finale e termina con l'ottimizzazione del processo, attraverso l'utilizzo di diversi materiali compatibilizzanti, per raggiungere migliori performance, fino ad un primo calcolo dei costi.

Innanzitutto, è stato doveroso procedere ad un analisi approfondita delle ceneri, essendo queste un prodotto di scarto con proprietà non tabulate.

Dopo una prima analisi sugli elementi presenti, la caratterizzazioni delle ceneri è proseguita con un analisi ai raggi X e ad infrarossi che ci hanno fornito rispettivamente informazioni su tipo e quantità di composti presenti e sui loro legami intramolecolari.

Le molecole riscontrate nella cenere sono in ordine decrescente calcite, ossido di calcio, magnetite e ossido di ferro con una vasta gamma di altri composti presenti in una percentuale minore dell'8%.

L'analisi termogravimetrica ha rilevato il grado di adsorbimento e ossidazione dei componenti presenti nelle ceneri mentre le immagini prodotte dal microscopio a scansione ottica hanno portato alla luce la grande disomogeneità di forme e dimensioni dei granelli di cenere.

Per approfondire questo aspetto è stata svolta un'analisi dimensionale che ha confermato la disomogeneità dei granelli e le dimensioni di questi, principalmente maggiori di 25 μm.

Per finire ne è stata misurata la densità e l'angolo di contatto ottico con una goccia di acqua che ha rivelato la natura idrofila della cenere.

Anche le prime ceneri prodotte nell'impianto di prova, con la caldaia a biomassa alimentata da legna di un fornitore diverso da quello attuale, sono state analizzate per sottolinearne le differenze dalla cenere prodotta nell'impianto odierno.

Questo paragone ha evidenziato un grado di disidratazione maggiore e una presenza più rilevante di composti derivati dal calcio e una diminuzione di quelli derivati dal ferro rispetto alle ceneri attualmente prodotte.

La Trellegorg ha fornito la formulazione standard per produrre il composto di gomma usato per le ruote, principalmente costituita da gomma naturale.

Dopo di chè, sono state effettuate sul composto prove dinamiche meccaniche e di trazione e infine un'analisi della dispersione degli agenti di riempimento nel composto finito.

Questi risultati sono stati presi come riferimento e sono stati confrontati con le proprietà del composto prodotto con una formulazione modificata dall'aggiunta della cenere come riempitivo.

La cenere è stata aggiunta in diverse quantità nella formulazione mantenendo le parti per cento di gomma (phr) degli altri materiali che compongono il prodotto finito. Nel caso dell'utilizzo di 15 phr di cenere nella formulazione, il risparmio sul costo del prodotto finale è del 7%.

Dalle misurazioni sopraccitate è stato possibile rilevare 1 phr di cenere aggiunta alla composizione come la quantità limite che stravolge le proprietà del prodotto finito. Aumentando progressivamente la quantità di cenere si raggiungono i 5 phr dove il composto sembra avere prestazioni migliori rispetto a quello con quantità di cenere minore ma comunque peggiori del composto standard. Aumentando la quantità di polveri le proprietà decadono nuovamente. Dall'analisi di dispersione è stato possibile ipotizzare che le 5 phr di cenere contribuiscono a creare agglomerati dei riempimenti di dimensioni non ancora eccessive diminuendo i possibili siti di attivazione dei difetti, presenti in maggiore quantità nel caso dei granelli non agglomerati che comunque hanno dimensioni che rendono la loro azione non rinforzante.

Per ovviare il problema si è cercato di ridurre le dimensioni delle polveri con diversi metodi, il più efficiente si è rivelato essere il Wet Ball Milling che porta il valore della moda misurato dal test dimensionale da 26 μm a 8 μm.

In questo caso, le ceneri hanno un effetto meno negativo sulle proprietà meccaniche del composto finito ma comunque inferiori al composto standard.

Dalla letteratura è stato possibile indicare come causa del degrado delle proprietà del composto, oltre alle dimensioni eccessive dei granelli, anche l'elevata idrofobia della cenere poco compatibile con la gomma naturale altamente indrofila.

Per modificare tale natura della cenere, principalmente composta di calcite, sono stati usati degli acidi grassi che grazie alle loro lunghe catene organiche si adsorbono sulla

cenere rendendola idrofobica, come evidenziato dall'analisi a raggi infrarossi, dall'analisi termogravimetrica e dall'analisi ottica dell'angolo di contatto. La quantità ottimale di acido stearico risulta essere il 3% in peso rispetto al peso delle ceneri e il 5% in caso dell'acido oleico che è una molecola più reattiva per la presenza di un legame insaturo ma anche più ingombrante, infatti risulta avere meno effetto sulla cenere a parità di peso rispetto all'acido stearico.

Suddetti acidi contribuiscono anche a diminuire le dimensioni dei granelli della cenere, infatti le proprietà del composto sono buone ma ancora non paragonabili a quelle del composto standard.

Un'altra strada percorsa, suggerita dalla presenza dell'elemento ferro nella cenere, è stata utilizzare i silani per modificare la natura della cenere, in particolare il TESPT.

Il TESPT crea legami più forti con la cenere, non solo fisici come accadeva con gli acidi grassi, infatti le proprietà del composto finito sono risultate quasi paragonabili a quelle del composto standard ad eccezione della forza a trazione che è notevolmente peggiorata per il fatto che il TESPT tende a creare agglomerati degli aggenti di riempimento di grandi dimensioni e seguenti numerosi siti di attivazione dei difetti.

Con gli ultimi tentativi si è cercato di intervenire direttamente sulla formulazione del composto aggiungendo agenti compatibilizzanti quali l'anidrite graffata maleica e la gomma epossidata. Nel primo caso le proprietà del composto finito risultano notevolmente diverse da quello di partenza anche se c'è quasi un dimezzamento dei costi.

Per quanto riguarda l'aggiunta di 5 phr di gomma epossidata alla formulazione, le proprietà del composto finale risultano addirittura migliorate rispetto al composto standard, a parità di costo, ed inoltre è stato possibile riutilizzare 15 phr di cenere prodotta come scarto dall'impianto di produzione stesso della gomma, in un ottica perfetta di economia circolare.

Aim of the thesis

In the framework of circular economy, the aim of this work is to find a process to transform the bioash, produced as waste by Trelleborg Wheel System S.p.a. plant, in a filler of rubber compound for tyres, preserving the properties of standard rubber compound.

It is done to avoid the disposal of waste in order to reduce the carbon dioxide emission produced by its transport and to decrease the quantities of non-renewable materials used in rubber compounding.

Moreover, the reintroduction of bioash in the internal product can be consider a no cost process with consequent materials and money saving.

All these aspects can have positive effects for the company and for the environment on condition of maintaining the standard rubber compound properties and using cheap and easy industrial method and low-cost and low-toxic functionalizers.

1. Introduction

1.1. Overview on Circular Economy

"Mottainai" is one key aspect of the "Kaizen".

Kaizen (改善) is the composition of two Japanese terms, KAI (change, improvement) and ZEN (good, better), and it means changing for the better, continuous improvement. It was coined by Masaaki Imai in 1986 to describe the corporate philosophy that supported the success of the Japanese industry in the 1980s, with particular reference to Toyota.

The expression Mottainai (勿体無い) was taken up by Wangarĩ Muta Maathai, Kenyan environmental political activist and 2004 Nobel Peace Prize winner, as a term that relates to the spirit of her Green Belt Movement; Mottainai is a word derived from one of the beliefs of Japanese Buddhism and nowadays it is used in a variety of contexts, but it always means one thing: "Such a pity it is not used its full potential"; it's often said with a sigh. It expresses that it is a shame for something to go to waste without having made use of its potential in full; something that happens regularly in a linear economy: raw materials are used to make a product and, after its use, any waste is thrown away [1].

On the other hand, the circular economy (CE), according to mottainai concept, is a new way of creating value and, ultimately, prosperity. It works by extending product lifespan through improved design and servicing and relocating waste from the end of the supply chain to the beginning-in, a schematic illustration is presented in Figure 1.1.

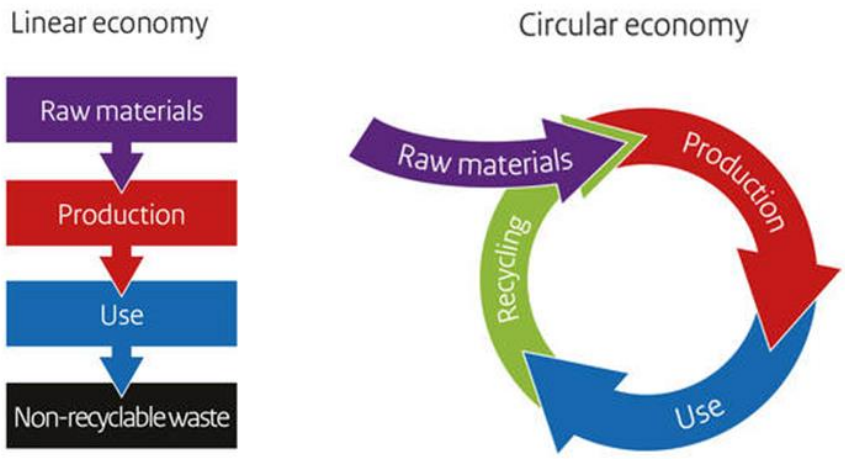

Figure 1.1 Models of linear and circular economy.

The concept of circular economy has been discussed since the 1970s but switching from the current linear model of economy to a circular one has recently attracted increased attention from major global companies and policymakers thanks to report of the Ellen MacArthur Foundation and McKinsey Company published during the World Economic Forum of 2012 [2].

The report evaluates the potential monetary benefits of the transition to a circular economy: it could create an opportunity of 630 American dollars billion per year for only a subset of the European Union manufacturing sectors.

Next to the huge economic benefits, the Ellen MacArthur Foundation pointed out the significant environmental and social benefits derived from a circular economy [3].

The major goals of the circular economy are reducing environment footprint, generate increased income, reduce resource dependency and minimize the waste.

The main means are encouraging a clear industrial production using fewer resources, developing a better service to extend goods lifespan, collecting products at end-of-life, separating waste and re-using resources, using green, toxin-free, long-life, recyclable products [4].

All these aspects are summarized in the Figure 1.2 below.

Figure 1.2 Main goals and means of circular economy.

However, there are more than one hundred definitions of EC and the perimeter is very broad. Above all, there are no clear Key Performance Indicators (KPIs) to answer the question: how can a circular a system be measured?

For this reason, a technical committee in International Organization for Standardization (ISO) was born, it is called ISO/TC 323.

Italy is the first country in the European rankings of the circularity index.

The "Ministero delle Sviluppo Economico" and the "Ministero dell'ambiente e della tutela del territorio e del mare" have drafted a report that provide a general framework for the circular economy as well as to define country's strategic positioning on the theme, in continuity with the commitments adopted under the Paris Climate Change Agreement, the United Nations Agenda 2030 on Sustainable Development, the G7 Communiquè and within the European Union [5].

In fact, the circular economy is the 12th goal of the United Nations Sustainable Development Goals (SDGs), collected in the Figure 1.3 below.

Figure 1.3 United Nations Sustainable Development Goals.

The aim of the 12th goal is the sustainable consumption and production: "doing more and better with less". The net welfare gained from economic activities can increase by reducing resource use, degradation and pollution along the whole life cycle, while increasing quality of life.

Many government associations monitor the improvements to reach the goals every year, such as ASviS: Italian Alliance for Sustainable Development born with the aim of

growing, in the society and in the State, the awareness of the sustainable development objectives importance or the European Commission at European level [6].

At global level, many conferences are organized every year to discuss the question of the sustainable economic grow, World Economy Forum can be mentioned.

The scope of it is helping countries and businesses identify ways to transform their production systems to achieve sustainable growth while supporting their commitments under and boosting their competitive capabilities [7].

Since 1900, the world population has grown by a factor four while resource consumption has grown by a factor ten and it is expected to double by 2030.

In the face of a rising global population and the associated growing resource consumption and negative environmental impacts, it becomes increasingly apparent that traditional business is not an option for a sustainable future.

So, the governments are encouraging many companies, in some cases requiring, the adoption of circular economy principles and practices [8].

1.2. The case of Trelleborg Wheel System S.p.a.

Trelleborg Wheel Systems S.p.a. (TWS) is a leading global supplier of tires and complete wheels for agricultural machines, material handling and construction vehicles, and two-wheeled vehicles.

Material Handling and Construction Tires sector produce solid tyres and has four plants located around world: in China, in Sri Lanka, in Czech Republic and in Brazil.

The production cycle of solid tyres is shown in the Figure 1.4 below.

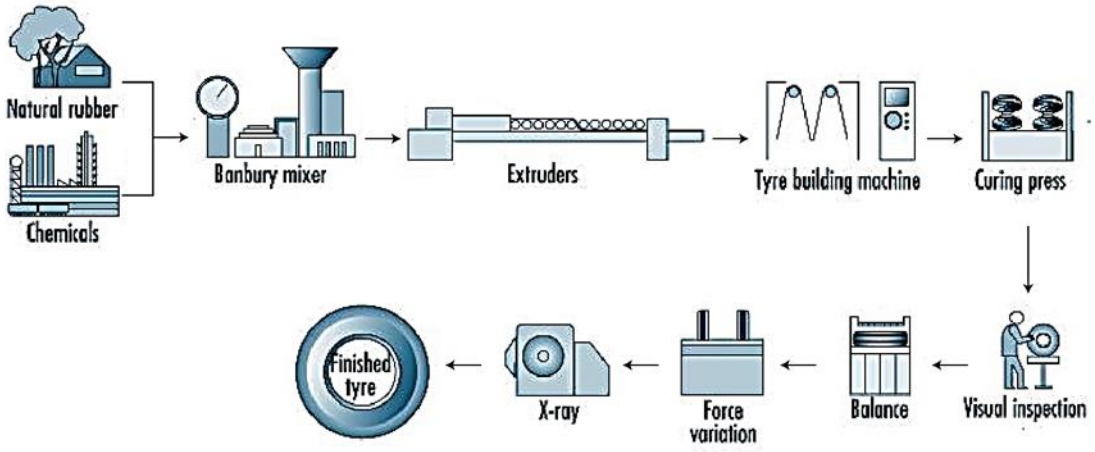

Figure 1.4 Production cycle of solid tyre.

Natural rubber, synthetic rubber and various chemicals, which act as accelerators, anti-oxidants, anti-ozonates, vulcanizers, plasticizers and reinforcing agents, are provided by suppliers in pre-weighed packages. All these materials are mixed together in the Banbury Mixer that works at a temperature just under one hundred Celsius grades to avoid the premature vulcanization of rubber compound.

After the completion of the Banbury mixing cycle, compound is extruded: the rubber is shaped into flat, long strips by forcing it through two set rolls rotating in different directions at different speeds.

The compound is transported up to Tyre Building Machine where it is left to cool and to rest.

In the Curing Press the compound undergoes heating at a temperature of about 150°C.

At the first stage, within few minutes, called scorch time, the softening of rubber compound happens and so it can be moulded, then, the cross-linking process occurs up to

the rubber stabilization when the material obtains the mechanical properties needed to be use as tyre.

At this point, the tyre is ready to the visual inspection where the presence of possible superficial defects can be detected.

The final tyre is weighted by a balance for logistic necessities.

Some tyres are sampled from the production line and various test is performed on them to ensure the required quality such as tensile test to evaluate mechanical strength and X-ray analysis to detect any hidden weaknesses or internal failures of the rubber.

In the TWS plant in Sri Lanka (Figure 1.5), the heat employed to compound mix in the Banbury is generated by a Biomass Fired Boiler where the wood provided by a supplier is burned to produce hot steam directed to Banbury.

Figure 1.5 Trelleborg Wheel System S.p.a. plant in Sri Lanka.

The Biomass Furnace is a green alternative to the traditional Oil Furnace.

In fact, the Biomass Furnace permits a reduction of CO_2 emissions of about 91% and a decrease of running rete cost of 50% compared with Oil Furnace.

A schematic overview on the Biomass Furnace system in TWS plant in Sri Lanka is illustrated in Figure 1.6 below.

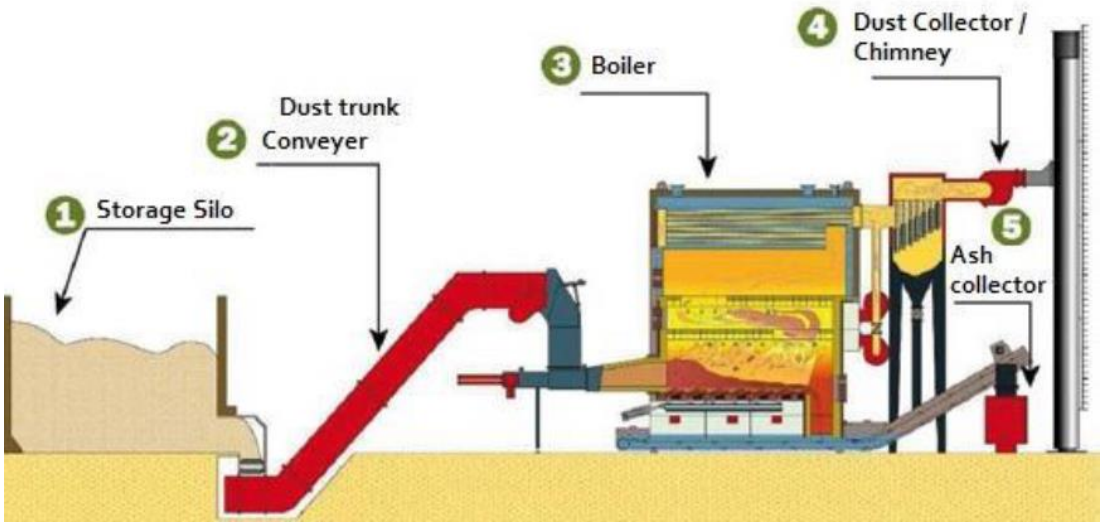

Figure 1.6 Schematic illustration of Biomass Furnace system.

A supplier provides the wood chips that is stored in silos.

The process starts with the wood chips unloading on a moving floor, powered by a fuel handling system of hydraulic drives, that transport wood chips, through a chain conveyor and a bucket elevator, into the dosing bin. The biomass reaches the boiler.

The main part of the system consists of the reciprocating grate furnace.

The furnace is made up of three sections (Figure 1.7): the fuel dryer, the firing zone and the cooling zone.

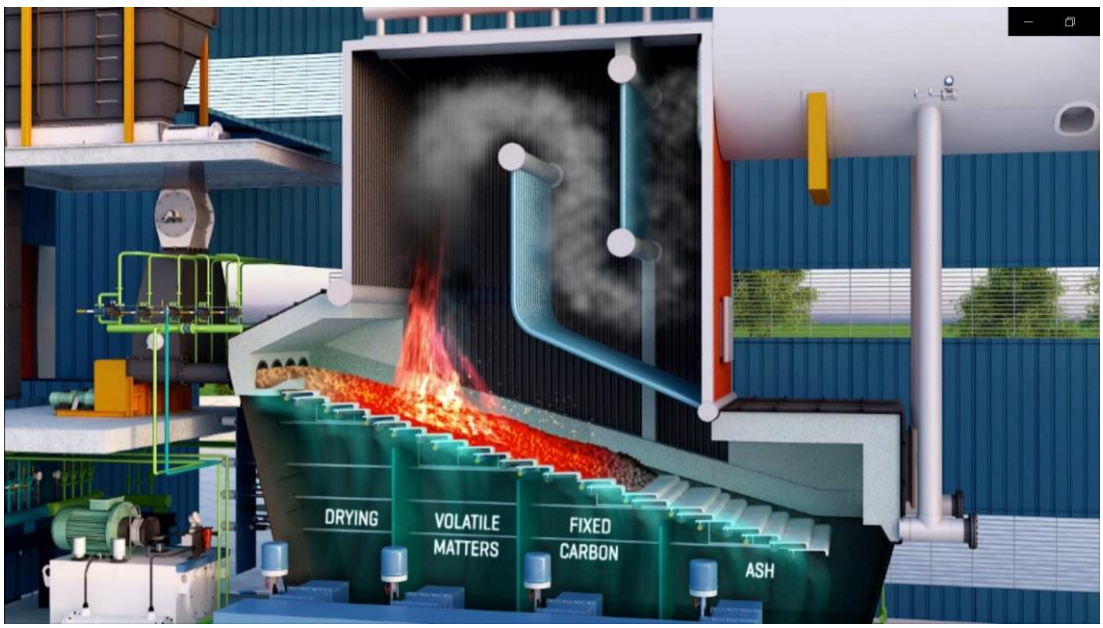

Figure 1.7 Rendering of furnace section of Biomass Fired Boiler.

Inside the furnace the wood chips are dried, and the humidity is controlled to guarantee the optimum value to promote the combustion.

The reverse flame boiler consists of inclined grate above which the wood is burnt evenly, increasing the efficiency.

A series of air fans conveys the hot steam coming from combustion to the steam outlet system, while at the end of the path, the fixed carbon and the ash are found as the last residual product.

The fuel gas at 330-340°C is convoyed to the economiser: a heat exchange that recovers the enthalpy of the hot fluid, improving the boiler's energy efficiency.

After that, the steam path goes on in the electrostatic precipitator (ESP): a filtration device that removes fine particles, like dust and smoke, by flowing gas using the force of induced electrostatic charge and minimally impeding the flow of gases through the unit.

In this way, the emission of the chimney is free of SO_x and it has a particulate matter (PM) lower than 50 mg/m^3.

Instead, the fly ash is conveyed through the moving bed to storage area, ready to be transported by biomass supplier for the disposal.

The plant produces 3 tons of ash per day, in an annual average. It is a high hydrophilic material. Since the ash comes from biomass combustion, it will be nominated bioash into this work.

Trelleborg Wheel System S.p.a. has taken care of the sustainable industrial production and has implemented a large number of measures to achieve the Sustainable Development Goals of United Nations.

At social level, together with Star for Life, TWS runs a school program at the Kelani and Bellana Colleges in Sri Lanka to support the education.

The Company also supports Antonio Bianchi’s House, a pre-school in Colombo for disabled children, in cooperation with Child Action Lanka.

At environment level, TWS uses, when possible, renewable raw materials as fibres derived from coconuts for rubber compounding and it reintroduces rubber waste products in the production cycle.

Moreover, thanks to patented Pit-Stop line technology, TWS indicates to customers the right moment to change tyres through a coloured indicator that appears

when the tyre reaches the limit of wear, reducing in this way the waste caused by a premature discarded of the tyres.

Thanks to the TWS partnership with COVA, the tyres at end of them life cycle are collected and recycled in accordance to the Art. 228 of D. Lgs 152/06.

On the other hand, the bioash produced from the boiler is a large amount of waste in the Sri Lanka plant but the bioash could have a high added value if it would be used as new filler in the rubber compounding, avoiding its disposal as waste.

To better explore this possibility, the features of rubber compound with bioash filler are discussed in the next chapters.

The problem of the bioash recycling as filler is the low compatibility between the polar rubber compound and the apolar bioash.

In this work, the possible treatments to improve the compatibility between rubber and bioash are investigated.

1.3. The rubber compounding

1.3.1. Overview on rubber

The unique properties of rubber as an engineering material start from its low modulus of elasticity and so its capability of sustaining a deformation of several hundred per cent. After such deformation, it quickly and forcibly retracts to its original dimensions. So, rubber is a resilient material and yet exhibits internal damping.

The high extensibility of rubber is due to vulcanization process.

Anyway, the raw state rubber is referred to as an elastomer with high molecular weight chains. An unvulcanised rubber lacks structural integrity and will “flow” over a period of time while vulcanization imparts dimensional stability, strength, and resilience.

The vulcanization process forms chemical bonds between adjacent elastomer chains and so the final rubber structure is a three-dimensional network composed of mutually cross-linked polymer chains that assume random coil conformation when no external perturbation is applied.

This conformation can be easily deformed by the action of an even small external stress thus generating highly elongated conformations.

In the cross-linked rubber network, physical couplings are also present as hydrogen bonds, polar, dispersion forces between elastomer chains and various intramolecular and intermolecular entanglements [9].

Moreover, mechanical properties of rubber are strongly improved by addition of fillers such as carbon black, due to the creation of new bonds between polymer and filler particles. In many cases, fillers in a rubber matrix are not found in the form of single particles, but as fractal clusters, generally called aggregates. Aggregates can further join together, and form superstructures called agglomerates.

Rubber can be compounded to have widely varying properties and can be processed into a variety of shapes.

The load-deflection curve can be altered by changing rubber compound and shape.

Typical rubber compound formulations consist of 10 or more ingredients that are added to improve physical properties, affect vulcanization, prevent long-term deterioration, and improve processability.

These ingredients are given in amounts based on a total of 100 parts of the rubber (parts per hundred of rubber).

Although the term rubber is used rather loosely, it usually refers to the compounded and vulcanized material [10].

All these rubber features are discussed in this chapter, with particular attention to filler effects, to understand the results of study presented in the chapter 3.

1.3.2. Vulcanization process

Vulcanization is the process by which the elastomer molecules become chemically cross-linked to form three-dimensional structures having dimensional stability.

Usually, the vulcanization technique for tyres favours the use of the cheapest method based on high pressure and high temperature environment. A typical vulcanization temperature for industrial solid tyres is 150°C for 30 minutes. This type of vulcanization is called compression moulding, in which the tire rubber is intended to adopt the shape of the mould.

The process occurs due to the presence of a vulcanizing agent: typically, the sulphur. However, the use of sulphur alone leads to a slow reaction, so activators and accelerators are added to increase the cure rate. Their type and quantity affect the rate of vulcanization, the cross-link structure, and the final properties of the compound.

During the thermal process, sulphur is able to react with the double bonds of the polymeric chains, forming chemical crosslinks, as illustrated in the Figure 1.8.

The vulcanized rubber forcibly retracts to its approximately original shape after a rather large mechanically imposed deformation, reducing the amount of permanent deformation remaining after removal of the deforming force.

Thus, vulcanization increases elasticity while it decreases plasticity.

The main disadvantage of this process is its irreversibility: at the end of the vulcanization process, the compound has to assume the desired shape.

According to the theory of rubber elasticity (Flory, 1953), the retractile force to resist a deformation is proportional to the number of network-supporting polymer chains per unit volume of elastomer.

In fact, the stiffness of the rubber compound increases with the formation of the crosslinks during vulcanization [11].

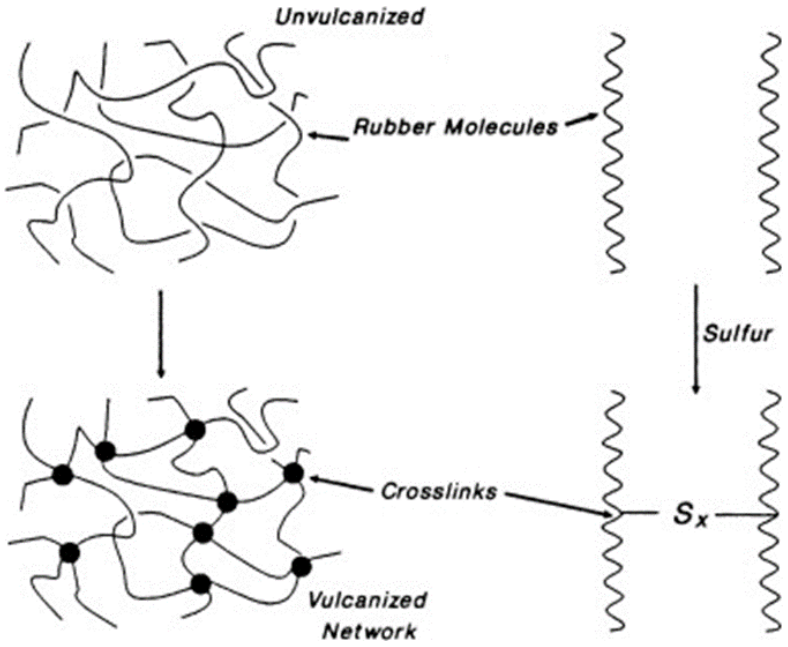

Figure 1.8 Effect of sulphur on the cross-linking of elastomer chains.

The grade of vulcanization is directly proportional to the Dynamic Modulus of the rubber: the ratio of stress to strain under vibratory condition.

Dynamic modulus is generally measured with the imposition of a sinusoidal, small strain at a frequency in the range between 1 and 100 Hz.

As vulcanization proceeds at the specific fixed temperature of 150°C, the torque required to shear the compound is monitored and a curve of torque versus time can be generated: the so called vulcanization curve, an example is shown in Figure 1.9.

The guidelines to determine the vulcanization characteristics is specified in ASTM D 2084 [12].

Generally, three stages are clearly represented by a vulcanization curve. The first stage is the induction period which is characterized by slow chemical reaction between rubber and additives. The end of this stage of few minutes is called scorch time (t sc).

The scorch time enables safe processing and good flow of the rubber compound inside a mould cavity since within this range the rubber is softened and can be deformed.

The second stage is where curing of rubber molecular chains occurs to form the network structures.

Vulcanization rate can be considered as the rate of this stage.

Optimum cure time (t 90) is the time required for the torque to reach 90% of the maximum achievable torque (T 90) and relates to the time necessary for the cured rubber to achieve optimal properties.

The last stage can involve over-curing reactions depending on rubber type, curatives and temperature. In an ideal case, equilibrium degree of vulcanization is obtained and the torque versus time graph plateaus. However, some compounds show reversion due to overheating that corresponds to break down of the rubber networks. Conversely, additional crosslinks may occur that produce a marching; this phenomenon is induced by the presence of very reactive vulcanization agent.

It is well known that over-cure of rubber compound usually has an undesirable effect on product quality. Therefore, a precise determination of cure time is necessary to ensure the final products having optimum performance with competitive cost [13].

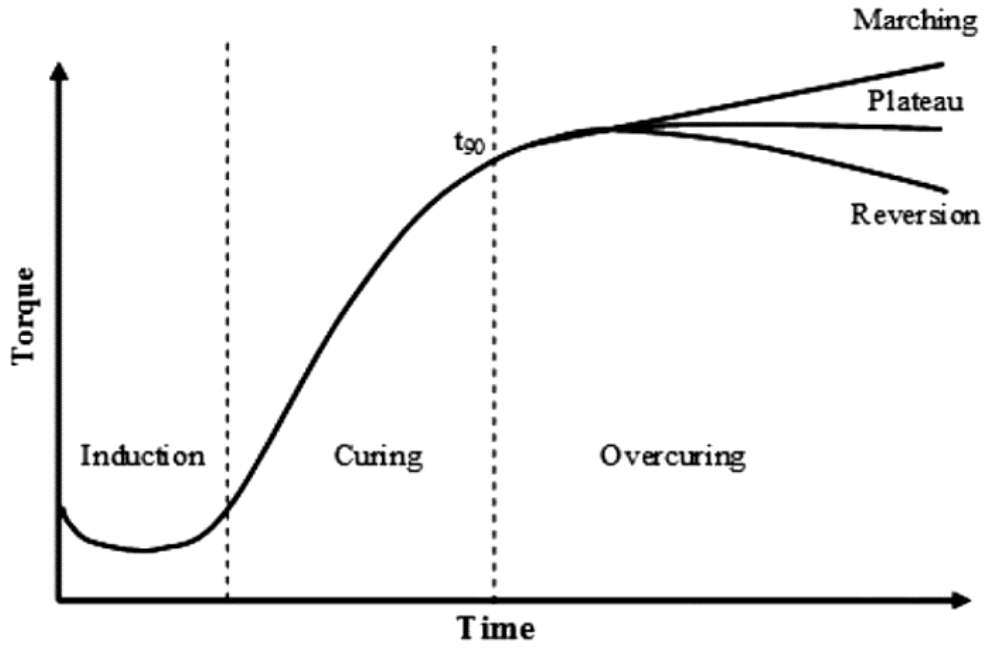

Figure 1.9 Vulcanization curve of a general rubber.

For filled elastomers, the cure time is usually shorter than unfilled elastomers and the maximum torque value increase as filler content increases.

While unfilled rubber can be properly modelled by purely viscoelastic models, filled rubbers, show a pronounced strain amplitude dependence of the storage and a loss modulus.

Hooke's law expresses the elastic modulus or Young modulus.

Young's modulus is the ratio between stress and strain: the stiffness of a material at the elastic stage of a tensile test.

Stress is the force on unit areas within a material that develops as a result of the externally applied force. Strain is the relative deformation produced by stress.

Hooke's law describes the elastic properties of materials only in the range in which the force and displacement are proportional: pure elastic material.

In case of shear force, the ratio of the shear stress τ to the shear strain γ defines the shear modulus G.

$$G = \frac{\tau}{\gamma}$$

The relation between shear strain and uniaxial strain is mediated by Poisson's ratio υ, as illustrated in the equation below. When the material is considered incompressible, such as the rubber, the Poisson's ratio υ is close to 0.5; so, in this case, it is assumed that the Young modulus is three times the shear modulus.

$$G = \frac{E}{2(1 + \upsilon)} = \frac{E}{3}$$

The dynamic properties of a filled rubber are usually expressed in terms of the complex modulus, which consists of a storage modulus (G') and a loss modulus (G"):

$$G^* = G' + G''$$

The complex modulus is a measure of the resistance of a material to deformation, and it encompasses both the elastic and viscous responses.

The loss modulus G'' or out-of-phase component represents the energy dissipated as heat during the deformation.

The storage modulus G' or in-phase component represents an immediate response to the application of the force and is directly proportional to torque of machine for rubber mixing. It is a measure of sample's elastic behaviour or, on other words, its stiffness.

The difference between the lower and the higher value of storage modulus in its curve against time, at the vulcanization temperature, is directly related to the crosslink density of the polymer network.

Fillers added to polymer systems cause a considerable change in dynamic properties and they affect not only the storage and loss moduli, but also their ratio, named damping factor (tan δ), which indicates the amount of hysteresis present during

deformation, considering that the behaviour, as a load is removed, is not the same as that when the load is being increased [14]. Tan δ is described by equation below.

$$\tan\delta = \frac{G''}{G'}$$

The mathematical relationship between shear modulus G and molecular weight between crosslinks M_c, and therefore, the crosslinking density, in terms of the elementary Gaussian network theory, is given by following equation:

$$G = \frac{\rho RT}{M_c}$$

where ρ is the density of the network, T is absolute temperature, and R the gas constant. The equation is valid for polymer networks synthesized with low crosslinker content.

From these equations we can extract some important conclusions:

- The modulus increases with temperature, just as with the spring constant of a single chain, due to its entropic origin;
- The modulus increases as a function of cross-link density, because M_c decreases; a "tighter" network is "stiffer";
- The modulus is independent of the functionality of the cross-links [15].

As can be seen in Figure 1.10, three stages of curing process can be observed in the tan δ curve. It suggests that, this parameter and its changes with time, apparently reflect the development of crosslinking reaction inside the rubber. In induction period, tan δ increased to a maximum which indicates the softening of the material and slow chemical reaction between vulcanizing agent, rubber and other compound constituents. The peak could relate to where optimum flow of the rubber compound through the mould cavity can occur giving the compound its final shape for curing. In the curing stage, tan δ was found to decrease rapidly which can again be explained by development of crosslinks between the rubber molecular chains that increase the elasticity of the material. As previously discussed, the end of this stage corresponds to the optimum vulcanization time (t 90) [16]. The last stage is again referred to the compound over-curing.

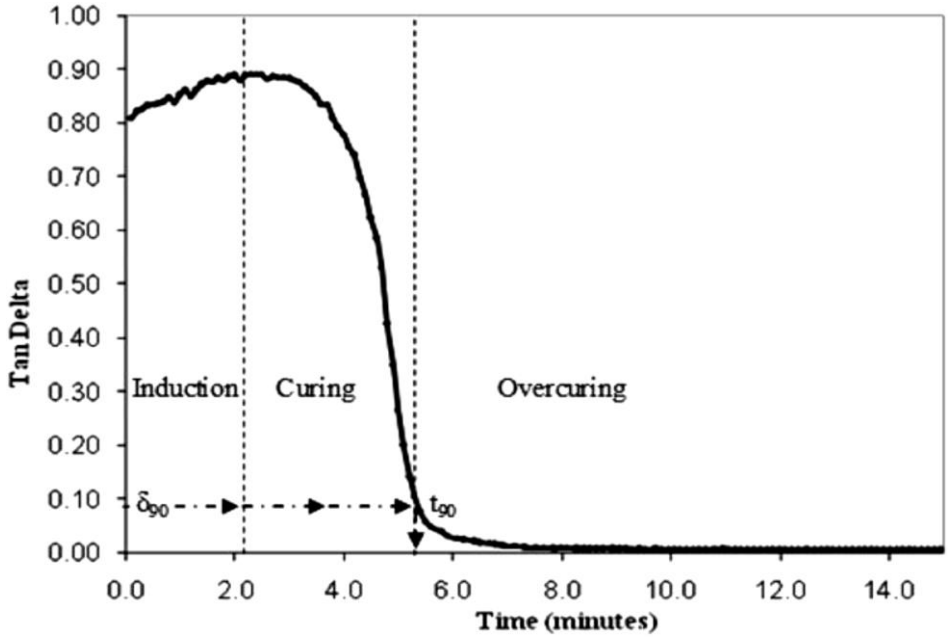

Figure 1.10 Tan δ curve as function of time for a general rubber compound.

1.3.3. Mechanical properties of rubber

Rubber has elastic properties similar to those of a metallic spring and has energy absorbing properties like those of a viscous liquid.

These viscoelastic properties allow rubber to maintain a constant shape after deformation, while simultaneously absorbing mechanical energy. The viscosity increases with reduced temperature.

The elasticity follows Hooke's law and increases with increased strain, while the viscosity follows Newton's law and increases with increased strain rate.

Therefore, when applying a strain, the resultant stress will increase with increasing strain rate. Springs or dashpots are frequently used to make theoretical models which illustrate the interaction of the elastic and viscous components of rubber. The springs and dashpots can be combined in series or in parallel, representing the Maxwell or Voigt elements. Rubber actually consists of an infinite number of such models with a wide spectrum of spring constants and viscosities [17].

At last, rubber can be essentially considered an incompressible substance that deflects by changing shape rather than changing volume.

A typical stress-strain curve is presented in Figure 1.11.

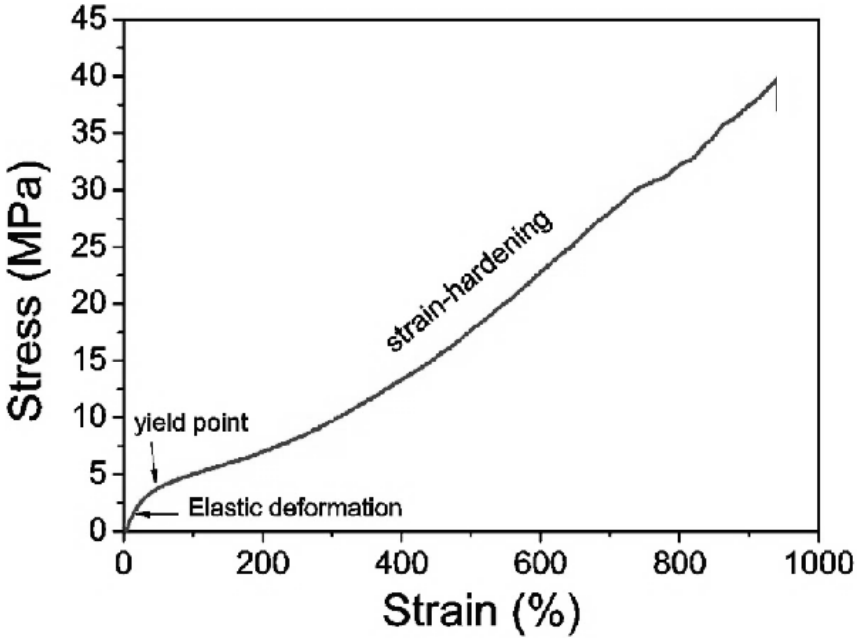

Figure 1.11 Stress-strain curve of a general rubber.

The elastic deformation of the rubber in the first stage of tensile test and the correspondent Young Modulus is limited at very low deformation. After then, the yield point, or elastic limit, is soon reached and the slop of curve drastically decrease in the strain-hardening region.

It is conceivable that the network of vulcanized rubber is composed of a broad distribution of chains with various lengths between the network points, since the practical vulcanization process cannot create a homogeneous network distribution.

Under stretching, only the chains with small length, among the densely packed network, can be oriented and form a crystal structure, whereas the chains with much longer lengths remain in the random coil state.

These crystal structures are connected by the oriented chains in amorphous state, this phenomenon forms a second network structure that is primarily responsible for the tough mechanical properties of vulcanized rubber. As the initial chemical network topology becomes more homogeneous, the strain required to induce the crystallization becomes larger and the fraction of the oriented amorphous chains also increases.

In other words, rubber compound undergoes strain-induced crystallization that accounts for the large increase in modulus at high deformation because the crystallites act as additional cross-links in the network. From this point of view, strain-induced crystallization can be considered as an auto-reinforcement of the elastomer [18].

In fact, although the Young's modulus and the yield stress values are both small, the stress and the strain values at break is relatively high, and particularly, the elongation at break. It is worth noting that, in this example, the stress at break is around 10 times of that yield stress, indicating the substantial enhancement on the mechanical performance induced by the strain-hardening.

To sum up, such enhancement could be ascribed to two aspects: on one hand, the stretching will induce the crystallization of rubber segments; on the other hand, the rubber chains will orient along the stretching direction [19].

Filled polymers generally exhibit nonlinear viscoelasticity under strains, which is often referred to as the Payne effect. The Payne effect is observed under cyclic loading conditions with small strain amplitudes and it is manifest as a dependence of the viscoelastic storage modulus on the amplitude of the applied strain. Above approximately 0.1% strain amplitude, the storage modulus decreases rapidly with increasing amplitude. At sufficiently large strain amplitudes, roughly 20%, the storage modulus approaches a lower bound. In that region where the storage modulus decreases the loss modulus shows a maximum [20].

This phenomenon has been related to filler network breakdown, filler deagglomeration, polymer-filler debonding from the filler surface, and strain softening of the polymer shell surrounding the fillers. However, underlying mechanisms for the Payne effect of filled polymers are not yet fully clarified. For example, the concepts of filler deagglomeration and network breakdown do not consider the contributions from the matrix and the filler-polymer interactions [21].

The stress-strain properties of rubber compounds are usually measured under tension as per ASTM D412-16 procedure [22].

The strength of a material is defined as the maximum stress that the material can sustain under uniaxial tensile loading.

The mobility of the chains can be measured from the deformation at the break point.

Stress measurements are made at specified percentages of elongation and reported as modulus values. For example, 300 percent modulus is defined as the stress per unit cross-sectional area (in MPa units) at an elongation of 300 percent.

These values describe the main physical properties of rubber compounds.

1.3.4. Effect of fillers in rubber compound

Rubber technology continues to develop over time, and a great deal of products come from the rubber industry every day.

Usually, at industrial level, the higher percentage of rubber compound consist of Natural Rubber due to its elasticity, low hysteresis, high durability and excellent toughness but to increase the application-oriented value of natural rubber some modifications are needed. Lot of other materials can be mixed with natural rubber to achieve the desiderate properties depends on final product application.

In tyre production, the required performances are essentially three: excellent abrasion resistance (good tyre tread wear), great traction (good mechanical properties) and low rolling resistance (good fuel economy) that can be achieved in case of low glass transition temperature (Tg) [23].

And so, a small part of compound can be made of synthetic rubber to give higher chemical stability at the final product. Sulphur is needed to create the network of cross-linked chains that permit at the rubber to recover its original shape after deformation. This process takes place thanks to a small quantity of accelerant and activators. To improve the properties of the final product also antioxidant and antiaging can be added.

Finally, carbon black filler functions to strengthen, increase the volume, improve the physical properties of rubber, and strengthen vulcanization. In fact, the addition of fillers like carbon black increase the modulus, tensile strength and wear resistance of the rubber material.

Moreover, it is possible to add other fillers, such as clay or similar, as semi-reinforcing fillers and for cost purposes, decreasing the needed quantities of other materials to load into the compound.

Filled rubber compounds exhibit very different rheological properties when compared with pure, unfilled elastomers, for instance:

- Disappearance of any linear viscoelastic region;
- Lower extrudate swell with increasing filler content;
- Smoother melt fracture defect with increasing filler content;
- Anisotropic effects in flow [24].

The state of filler dispersion plays a major role on the final properties of the material and also is influenced by the nature of the polymer-filler (P-F) and filler-filler (F-F) interactions.

Usually, the filler/rubber blends show decreasing trend of cure time with increasing filler loading. This indicates that fillers can have the ability to activate the vulcanization process through the promotion of hydrogen sulphide formation, they participate to the creation of cross-linkages turn out to decrease time to chains networks creation. And so, it is obvious that increasing loaded filler, the scorch time available to compound moulding comes down.

The incorporation of fillers in rubber blends increases the minimum torque, this effect is mainly attributed to polymer-filler interaction.

A similar trend was observed for maximum torque. Because maximum torque is correlated to modulus, polymer-filler interaction and filler-filler interaction will contribute to the value of maximum torque.

It is believed that uniform dispersion of filler and better filler-polymer interaction enhance the tensile strength of compounds. On the other hand, sometimes, the deterioration of tensile strength is observed. It is caused by decreasing polymer-filler interaction and increasing of filler-filler interactions due to the formation of agglomeration, in case of high presence of fillers inside the rubber matrix or due to the nature of filler to create stronger F-F interaction than P-F interaction.

Tensile stress at a relatively large strain (>100%) is closely related to the filler-rubber interaction.

Moreover, the loading of reinforcing fillers in the compounds gives lower values of elongation at the break and higher values of modulus at given percentage of deformation. It is expected as reinforcing agent has strong polymer-filler interaction, which restricts the mobility of natural rubber chains.

The opposite case occurs in presence of agglomeration due to high fillers presence or to fillers with strong F-F interaction.

It is clear that increasing the loaded reinforcing filler, the hardness value becomes higher. As tensile properties and hardness depends also on the behaviour of particulate fillers in the compounds, the fillers that have strong filler-filler interaction or the agglomerations induce lower tensile strength, higher deformation at break, lower modulus

and higher hardness compared to filler that has strong polymer-filler interaction. As hardness increases, reduction in resilience will occur [25].

The new filler analysed in this study is the bioash, in some cases, a similar material has been used as a road stabilization product [26]. The mechanisms of the bioash interaction with rubber are discussed in the chapter 3.

To sum up, the nature of the fillers and their interactions with rubber matrix have an intrinsic effect on mechanical and rheological behaviour of filled rubber compound.

A large variety of powdered minerals can be compounded with elastomers but not all have reinforcing capabilities.

There are certain minerals used to reinforce the elastomers, which may have several particle sizes [27]. As shown in Figure 1.12, particles larger than 0.1 μm do not have high reinforcing capabilities (at best) or have a detrimental action.

Reinforcement is readily obtained with sizes smaller than 0.1 μm but particle structure appears as a more decisive factor. In fact, also the structure of aggregates influences the rule of fillers in compound properties. The large aspect ratios of fillers are thought to be mainly responsible for the enhanced mechanical properties of rubber compound.

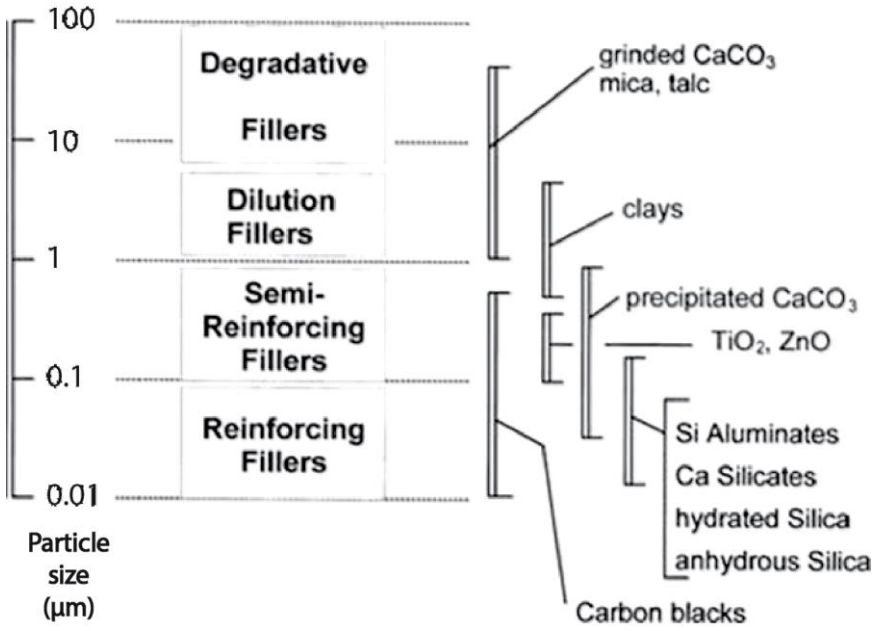

Figure 1.12 Classification of fillers according to average particle size.

The carbon black that has a reinforcing effect, for example, is made up of complex and longitudinal branched arrangements of spherical entities whose diameter ranges from 0.01 to 0.09 μm.

On the other hand, particulate fillers with high F-F interaction are arranged in aggregates of main dimension between 0.1 and 10 μm and several aggregates further give weak giant assemblies called agglomerates with size of 10 - 100 μm.

The agglomerates have poor, if any, reinforcing properties and their presence in a vulcanized compound are failed initiation sites.

The strength of the material (the break stress) increases with smaller particles. The increasing surface area of the filler particles turns out to a more efficient stress transfer mechanism.

Mechanically, filler particles affect the strength in two ways: on one hand, the weakening effect is due to the stress concentration, on other hand, the particles may serve as barriers to crack growth and so they can have a reinforcing effect [28].

Despite tensile strength and modulus at 300% elongation can be considered a qualitative way to measure the grade of filler reinforcement, the energy at rupture is the best single criterion for reinforcement.

2. Materials and methods

2.1. Materials for standard rubber compound

The base formulation of the compounds present in this work refers to obtainment of standard rubber compound for tyres and it has been kindly given by Trelleborg Wheel System S.p.A. (T.W.S.); the main materials used in the compounding [29] are here listed and discussed in this sub-chapter. The information about suppliers are confidential.

2.2.1 NR SIR20
2.2.2 SBR EUROPRENE 1500
2.2.3 CB N330
2.2.4 MES-OIL
2.2.5 Zinc oxide
2.2.6 Stearine N
2.2.7 6PPD
2.2.8 TBBS 80%
2.2.9 Oiled sulphur & silica

2.1.1. NR SIR20

SIR20 is the commercial name of Standard Indonesian Rubber (SIR) 20 grade: a type of the natural rubber (NR) with a medium grade of purity; it belongs to the class of TSR: Technically Specified Rubber.

The natural rubber is cis-1,4-polyisoprene (Figure 2.1) with a molecular weight of 200’000-500’000 Daltons. It can be isolated from more than 200 different species of plant but only one tree source is commercially significant: the Hevea Brasiliensis.

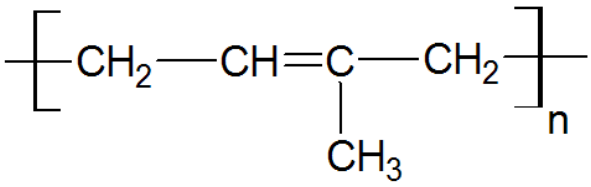

Figure 2.1 Structural formula of natural rubber.

Latex is an aqueous colloid of NR and is obtained from the tree by ‘tapping’ into the inner bark and collecting the latex in cups. The latex typically contains 30-40% dry rubber by weight, and 10-20% of the collected latex is concentrated by creaming, or centrifuging, and used in its latex form.

The remaining latex is processed in the producer country into dry rubber as sheets, crepes and bales. There is an International Standard for the Quality and Packing for Natural Rubber grades, the so-called “Green Book”, published by the Rubber Manufacturers’ Association in 1969.

The technical specifications on composition guaranteed by the supplier are reported in Table 2.1.

Table 2.1 Guaranteed specifications of SIR 20.

Raw Material form	*Dirt Content % max*	*Ash Content % max*	*Volatile Matter Content % max*	*Nitrogen Content % max*
Coagulum	0.16	1	0.8	0.6

Natural rubber has a high tensile strength and it is resistant to fatigue from wear such as chipping, cutting or tearing. On the other hand, since the main chain of NR contains unsaturation (residual double bonds) it is susceptible to attack by oxygen, ozone and light, and compounds therefore require protection against these agencies.

Natural rubber also has high adhesion to steel cord, which makes it an excellent material for use in tyres.

2.1.2. SBR EUROPRENE 1500

The chemical denomination of Europrene1500 is Emulsion Polymerized Styrene-Butadiene Rubber/Copolymer (E-SBR), dry type. It is a synthetic rubber derived from styrene and butadiene (Figure 2.2).

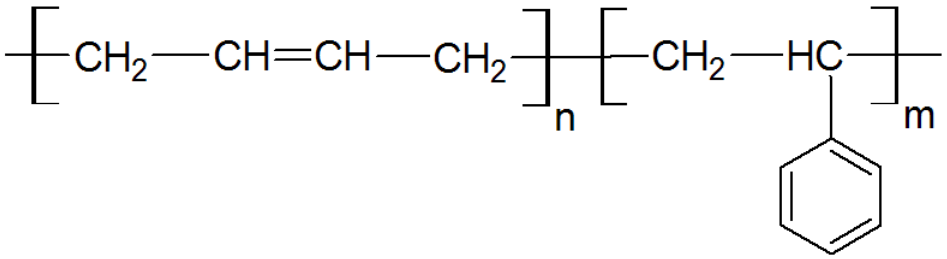

Figure 2.2 Structural formula of Styrene-Butadiene synthetic rubber.

The technical specifications guaranteed by the supplier are reported in Table 2.2.

Table 2.2 Guaranteed specifications of Europrene 1500.

Mooney viscosity MU ML 1+4 (100 °C) (ASTM D 1646)	*Bound styrene %wt (ASTM D 5775)*	*Organic acid %wt (ASTM D 5774)*
52	23.5	6

Synthetic rubber offers better resistance to abrasion than natural rubber, as well as superior resistance to heat and to effects of aging. Together with natural rubber, the physical and chemical properties of the addition of synthetic polymers determine the overall tyre performance.

2.1.3. CB N330

N330 is a hard particle furnace Carbon Black.

Carbon black (CB) is obtained using as feedstock heavy residues coming from refinery conversion units, so it can contain sulphur, oxygen and nitrogen residues from combustion.

The carbon black type N330 is defined as hard black grades: it is characterized by a normal structure and by a good ratio of porosity that guarantees a quite high superficial area available for interaction with rubber.

Carbon black N330 is used as reinforcing filler in rubber compounds since it offers very good abrasion resistance and provides also good tear resistance and high tensile strength.

2.1.4. MES-OIL

MES (mild extracted solvate) is environment friendly aromatic oil for rubber.

It is characterized by high stability, remarkable compatibility with rubber and rubber blends, low volatility both during the high temperature production phases and during the storage of the final products, suitable viscosity and appropriate plasticity in order to facilitate the processability without altering the physical properties of rubber compound.

MES-OIL facilitates the dispersion and the blending in the mixture of rubber with other components such as pigments, additives and carbon-black and it helps the elastomer workability.

2.1.5. Zinc Oxide

Zinc Oxide is a mineral chemical. The chemical formula is ZnO.

It proved to be the most effective activator to speed up the rate of curing; the unreacted portion of the zinc oxide remains available as an alkaline reserve to neutralize the sulphur-bearing acidic decomposition products formed during vulcanization.

Zinc oxide and stearic acid together form zinc soap that improves the solubility of zinc oxide in the compound, and that forms a complex with accelerator. This complex is particularly lively, it reacts with sulphur to produce a very strong vulcanizing agent.

Zinc oxide has also anti-aging properties, protecting rubber form UV light.

2.1.6. Stearine N

Stearine N is the commercial name of Stearic Acid (AS), a saturated fatty acid found in various animal and plant fats. Its IUPAC name is octadecanoic acid since it has an 18-carbon chain: the molecule sketch is illustrated in Figure 2.3 below.

It is a white solid with a mild odour and with chemical formula: $C_{17}H_{35}CO_2H$.

It is considered to be inexpensive and biocompatible, as well as of a low toxicity.

Stearic acid is used as activator, dispersing agent, plasticizer and lubricant in rubber compound processing.

The density of stearic acid is about 941g/l.

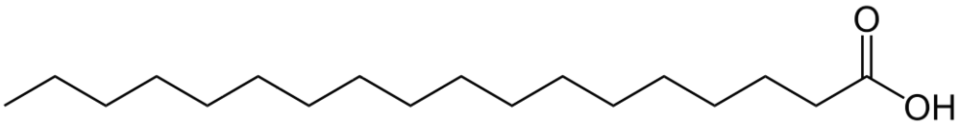

Figure 2.3 Structural formula of Stearic Acid.

2.1.7. 6PPD

6PPD or Vulkanox 4020/LG is the commercial name of N-1,3-dimethylbutyl-N'-phenyl-p-phenylenediamine, whose molecular formula is $C_{18}H_{24}N_2$.

It is used, in form of solid pellets, as antioxidant and antiozonant in rubber compounding. 6PPD improves the fatigue-resistance of the elastomers and acts as sacrificial surface layer against aging.

2.1.8. PREMIX TBBS 80%

Premix TBBS 80% is a delayed action accelerator that contains 80% by weight of the active substance: N-tert-butyl-2-benzothiazolsulfenamide.

TBBS 80% guarantees a considerably long scorch time, great processing safety and excellent modulus development for rubber compounding.

2.1.9. Oiled Sulphur & Silica

The Oiled sulfur & silica is a yellow power containing a percentage of pure Sulphur between 80% and 90%.

The role of Sulphur during rubber compounding is crucial for development of properties in final product: it is, indeed, a cross-linking agent.

The cross-linking reaction consists in formation of strong bonds between the long chain of rubber that makes the rubber hard, this process is also known as vulcanization.

The vulcanized rubber has better elasticity at low and at high temperatures. It also neither becomes soft nor brittle (§ 1.3.2)

For simplicity, in this study, when it is spoken about Sulphur, it is referred to above Oiled sulfur & silica.

2.2. Materials for circular process implementation

To implement the circular economy in the current process of tyre rubber compounding, the standard compound formulation is modified to allow the loading of bioash: the waste element that it is wanted to reintroduce into the production cycle.

Moreover, also other materials have been used to modify the bioash chemistry with the aim of improving the properties of the final product. The list of materials added to the standard composition, is here presented and discussed in next sub-chapters:

2.2.1 Bioash
2.2.2 Oleic Acid
2.2.3 Silane coupling agent (TESPT)
2.2.4 Polyisoprene-graft-maleic anhydride (gMAH)
2.2.5 Epoxidized natural rubber 50 (ENR)

Besides, the standard formulation has been modified by addition of the bioash, functionalized bioash, bioash and epoxidized natural rubber 50 or bioash and polyisoprene-graft-maleic anhydride. The presence and the quantity of these components change in each compound (all the formulations are reported in § 2.3).

2.2.1. Bioash

The bioash used in this research is the waste produced by the Biomass Fired Boiler, a segment of Trelleborg Wheel System S.p.a. plant in Sri Lanka, for the generation of hot steam needed for compound mixing (§ 1.2).

The preliminary studies have been done on two types of bioash:

- Bioash from the trial plant
- Bioash from the actual plant

The bioash from the actual plant comes from the combustion of wood of the Ipil-Ipil and natural rubber trees.

The wood for trial plant has been provided by a different temporary supplier.

After the analysis on the difference between the two types of bioash, the bioash produced by actual plant is used as reference since it is closer to possible industrial application.

2.2.2. Oleic acid

Oleic acid is a colorless to pale yellow liquid with a mild odor. It occurs naturally in various animal and vegetable fats and oils; it has been provided by Sigma- Aldrich Corporation.

Oleic acid is a saturated long-chain fatty acid, octadec-9-enoic acid, in which the double bond at C-9 has Z(cis)stereochemistry induces oleic acids to create bonds with other elements and this distinguishes it from stearic acid.

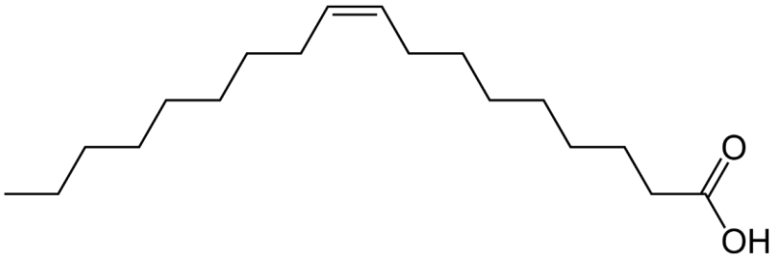

Figure 2.4 Structural formula of Oleic Acid.

2.2.3. Silane coupling agent (TESPT)

Bis(triethoxysilylpropyl)tetrasulfide (TESPT), commercially named Si69, with chemical formula: $C_{18}H_{42}O_6S_4Si_2$, is an organosulfur compound. The molecule consists of two trialkoxysilyl propyl groups linked with a polysulfide. The molecule is shown in Figure 2.5 below.

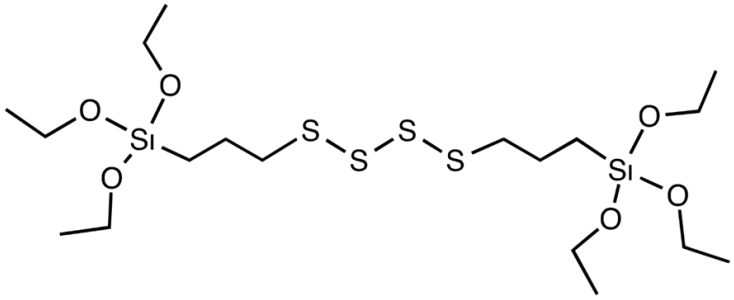

Figure 2.5 Structural formula of TESPT.

It has been supplied by Sigma-Aldrich Corporation and it is presented as a colourless viscous liquid or white solid pellet at 5°C.

TESPT is generally used as a crosslinking agent and reinforcing filler in the manufacturing of rubber.

Hence, the ethoxy group of TESPT can react with carboxyl or hydroxyl group on the carbon black surface to form a siloxane bond. Carbon black has various functional groups on the surface such as carboxyl, aldehyde, and hydroxyl groups though total amount of the functional groups is small.

TESPT interacts also with natural rubber [30]. Its mechanism of reaction is illustrated in the Figure 2.6 below.

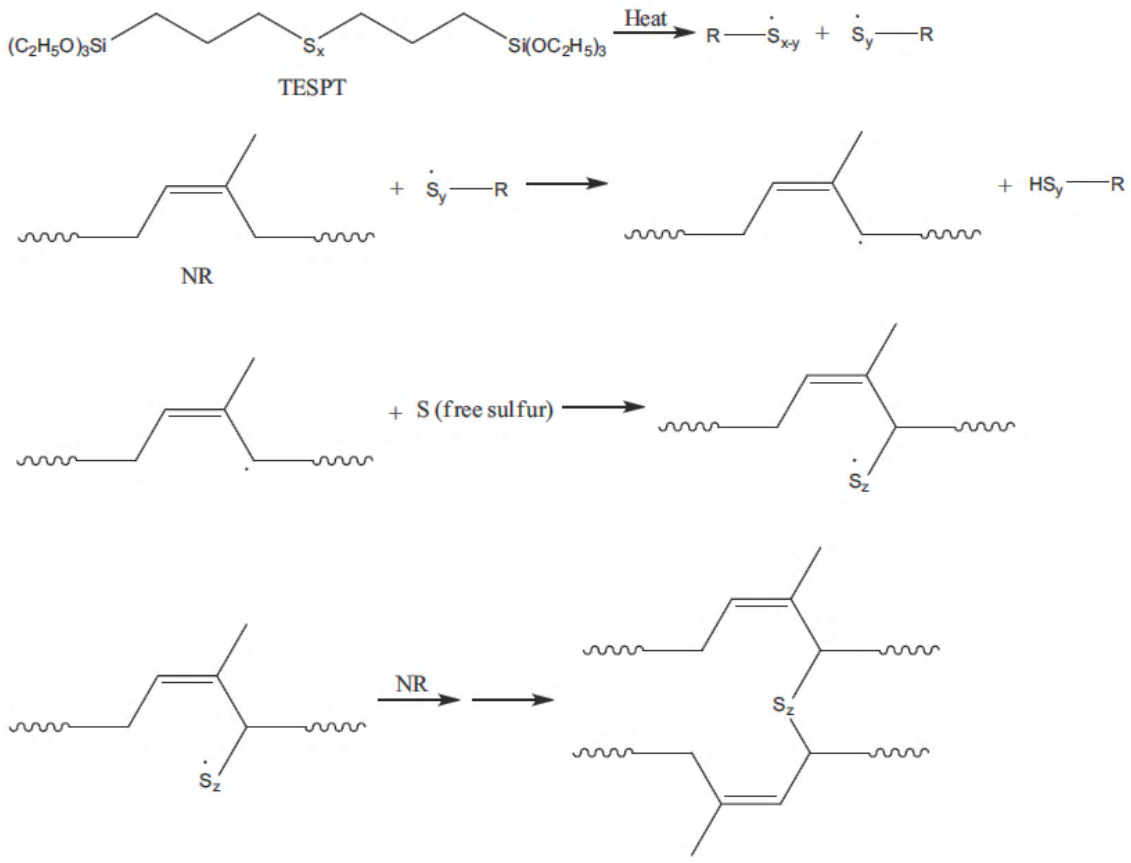

Figure 2.6 Schematic illustration of interaction mechanism between TESPT and natural rubber.

2.2.4. Polyisoprene-graft-maleic anhydride (gMAH)

Polyisoprene-graft-maleic anhydride (gMAH) is a modified natural rubber with the presence of three oxygen atoms in a pentacycle, as showed in Figure 2.7.

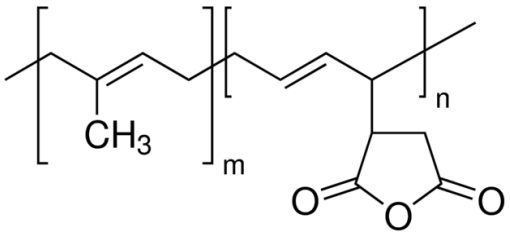

Figure 2.7 Structural formula of polyisoprene-graft-maleic anhydride.

As it happens in the case of epoxidized natural rubber (ENR), the NR segment interacts with the NR matrix while the polar segment is compatible with the bioash; with respect to the ENR, three sides for reaction are available and the presence of double bonds in the pentacycle improve the compatibility with the hydrophilic bioash.

gMAH is a transparent sticky gel. It has been provided by Sigma-Aldrich Corporation; its main properties are shown in the Table 2.3 below.

Table 2.3 Guaranteed specifications of polyisoprene-graft-maleic anhydride.

Viscosity, 20% in toluene, 30°C (cp)	*Density, at 25°C (g/mL)*	*Average Mw*
10-50	0.92	25’000

2.2.5. Epoxidized natural rubber 50 (ENR)

Epoxidized natural rubber (ENR) is the result of the chemical modification of natural rubber by introducing a hydrophilic group along the isoprene backbone, specifically by epoxidation carried out with a peracid formed by the reaction of acetic or formic acid with hydrogen peroxide (Figure 2.8).

In this way the common structure of cis-1,4-polyisoprene, which contains double bonds that are prone to thermal and oxidative degradation, is stabilized by the presence of an oxygen atom instead of the unsaturated bond.

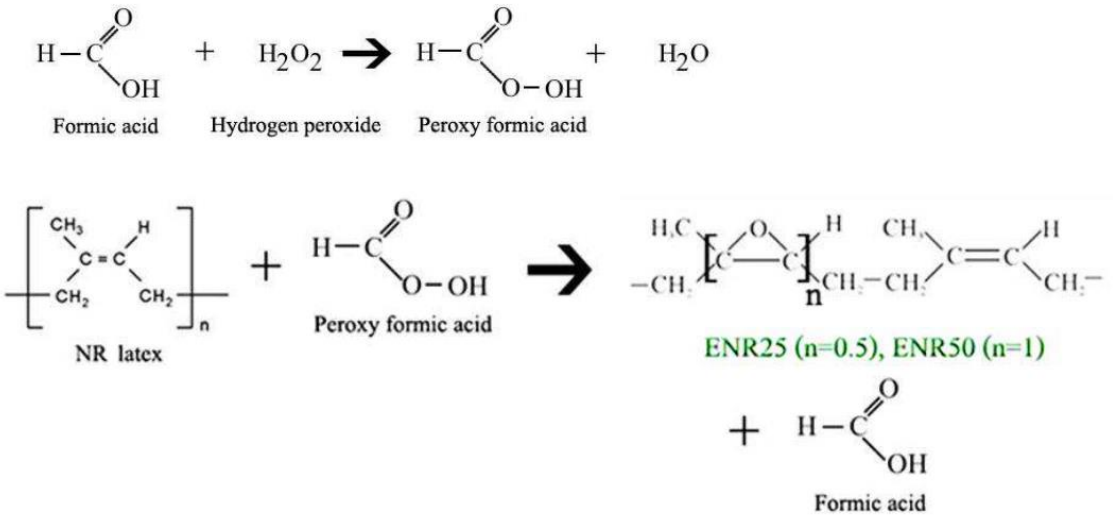

Figure 2.8 Reaction mechanism for ENR production.

Epoxidized natural rubber has improved heat and chemical resistance because the oxirane ring increases the hydrophilicity and reduces the number of double bonds in the backbone. The advantages in the use of ENR as tyre tread material are low rolling resistance, low heat build-up, higher oil resistance and anti-vibration property.

But, ENR has probably still to find its market niche.

All these improvements are due to increase of interfacial adhesion between hydrophilic bioash and hydrophobic natural rubber matrix: the polar part of ENR may react with the bioash, while NR part of ENR may be miscible with NR.

Specifically, in this work, the level of epoxidation of natural rubber is 50 mole percent, so it is called ENR-50. The supplier Sanyo Trading India Private LTD has provided the following technical specifications:

Table 2.4 Guaranteed specifications of ENR50.

Mooney viscosity MU ML 1+4 (100 °C) (ASTM D 1646)	*Ash Content % max*	*Glass Transition Temperature (°C)*	*Epoxidation level (mole%)*
70-100	0.50	-24	50 ± 2

2.3. Compound formulations

Several compound formulations have been prepared and tested.

The base formulation is the standard rubber formulation for tyres provided by TWS, so it is called STD. At the standard formulation different parts of raw bioash or modified bioash, for hundred of rubber, are added. Moreover, the last formulations include the presence of grafting agent since it is added directly during compound mixing.

All the quantities of materials in the rubber compound are expressed by "parts for hundred of rubber" (phr). The following tables summarize the composition of the formulations in terms of phr and respective grams to produce a final crude rubber compound which occupies a volume of 35 cm^3: about 39 g of materials.

The choice of producing 39 g per batch is related to the capacity of the mixer of 45 cm^3 (§ 2.4.1) and to maintain a low torque resistance during the process, avoiding an increase of temperature that could lead to a premature rubber vulcanization.

From the indication of phr of ingredients and the knowledge of their density, the occupied volume is calculated and then scaled by their ratio called fill factor, according to desired volume of final product.

2.3.1. Formulation without ash

The first formulation refers to standard rubber compound for tyres, without bioash. It is nominated STD0.

The Table 2.5 below indicates the density, phr, weight percentage and grams of each ingredient used in compounding.

Table 2.5. Formulation for standard rubber compound (without bioash): STD0.

STD0	*Density (g/cm3)*	*phr*	*Weight percentage (%)*	*Quantities (g)*
NR TSR20	0.92	80	48.48	18.99
SBR S1500	0.94	20	12.12	4.75
CB N330	1.80	50	30.30	11.87
MES OIL	0.91	5	3.03	1.19
ZINC OXIDE	5.55	4	2.42	0.95
STEARIC ACID	0.85	2	1.21	0.47

6PPD	1.00	1	0.61	0.24
TBBS 80%Active	1.17	1	0.61	0.24
SULFUR	2.00	2	1.21	0.47

2.3.2. Formulations with the bioash

The following tables refer to standard formulation modified with different quantities of bioash: the waste of rubber production reintroduced in process as part of final product. The foreign ingredients with refers to standard formula are underlined.

The Table 2.6 below shows the composition of compound STD1: standard rubber compound formulation with the addition of 1 phr of bioash.

Table 2.6. Formulation of rubber compound with 1 phr of bioash: STD1.

STD1	*Density (g/cm3)*	*phr*	*Weight percentage (%)*	*Quantities (g)*
NR TSR20	0.92	80	48.19	18.87
SBR S1500	0.94	20	12.05	4.72
CB N330	1.80	50	30.12	11.80
MES OIL	0.91	5	3.01	1.18
ZINC OXIDE	5.55	4	2.41	0.94
STEARIC ACID	0.85	2	1.20	0.47
6PPD	1.00	1	0.60	0.24
TBBS 80%Active	1.17	1	0.60	0.24
SULFUR	2.00	2	1.20	0.47
BIOASH	1.09	1	0.60	0.24

The Table 2.7 shows the composition of compound STD3: standard rubber compound formulation modified with the addition of 3 phr of bioash.

Table 2.7 Formulation of rubber compound with 3 phr of bioash: STD3.

STD3	*Density (g/cm3)*	*phr*	*Weight percentage (%)*	*Quantities (g)*
NR TSR20	0.92	80	47.62	18.64
SBR S1500	0.94	20	11.90	4.66
CB N330	1.80	50	29.76	11.65
MES OIL	0.91	5	2.98	1.17
ZINC OXIDE	5.55	4	2.38	0.93
STEARIC ACID	0.85	2	1.19	0.47
6PPD	1.00	1	0.60	0.23
TBBS 80%Active	1.17	1	0.60	0.23
SULFUR	2.00	2	0.19	0.47
BIOASH	1.09	3	1.79	0.70

The Table 2.8 below shows the composition of compound STD5: standard rubber compound formulation with the addition of 5 phr of bioash.

Table 2.8 Formulation of rubber compound with 5 phr of bioash: STD5.

STD5	*Density (g/cm3)*	*phr*	*Weight percentage (%)*	*Quantities (g)*
NR TSR20	0.92	80	47.06	18.42
SBR S1500	0.94	20	11.76	4.60
CB N330	1.80	50	29.41	11.51
MES OIL	0.91	5	2.94	1.15
ZINC OXIDE	5.55	4	2.35	0.92
STEARIC ACID	0.85	2	1.18	0.46
6PPD	1.00	1	0.59	0.23
TBBS 80%Active	1.17	1	0.59	0.23
SULFUR	2.00	2	1.18	0.46
BIOASH	1.09	5	2.94	1.15

In case of the addition of 5 phr of bioash at the standard formulation, considering the zero cost of the recycled bioash, the money saving amounts to 1.63 % of standard compound price.

The Table 2.9 below shows the composition of compound STD8: standard rubber compound formulation with the addition of 8phr of bioash.

Table 2.9 Formulation of rubber compound with 8 phr of bioash: STD8.

STD8	*Density (g/cm3)*	*phr*	*Weight percentage (%)*	*Quantities (g)*
NR TSR20	0.92	80	46.24	18.09
SBR S1500	0.94	20	11.56	4.52
CB N330	1.80	50	28.90	11.31
MES OIL	0.91	5	2.89	1.13
ZINC OXIDE	5.55	4	2.31	0.90
STEARIC ACID	0.85	2	1.16	0.45
6PPD	1.00	1	0.58	0.23
TBBS 80%Active	1.17	1	0.58	0.23
SULFUR	2.00	2	1.16	0.45
BIOASH	1.09	8	4.62	1.81

The Table 2.10 below shows the composition of compound STD15: standard rubber compound formulation with the addition of 15phr of bioash.

Table 2.10 Formulation of rubber compound with 15 phr of bioash: STD15.

STD15	*Density (g/cm3)*	*phr*	*Weight percentage (%)*	*Quantities (g)*
NR TSR20	0.92	80	44.44	17.37
SBR S1500	0.94	20	11.11	4.34
CB N330	1.80	50	27.78	10.86
MES OIL	0.91	5	2.78	1.09
ZINC OXIDE	5.55	4	2.22	0.87
STEARIC ACID	0.85	2	1.11	0.43

6PPD	1.00	1	0.56	0.22
TBBS 80%Active	1.17	1	0.56	0.22
SULFUR	2.00	2	1.11	0.43
BIOASH	1.09	15	8.33	3.26

In case of the addition of 15 phr of bioash at the standard formulation, considering the zero cost of the recycled bioash, the money saving amounts to 7.09 % of standard compound price.

From the test results (§ 3.1.3), it is notable that the higher differences in final rubber properties occur with the compounds that contain 5 phr and 15 phr of the bioash, so these quantities are taken as references for subsequent studies with treated bioash.

2.3.3. Formulations with the bioash and gMAH

To improve the compatibility between the bioash and rubber, gMAH is added in compounding so that the polar segment of gMAH can react with bioash while the NR segment can interact with the rubber matrix.

The Table 2.11 below shows the composition of compound STD5-gMAH: standard formulation with the addition of 5 phr of bioash and the double amount of gMAH that is 10 phr, since the bioash/compatibilizer ratio is 1:2 as reported in literature [31].

Table 2.11. Formulation of rubber compound with 5 phr of bioash and double phr of gMAH: STD5-gMAH.

STD5-gMAH	*Density (g/cm3)*	*phr*	*Weight percentage (%)*	*Quantities (g)*
NR TSR20	0.92	80	44.44	17.19
SBR S1500	0.94	20	11.11	4.30
CB N330	1.80	50	27.78	10.74
MES OIL	0.91	5	2.78	1.07
ZINC OXIDE	5.55	4	2.22	0.86
STEARIC ACID	0.85	2	1.11	0.43
6PPD	1.00	1	0.56	0.21
TBBS 80%Active	1.17	1	0.56	0.21
SULFUR	2.00	2	1.11	0.43

BIOASH	1.09	5	2.78	1.07
gMAH	0.92	10	5.56	2.15

The Table 2.12 below shows the composition of compound STD15-gMAH: standard formulation with 15 phr of the bioash and the double amount of gMAH, that is 30 phr.

Table 2.12. Formulation of rubber compound with 15 phr of bioash and double phr of gMAH: STD15-gMAH.

STD15-gMAH	*Density (g/cm3)*	*phr*	*Weight percentage (%)*	*Quantities (g)*
NR TSR20	0.92	80	38.10	14.45
SBR S1500	0.94	20	9.52	3.61
CB N330	1.80	50	23.81	9.03
MES OIL	0.91	5	2.38	0.90
ZINC OXIDE	5.55	4	1.90	0.72
STEARIC ACID	0.85	2	0.95	0.36
6PPD	1.00	1	0.48	0.18
TBBS 80%Active	1.17	1	0.48	0.18
SULFUR	2.00	2	0.95	0.36
BIOASH	1.09	15	7.14	2.71
gMAH	0.92	30	14.29	5.42

In case of the addition of 15 phr of bioash and 30 phr of gMAH at the standard formulation the great money saving amounts to 56.24 % of standard compound price.

2.3.4. Formulations modified with the bioash and ENR

Another tentative has been done with ENR that has a consistence similar to rubber commonly used in compounds for tyres. Similarly to gMAH, the ENR acts as a bridge between rubber and the bioash thanks to the presence of a polar group instead of all the unsaturated bonds of natural rubber.

The Table 2.13 shows the composition of compound STD5-ENR: standard formulation with the addition of 5 phr of bioash and 5 phr of ENR.

The quantity of ENR is 5 phr for every compound as suggested by literature [32].

Table 2.13. Formulation of rubber compound with 5 phr of bioash and 5 phr of ENR: STD5-ENR.

STD5-ENR	*Density (g/cm3)*	*phr*	*Weight percentage (%)*	*Quantities (g)*
NR TSR20	0.92	80	45.71	17.84
SBR S1500	0.94	20	11.43	4.46
CB N330	1.80	50	28.57	11.15
MES OIL	0.91	5	2.86	1.12
ZINC OXIDE	5.55	4	2.29	0.89
STEARIC ACID	0.85	2	1.14	0.45
6PPD	1.00	1	0.57	0.22
TBBS 80%Active	1.17	1	0.57	0.22
SULFUR	2.00	2	1.14	0.45
BIOASH	1.09	5	2.86	1.12
ENR	1.02	5	2.86	1.12

The Table 2.14 below shows the composition of compound STD15-ENR: standard formulation with the addition of 5 phr of bioash and 5 phr of epoxidized natural rubber.

Table 2.14. Formulation of rubber compound with 15 phr of bioash and 5 phr of ENR: STD15-ENR.

STD15-ENR	*Density (g/cm3)*	*phr*	*Weight percentage (%)*	*Quantities (g)*
NR TSR20	0.92	80	43.24	17.37
SBR S1500	0.94	20	10.81	4.34
CB N330	1.80	50	27.03	10.86
MES OIL	0.91	5	2.70	1.09
ZINC OXIDE	5.55	4	2.16	0.87
STEARIC ACID	0.85	2	1.08	0.43
6PPD	1.00	1	0.54	0.22
TBBS 80%Active	1.17	1	0.54	0.22

SULFUR	2.00	2	1.08	0.43
BIOASH	1.09	15	8.11	3.26
ENR	1.02	5	14.29	2.70

In case of the addition of 15 phr of bioash and 5 phr of ENR at the standard formulation, considering a cost of ENR under 5 €/Kg, the price is about the same of standard compound price.

2.4. Rubber processing

2.4.1. Brabender Measuring Mixer

The flow of rubber production starts with the mixing of all raw materials below the vulcanization temperature: 150°C, as conventionally fixed [33].

To achieve it at laboratory scale, the machine used has been an internal mixer Brabender R - Lab Station 7 with Roller Mixer W50, a detail of mixing camera is depicted in the Figure 2.9 below.

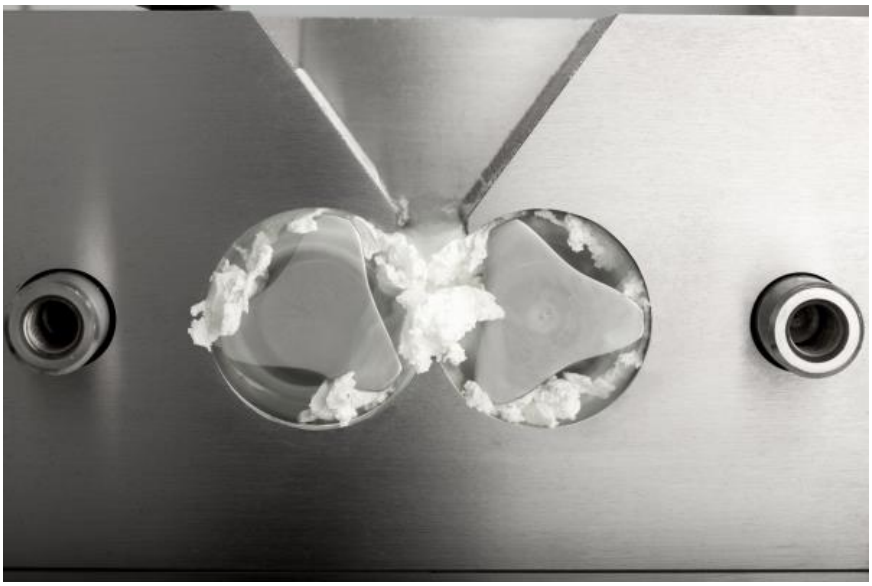

Figure 2.9 Brabender R - Lab Station 7 with Roller Mixer W50, detail of mixing camera.

The Brabender is an internal mixer for non-continuous production of homogeneous mixtures. The raw material is loaded through the top opening into the heated mixer bowl where the compound is homogenized by rollers: specially shaped mixing blades. The machine is connected to a drive unit to measure and to record torque and temperature during mixing process.

The torque mirrors the resistance the material opposes to the rotating rollers during the mixing process giving an idea about the viscosity changing of mixtures, at the other hand, the temperature path as a function of the time gives information about the structural changes of the material.

The starting temperature and the rotation speed of the rollers can be set, while the cooling of the mixer camera is ensured by compressed air system.

The main features of Brabender is summarized in the Table 2.15 below.

Table 2.15 Brabender main features.

Application	*Volume of mixer bowl (cm^3)*	*Max Torque (Nm)*	*Operating Max Temperature (°C)*
Thermoplastics	55	200	500

To guarantee a temperature under the vulcanization point, the rubber mixing is carried out in two stages, the rollers speed is fixed at 80 rounds/min.

In the first step, the different types of rubbers are introduced in the mixer bowl, afterwards the carbon black and eventually the bioash are loaded, the resistance of these materials highly increase the torque value, so the addition of the oil is necessary. Finally, the mixture is completed with the activators and the antioxidant and left to mix for some minutes.

The conditions of the first stage are showed in the Table 2.16, they have been chosen to guarantee a good mixing: about sixteen minutes allow the stabilization of the torque and the temperature, without the problem of possible vulcanization since the sulphur is absent.

An example of the resulted diagram with relationship between torque and temperature, over the time, is illustrated in the Figure 2.10.

Table 2.16 Conditions for compound mixing, Step 1.

Rubber mixing, STEP 1			
Start Temperature (°C)	*Final Temperature Avg. (°C)*	*Final Torque Avg. (Nm)*	*Time duration Avg. (min)*
55	120	25	16

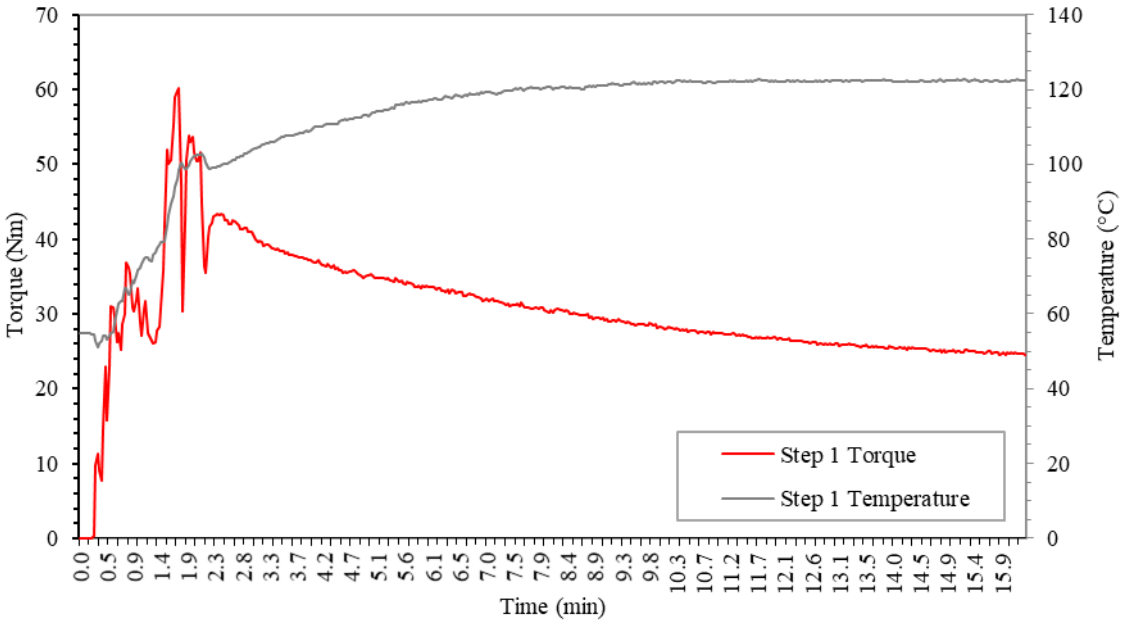

Figure 2.10 Monitoring of mixing in Brabender, Step 1.

The loading of the rubbers and the various fillers occurs in the first 2 or 3 minutes and it results in an increasing of torque at each loading as can be seen in the curves of compound mixing monitoring at the first step.

The sudden decrease of torque at about two minutes is due to the oil loading.

The increasing of torque causes a heat generation due to friction that results in increasing of temperature too.

After the loading of all materials in the Brabender mixer, the compound is left to stabilize, both from torque and temperature point of view.

In the second step, the previous compound is removed from the Brabender camera that is cooled by compressed air system up to start temperature, then the mixture of the step 1 is loaded again in the Brabender mixer and the vulcanization agent and the accelerator are added.

In this case the temperature cannot be set at more than 100°C for several minutes to avoid the premature vulcanization.

The conditions of the second stage are showed in the Table 2.17.

An example of the resulted diagram with the relationship between torque and temperature, over the time, is illustrated in the Figure 2.11.

More the curves of torque and of temperature are stable at the end of the mixing, higher is the quality of the final product.

Table 2.17 Conditions for compound mixing, Step 2.

Rubber mixing, STEP 2			
Start Temperature (°C)	Final Temperature Avg. (°C)	Final Torque Avg. (Nm)	Time duration Avg. (min)
55	100	24	5

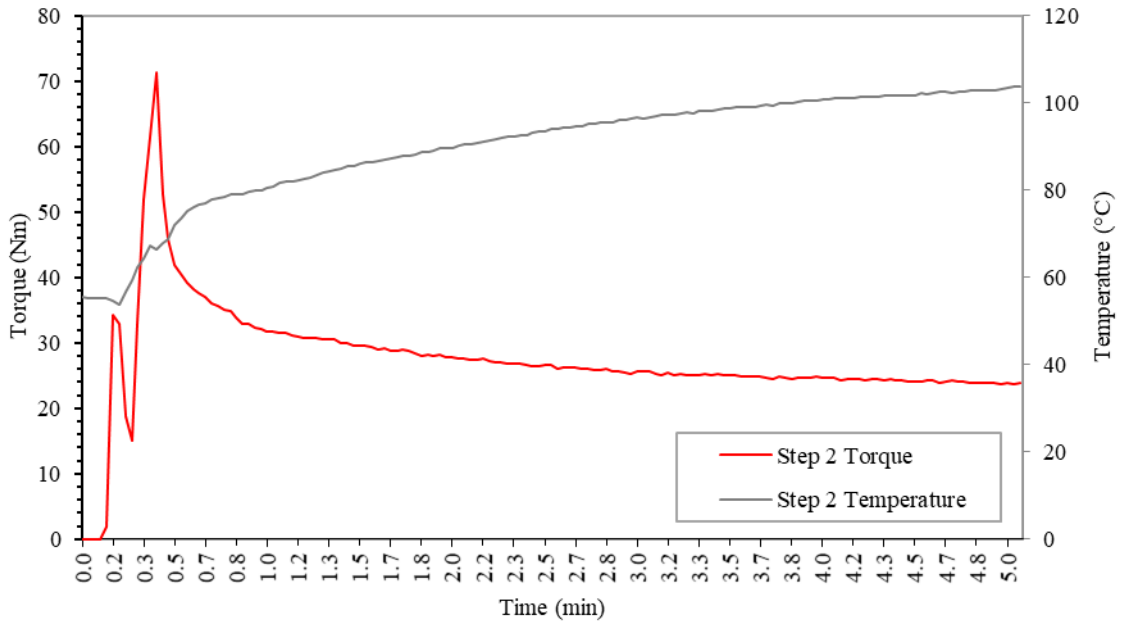

Figure 2.11 Monitoring of mixing in Brabender, Step 2.

2.4.2. Compression Moulding

To cross-link the rubber in a controlled way, a compression moulding apparatus has been used, specifically the JBT Engineering ® hydraulic press (Figure 2.12). This machine consists of two heated plated and a control system that allows to achieve a stable high temperature, monitoring the pressure. Cooling, when needed, is achieved by fluxing cold water.

Figure 2.12 JBT Engineering ® hydraulic press.

After the compounding process the rubber is cut in small pieces, an amount of about 12.5 grams of small pieces are placed in a square mould and heated at 151°C for 30 minutes. The output is a film of cross-linked rubber. The thickness of the sample is not controlled; therefore, it varies among the different samples.

2.5. Rubber characterization techniques

2.5.1. Dynamic Mechanical Analysis (DMA)

Dynamic Mechanical Analysis (DMA) is a technique used to measure the mechanical and viscoelastic properties of a material as a function of temperature, time and frequency while it is subjected to an oscillating stress.

The model DMA/SDTA 861^e by Mettler Toledo has been used (Figure 2.13).

Figure 2.13 Metter Toledo DMA/SDTA 861 ^{e}.

The crude rubber is cut in small circular discs that are clamped symmetrically between two fixed outer parts and a central part moving in shear mode at 1Hz and at a temperature of 151°C. The ratio between applied stress amplitude and strain amplitude response is measured as complex modulus that can be described by the storage modulus G', in phase with applied stress, and the loss modulus G'', out of phase.

The higher value of G' (G' max) measures stiffness in the rubber, while the lower G' value (G' min) indicates the initial viscosity of the rubber compound.

The ratio between the loss and storage modulus value is the loss factor δ. Moreover, the percentage of the difference between the maximum modulus and the modulus after 30 minutes from it, is used as indicator of stability of compound and it is here named Modulus Decadency %.

Modulus as a function of time provides important information on transition phase of vulcanization process: the time corresponding to the difference between the maximum

and the minimum modulus is considered as the vulcanization time. Vulcanization time changes according to the fillers loaded in the compound.

However, the main type of equipment used for producing vulcanization curves is the Rubber Process Analyser (RPA). By RPA, the torque required to shear the compound is monitored and the curve of torque versus time can be generated.

Optimum cure time (t 90) is the time required for the torque to reach 90% of the maximum achievable torque and it relates to the time necessary for the cured rubber to achieve optimal properties. On the other hand, it was studied that there is not a direct correlation between the t 90 and the G" or G' graph but since tan δ curve apparently reflects the development of crosslinking reaction of compound, an equivalent t 90 could be obtained, similarly to that obtained by RPA, from δ 90 according to following equation:

$$\delta\,90 = \delta\max - 0.9\,(\delta\max - \delta\min)$$

where now δ max and δ min are the maximum and the minimum tan δ values. It is assumed that t 90 could now be obtained from tan δ versus time graph at δ 90 [34].

Finally, it must be underlined that DMA machine reaches the set temperature gradually, so the scorch time cannot be calculated since it needs a totally isothermal test.

All the data from DMA are recorded at the temperature of 151°C, so the rubber softening range is out of the measures of this study.

2.5.2. Rubber Process Analyser (RPA)

Rubber process analyser (RPA) is an oscillating shear rheometer dedicated to the complete characterization of rubber at all stages of manufacture.

The RPA provides invaluable viscoelastic data on uncured rubber through the curing process, and in situ cured materials. Torque, viscosity and viscoelastic properties of elastomers over the widest ranges of testing conditions can be provided thanks to an accurate temperature control, absent in the DMA.

To monitor the vulcanization of rubber, a shear stress is applied to a disk of rubber at fixed temperature (Figure 2.14). For its high control of test conditions and its rapidity in performing, RPA is industrially used to measure the optimum cure time: t 90.

The RPA used in this study is located in the spaces of Trelleborg Wheel System S.p.a. and has been provided by TA Instruments.

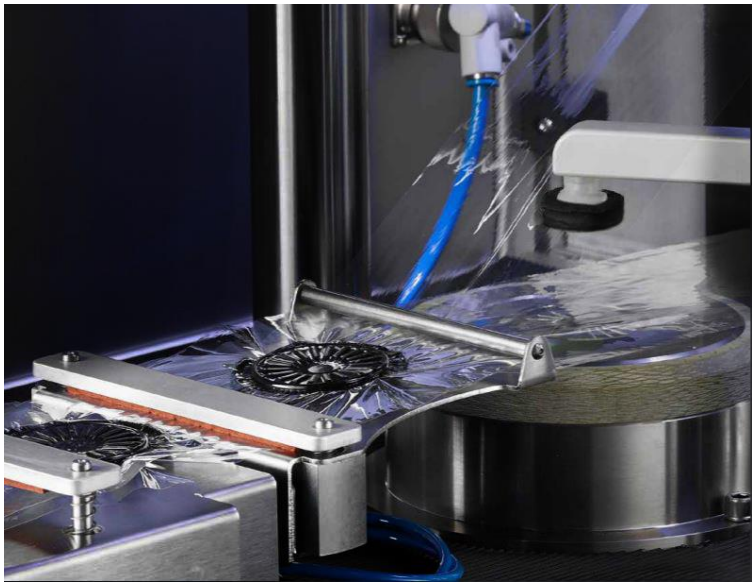

Figure 2.14 Detail of a rubber simple loaded in the RPA instrument.

2.5.3. Tensile Testing

Tensile testing machine is one of the most frequently instrument for mechanical material testing. It is used to characterize strength and deformation of samples under uniaxial tensile load in accordance with the respective standard method.

Standard Test Methods for Vulcanized Rubber is ASTM D412-16 [22].

Tensile test has been performed by Zwick/Roell Static Materials Testing Machine. Schematic illustration of the components of the machine is depicted in the Figure 2.15.

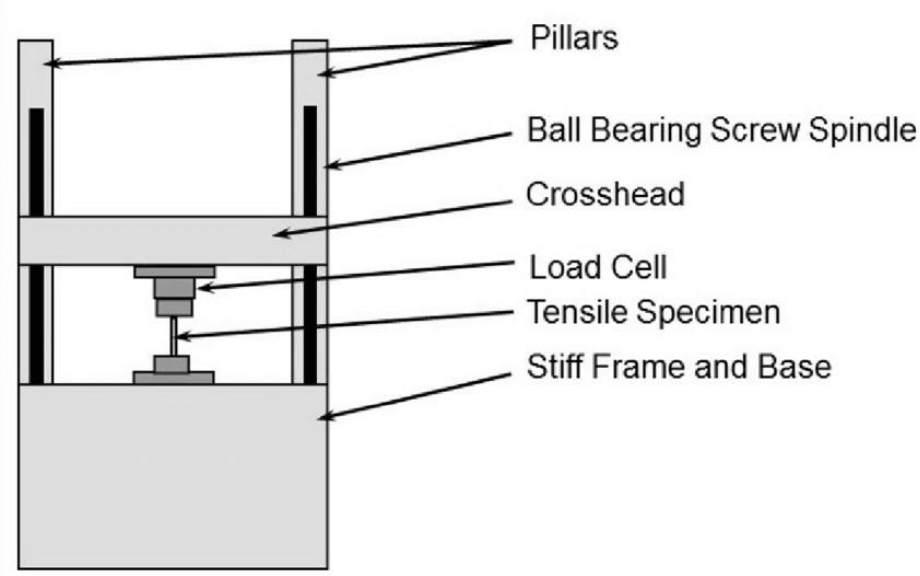

Figure 2.15 Schematic Illustration of the static materials testing machine.

In this study, the machine has been equipped with a load cell of 10 kN and a strain gages set at 20 mm distance. The pressed sheet of cross-linked rubber has been cut in a custom shape illustrated in detail in Figure 2.16, with dimension tolerance of ± 0.5 mm.

Samples have been fixed to the machine with milled metallic clamps and the deformation rate has been set at 100 mm/min.

The test output is the stress-strain curve, value of stress and of strain at the break point and elastic modulus at different percentage of deformation are reported.

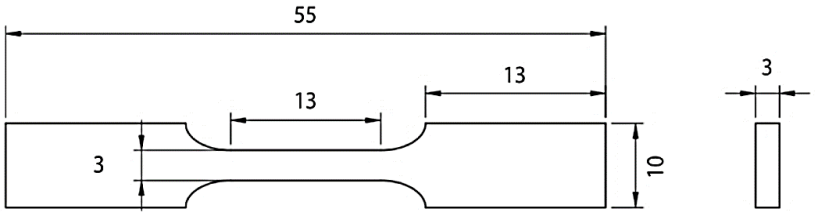

Figure 2.16 Dimension of sample for tensile test.

2.5.4. Dispersion Testing Analysis

Dispersion Testing Analysis has been performed with a Dispergrader™ αview provided by Alpha-Technologies (Figure 2.17): it is a reflected light microscope designed for optical dispersion analysis of fillers like carbon black in mixed rubber compounds.

The system explores, by a camera, the shadows cast by agglomerates present in freshly cut surface of a sample. The Enterprise™ software organizes data into reports that allow the statistically control of manufacturing product to verify the quality of mixing process.

Figure 2.17 Alpha-technologies Dispergrader™ αview.

2.6. Bioash characterization techniques

2.6.1. X-ray Diffraction (XRD)

X-ray diffraction (XRD) has been performed to characterize bioash constituents. The wavelength of the X-rays is of the same order of magnitude as spacings between atoms in a crystal. It means that interaction between X-rays and a crystal produces constructive interference when Bragg's law is satisfied ($n\lambda=2d\sin\theta$). This law relates the wavelength of electromagnetic radiation (λ) to the diffraction angle (θ) and the lattice spacing (d) in a crystalline sample. By scanning the sample, through a range of θ angles, all possible diffraction directions of the lattice should be attained due to the random orientation of the powdered material. Conversion of the diffraction peaks to d-spacings allows identification of the mineral by a database since each mineral has a set of unique d-spacings.

XRD analysis has been performed by D8 Advance instrument, produced by Brukel, with a radiation generated at 40kV and 40 mA, 2θ ranging from 2° to 80° with a step size of 0.02° and a scan time of 1.2 s, at room temperature (Figure 2.18).

Figure 2.18 Brukel D8 Advance XRD Analyzer.

2.6.2. Fourier Transform Infra-Red Spectroscopy (FT-IR)

Infrared spectroscopy is a qualitative analytical technique which reflects oscillations arising from vibration and rotation of molecules. The vibration of molecules that results from change in bond length (stretching) or bond angle (bending) can be used to characterize the structure of the molecule and investigate the interactions with surrounding environment [35].

Fourier transform infrared spectroscopy (FT-IR) has been performed on different samples to evaluate whether the bioash has linked at the functionalizers.

Thermo Nicolet NEXUS 470 FTIR, produced by GMI Inc., has been used (Figure 2.19).

Figure 2.19 GMI Inc. Thermo Nicolet NEXUS 470 FTIR.

The analysed powders have been blended with potassium bromide (KBr) powders, ground together and then pressed with a hydraulic press under 6 tons, for 2 min, into thin disks of a diameter of 13 mm. IR spectra region 4000-400 cm^{-1} has been recorded at room temperature. Each spectrum has an average of 32 scans and a resolution of 4 cm^{-1}.

Spectra analysis has been done using OMNIC Spectra Software by Thermo Scientific.

2.6.3. Kumagawa Extractor

Kumagawa extractor is a piece of laboratory apparatus.

It is composed of three main sections: a percolator which circulates the solvent (the solvent in the distillation flask is brought to boil, by electrical heat source, up to

condenser where the reflux starts); a thimble, usually made of thick filter paper, directly suspended inside the solvent flask, which retains the solid sample to be extracted; and a siphon mechanism, which periodically empties the thimble.

A schematic illustration of apparatus is available in Figure 2.20 below.

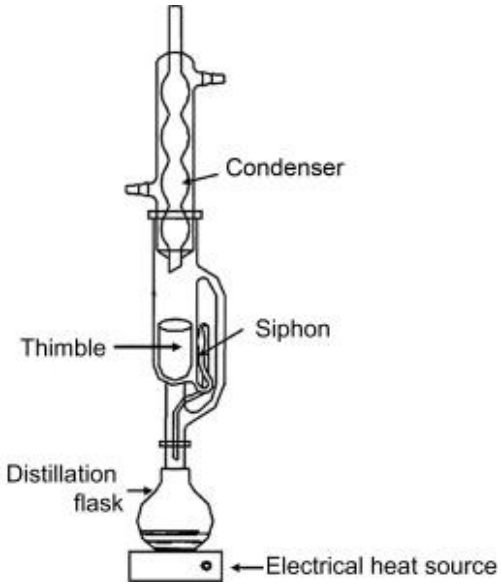

Figure 2.20 Schematic illustration of Kumagawa extractor.

It is designed for extraction of desired elements by a solvent that has a limited solubility with it and that is insoluble with regard to impurities.

In current work, Kumagawa has been used to understand how many grams of functionalizer are lost from the modified bioash by a solvent with high solubility grade relative to functionalizer. The time of extraction has been fixed at 4 hours for a total of 50 cycles, then the sample has been left dry overnight. The sample has been weighted before and after the extraction, from the difference in weight and the information on the quantities of functionalizer used, the efficiency of functionalization has been quantified, with the hypothesis (to validate, § Future developments) that all the weight lost refers to functionalizer. The proper solvent for each functionalizer has been found in the literature.

The solubility of stearic acid in ethanol, methanol, ethyl acetate, and acetone has been measured gravimetrically at various temperatures ranging from 301 to 313 K, at atmospheric condition. The solubility of stearic acid in Ethyl-Acetate was found to be the highest, followed by ethanol, acetone and methanol [36].

On the other hand, the technical data sheets report the acetone like an optimum solvent for oleic acid and TESPT.

2.6.4. Thermogravimetric Analysis (TGA)

Thermogravimetric analysis (TGA) has been performed on the modified bioash samples to characterize different decomposition steps. TGA is a technique that provides a very precise measurement of weight variation as a function of temperature or time. It can be performed in air or inert gas (N_2) atmospheres. Linear and ballistic heating rates is possible thanks to infrared furnace (Figure 2.21) and unique temperature control and measurement thanks to thermocouple assembly.

In this work, the experiments have been carried out by a TGA Q 500, produced by TA Instruments. All test have been performed in air atmosphere, from a temperature of 25°C to 800°C with a heating rate of 20°C/min.

Figure 2.21 Furnace detail of TA Instruments TGA Q 500.

2.6.5. Particle Size Analysis

The Mastersizer 3000 Hydro EV is a particle size analysis instrument by Malvern.

The Mastersizer 3000 uses the technique of laser diffraction to measure particle size distributions: the particulate sample is dispersed in water where a laser beam passes through it and angular variation in intensity of scattered light is measured. Large particles scatter light at small angles relative to laser beam and small particles scatter light at large angles. Sensitivity to sub 100 nm particles, or scattering light at wide angles, is achieved using advanced optics and a powerful of 10 mW from a solid state blue light source.

A schematic illustration of machine and its operation is showed in Figure 2.22.

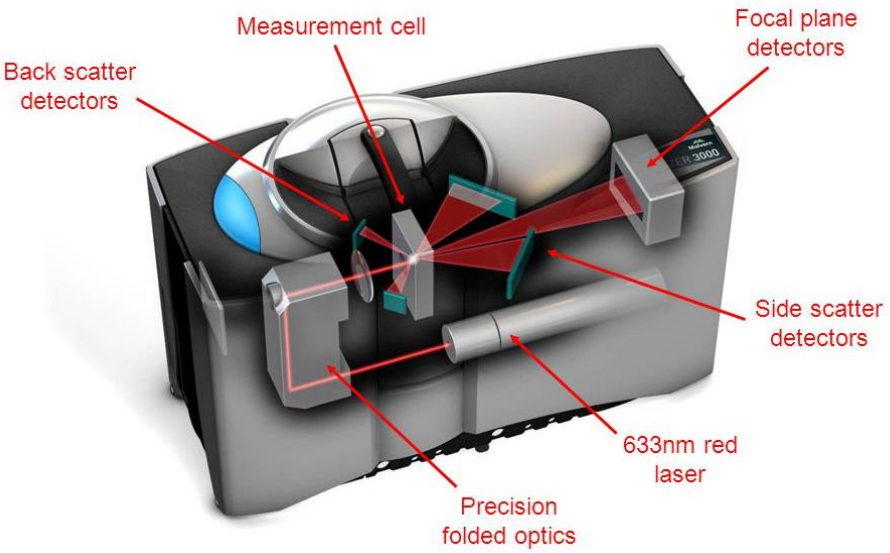

Figure 2.22 Illustration of Mastersizer 3000 Hydro EV Particle Sizing Analyzer operation

The angular scattering intensity data is then analysed to calculate size of the particles that created the scattering pattern, using the Mie theory of light scattering. Since the heterogeneity of simples, Fraunhofer approximation is used assuming opaque and not spherical particle. To ensure that values remained constant over time and to exclude phenomena of aggregation between the particles and phenomena of deposition of the sample, several consecutive replicas have run.

The particle size is reported as a volume equivalent sphere diameter.

To characterize the resulting curve of percentage of volume density compared to size class of particles, mode, mean and D[3/2] are used.

The mode is the size with higher frequency and the mean is average of data set. The Sauter Mean Diameter D[3/2], or surface area mean, is equivalent diameter of surface/volume defined by the equation:

$$D\left[\frac{3}{2}\right] = \frac{1}{\sum_i \frac{x_i}{d_i}}$$

Where x_i is mass fraction of particles with diameter d_i.

In other words, the Sauter Mean Diameter of a distribution of N particles is the diameter of a set of N spherical particles, all the same, that have the same external superficial/volume ratio of the real set of which the mean diameter must be calculated.

2.6.6. Scanning Electron Microscope (SEM)

A scanning electron microscope (SEM) is a type of microscope to detect sample topography and composition by scanning surface of specimen with a focused beam of electrons. The interaction between the electron beam and the surface of the sample generates secondary electrons, backscattered electrons, diffracted backscattered electrons, photons, visible light and heat. The software processes mainly secondary electrons and backscattered electrons and constructs SEM images while intensity of signals gives information about possible constituents of the sample.

The scanning electron microscope, that has been used in this work, was an EVO 50 Extended Pressure, produced by ZEISS (Figure 2.23). It works in a continuous vacuum up to $3 \cdot 10^3$ Pa and allows differentiation of the vacuum degree between filament chamber and the sample holder chamber thanks to a valve system. The electron source is a LaB_6 nanocrystal. Electrons are accelerated by a potential difference of 20kV.

Figure 2.23 ZEISS EVO 50 Scanning Electron Microscope.

2.6.7. Tap Density Testing

The tap density tester TAP-2S by Joint Analytical Systems has been designed for satisfied pharmaceutic standard of United States Pharmacopeial Convention, Incorporated (USP). It consists of two glass cylinders and holders (Figure 2.24).

Figure 2.24 Joint Analytical Systems TAP-2S Tap Density Tester.

The user loads the powders into a cylinder and places it on the platform. The test time or number of taps is entered using the instrument's keypad, in this case 2'000 taps have been run and two 50 ml glass cylinders have been used. During motion, the cylinder simultaneously taps and rotates, ensuring that the material being tested is packed evenly throughout the cylinder and levelled with the cylinder surface for direct reading.

In this way, Tapped Density has been calculated. It is the ratio of mass of the powder and volume occupied by the powder after it has been tapped for a defined period: the tapped density of a powder represents its random dense packing. Tapped density values are higher for more regularly shaped particles than irregularly particles.

It is contraposed to Poured Bulk Density that refers to volume measured after pouring powder into a cylinder, creating a relatively loose structure: it is the ratio of mass and volume, including interparticle voids volume.

2.6.8. Optical Contact Angle (OCA)

The Optical Contact Angle has been exploited to measure wettability and hydrophilicity of the bioash and of the modified bioash. As a matter of fact, a liquid in contact with a solid form a droplet with a precise angle ϑ, as defined in the Young's Law equation:

$$\gamma_s = \gamma_{sl} + \gamma_l(cos\vartheta)$$

where γ_s is the surface free energy, γ_l is the liquid surface energy and γ_{sl} is the interfacial tension.

In current work, the optical contact angle has been analysed using an OCA 20 produced by Dataphysics Co., equipped with a CCD photo-camera and with a 500 mL Hamilton syringe to dispense water droplet (Figure 2.25).

Figure 2.25 Dataphysics Co. OCA 20.

At room temperature, the drop of chosen liquid is left to drip on bioash compacted by hydraulic press, after 5 seconds of the droplet deposition on the samples, the camera captures the image and the software calculates the contact angle ϑ. It gives information about the hydrophilicity or hydrophobicity of the sample and so about its wettability.

2.7. Ash modification techniques

2.7.1. Ball Milling

The Ball Mill is a type of grinder consisting of a mechanical system that allows rotation of hollow ceramic shell around its axis. It is used to grind, blend and mix the materials. It works on the principle of impact and attrition: the mixing is performed by the rotation movement and the size reduction by grinding media such as zirconia balls.

Zirconia balls have smooth and gloss surface like pearl and guarantee the impact with powder particles and walls of shell. The dry or wet mixing method can be run. The machine is provided by MGS mills Italia (Figure 2.26).

Figure 2.26 MGS mills Italia Ball Mill

In current study the raw bioash (RAW) has an electrostatic charge that does not allow the maximum efficiently since the bioash particles are attracted by plastic walls of container and so have less freedom of movement. This phenomenon reduces probability of interactions that permit the decrease of particle size.

Therefore, the Wet Ball Mill is exploited: to the zirconia balls and to the components of the mix, a medium is added, for example water. The water, which is a very good conductor, can improve the capability of powered dispersion.

As a result, the quantities, used in this work to obtain an optimum output in size reduction and mixing, according with article [37] are the following:

- 30 g of bioash
- 300 g of zirconia balls
- 120 g of distilled water

The ball mill is left to operate for at least thirty hours. After that, the mixture is left to dry in an oven at 50°C for a day to eliminate superfluous water.

This method is used to obtain smaller powder particles sizes, the resulting modified bioash is called RAW BMW:

- **RAW BMW →** Raw Bioash treated by Ball Milling Wet

The rubber compounds, created with the addition of RAW BMW, are the following:

- **STD5-RAW BMW →** Compound with 5 phr of the bioash treated by wet ball milling
- **STD15-RAW BMW →** Compound with 15 phr of the bioash treated by wet ball milling

2.7.2. Functionalization of bioash with stearic acid

The bioash functionalization with solid grains of stearic acid, thanks to their long carbon chain, makes bioash surface hydrophobic so the resulting mixture has a neutral electrostatic charge.

The dry ball milling method is exploited: the zirconia balls and the bioash are introduced in a suitable case, without adding liquid substance as medium, and the ball milling is left to start for at least thirty hours.

The zirconia balls must be enough to ensure the Ball Milling effect: the quantity of bioash grains to add in a plastic bottle is about 15% by weight of zirconia balls, in accordance with literature [38].

The quantities applied are listed following:

- 15 g of bioash
- 100g of zirconia ball

A small quantity of stearic acid (AS) is added in the previous rubber compound formulation to modify the bioash nature.

Different percentages of functionalizer are exploited to find the right quantity that can give the desired properties to the final rubber compound.

The quantities of stearic acid added at 15 g of raw bioash, are summarized in the Table 2.18 below:

Table 2.18 Stearic acid added at 15 g of raw bioash in Dry Ball Mill.

AS1	*AS3*	*AS5*	*AS10*
1% w/w of bioash	3% w/w of bioash	5% w/w of bioash	10% w/w of bioash
0.15 g	0.45 g	0.75 g	1.50 g

The structure of stearic acid molecule is constituted by a hydrophilic head and a hydrophobic tail. And so, the stearic acid is adsorbed on the bioash surface vertically due to low surface area occupied by its molecules.

In vertical orientation, the molecules occupy small area on the surface, hence the density of stearic acid molecules would be high. Vertical orientation leads to more hydrophobic surface compared to horizontal orientation for which the density of molecules is low and the surface results less hydrophobic [39].

For the practical application, if the amount of fatty acid is low, the desired effect is not achieved, while use of excessive amount of organic phase leads to processing problems, inferior mechanical properties and increased price.

Possible structure of adsorbed layer presented in Figure 2.27 shows the chemisorption of stearate due to the steric effect and oblique conformation of hydrocarbon chains. Acid molecules can be adsorbed both physically and chemically by hydrogen bonds, or as dimers due to the interaction of hydrocarbon chains. This generally indicates the inhomogeneity of modified bioash.

Molten stearic acid is presumed dissociated on bioash surface mainly composed by calcite. The stearic acid H+ ion moves to the surface carbonate ion (−) of the bioash and stearic ion is chemisorbed on the primary surface centre of Ca+ ion.

Due to the steric effect, a part of surface bioash centres can be blocked, it affects the amount of the chemisorbed organic component [40].

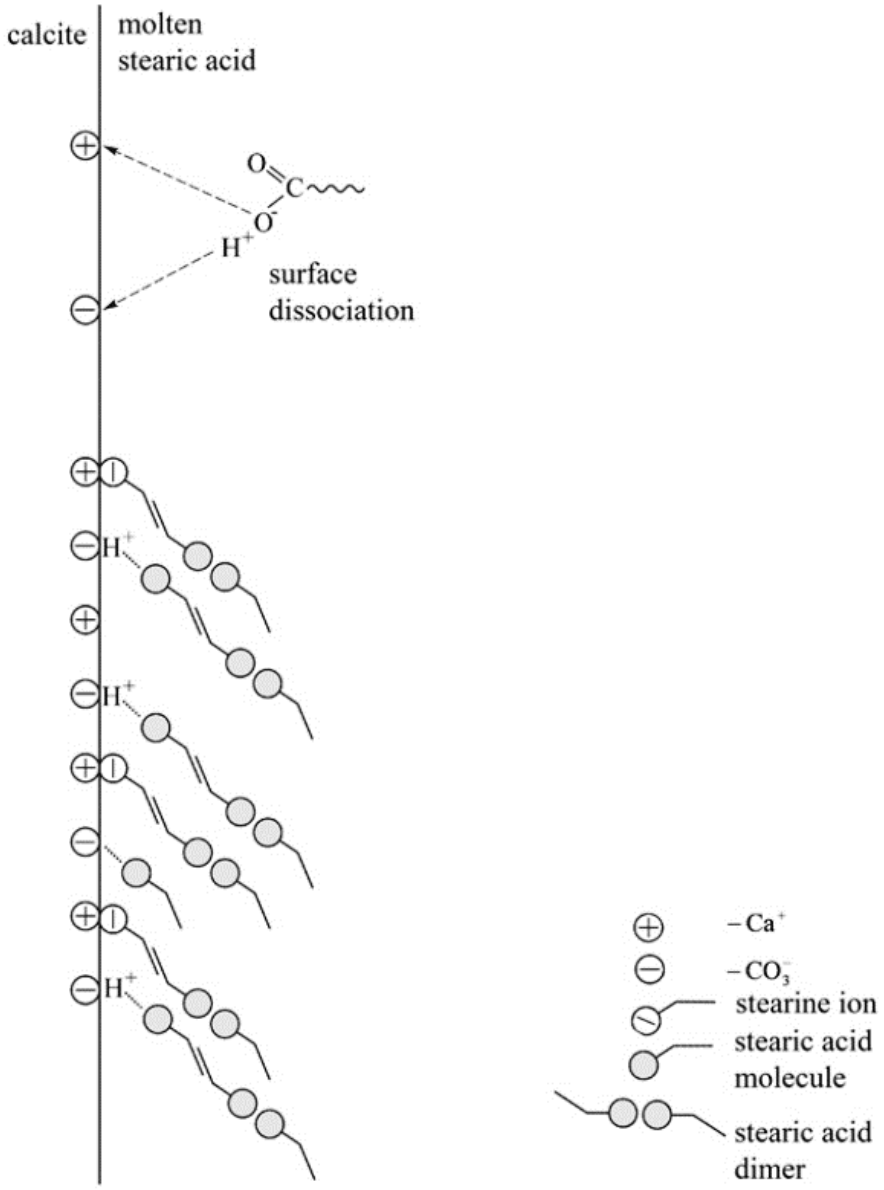

Figure 2.27 Schematic illustration of stearic adsorption on calcite surface.

The resulting modified bioash are named as follows:

- **RAW AS1 →** Raw bioash with 1% w/w stearic acid
- **RAW AS3 →** Raw bioash with 3% w/w stearic acid
- **RAW AS5 →** Raw bioash with 5% w/w stearic acid
- **RAW AS10 →** Raw bioash with 10% w/w stearic acid

The rubber compounds, created with the addition of RAW AS, are the following:

- **STD5-RAW AS1 →** Compound with 5 phr of bioash functionalised by 1% w/w stearic acid
- **STD5-RAW AS3 →** Compound with 5 phr of bioash functionalised by 3% w/w stearic acid
- **STD5-RAW AS5 →** Compound with 5 phr of bioash functionalised by 5% w/w stearic acid
- **STD5-RAW AS10 →** Compound with 5 phr of bioash functionalised by 10% w/w stearic acid
- **STD15-RAW AS1 →** Compound with 15 phr of bioash functionalised by 1% w/w stearic acid
- **STD15-RAW AS3 →** Compound with 15 phr of bioash functionalised by 3% w/w stearic acid
- **STD15-RAW AS5 →** Compound with 15 phr of bioash functionalised by 5% w/w stearic acid
- **STD15-RAW AS10 →** Compound with 15 phr of bioash functionalised by 10% w/w stearic acid

2.7.3. Functionalization of bioash with oleic acid

Since the oleic acid is liquid at ambient temperature the mixing by ball mill is not efficiency for the bioash modification.

A reaction in solvent is done to permit a good interaction between oleic acid and the bioash: in a flask, 5 g of bioash with opportune quantity of oleic acid is mixed by magnetic agitator in a solution of toluene for 24 hours at room temperature.

Since chemical nature of the oleic acid (AO) is similar to stearic acid, similar results in rubber compound are expected.

And so, only AO at 5% and 10% by weight of bioash are studied, the quantities are reported in the Table 2.19 below.

Table 2.19 Oleic acid added at 5 g of raw bioash in solution with toluene.

AO5	AO10
5% w/w wrt bioash	10% w/w wrt bioash
0.25 g	0.50 g

The oleic acid molecules are more bulky than stearic acid molecules, a schematic representation of oleic acid adsorbed on bioash surface is presented in Figure 2.28 below.

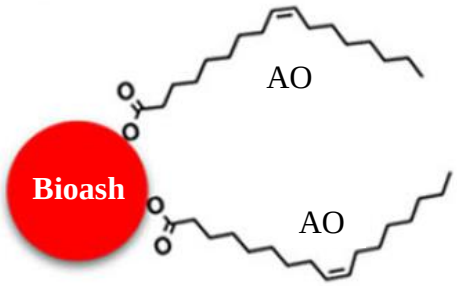

Figure 2.28 Schematic illustration of oleic acid adsorption on bioash surface.

The resulting modified bioash are named as following:

- **RAW AO5 →** Raw bioash with 5% w/w oleic acid
- **RAW AO10 →** Raw bioash with 10% w/w oleic acid

The rubber compounds, created with the addition of RAW AO, are the following:

- **STD5-RAW AO5 →** Compound with 5 phr of bioash functionalised by 5% w/w oleic acid
- **STD5-RAW AO10 →** Compound with 5 phr of bioash functionalised by 10% w/w oleic acid
- **STD15-RAW AO5 →** Compound with 15 phr of bioash functionalised by 5% w/w oleic acid
- **STD15-RAW AO10 →** Compound with 15 phr of bioash functionalised by 10% w/w oleic acid

2.7.4. Functionalization of bioash with TESPT

The problem in the presence of highly hydrophilic bioash as filler in rubber compounding is that interaction between filler and itself is higher than filler-polymer interaction. For enhanced dispersion, coupling agents such as bis-3-triethoxysilylpropyl-tetrasulfane (TESPT) can be used: it modifies the surface of bioash particles to increase the filler-rubber interaction.

However, it is to be underline that this coupling agent is usually used in presence of silica, and the presence of silica, in the bioash of this study, is quite low.

A schematic representation of the coupling reaction between bioash hydroxyl groups and the Si site of TESPT in the presence of catalytic amount of a mineral acid in a solution of toluene is depicted in the Figure 2.29 below.

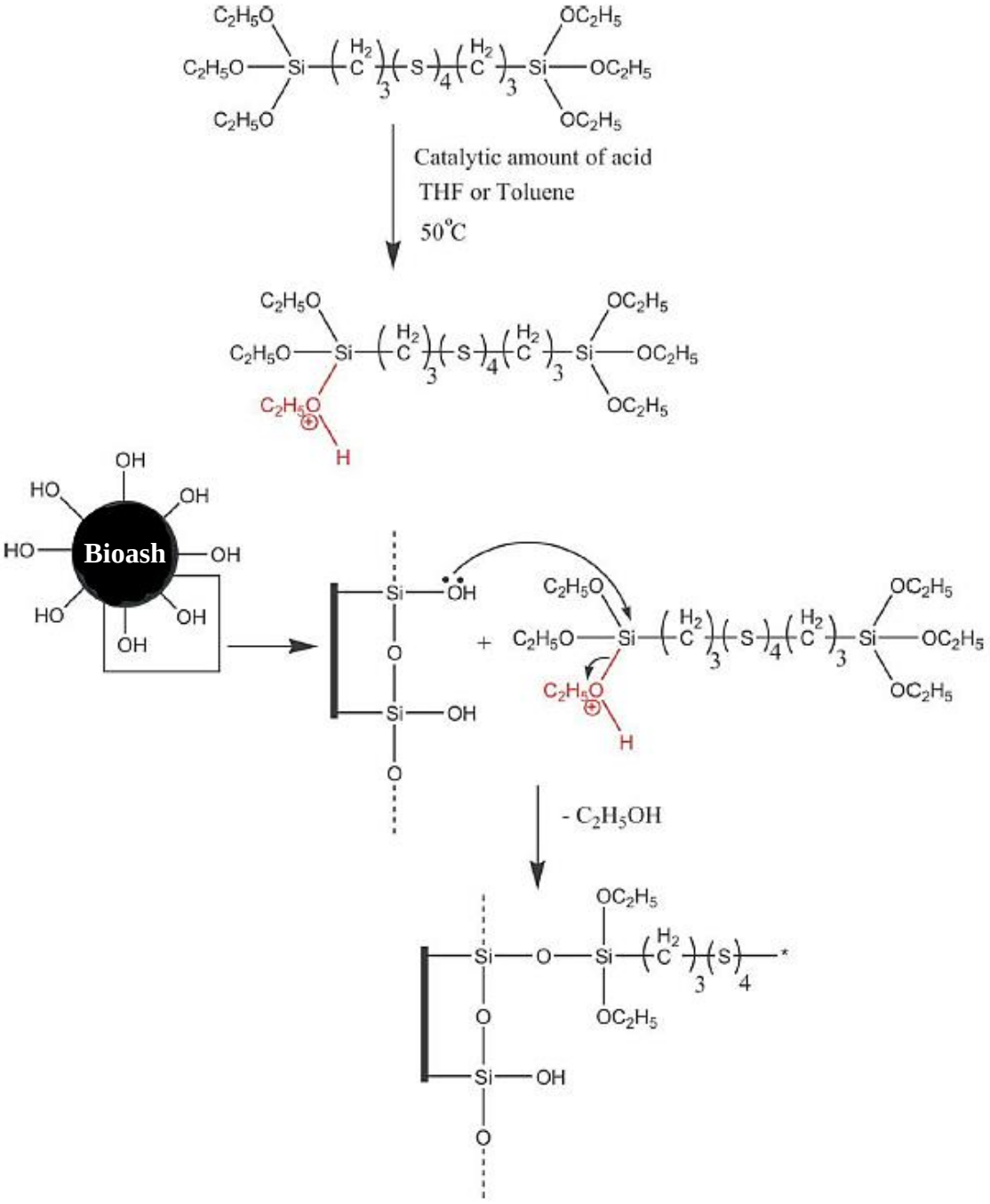

Figure 2.29 A schematic representation of the coupling reaction between bioash hydroxyl groups and TESPT.

First of all, toluene is dried by molecular sieves to minimize secondary reactions due to water presence. The molecular sieves are purified by heating at 300°C for four hours in vacuum atmosphere, then toluene can be inserted in a flask with an inert nitrogen atmosphere where the molecular sieves occupying half of the flask total volume.

Toluene is left to dry for at least 48 hours.

Next, in another flask with inert atmosphere, TESPT, corresponding to 7% of bioash weight is stirred in dehydrated toluene by a magnetic stirrer to complete TESPT dissolution. A catalytic amount of a mineral acid, such as sulphur or chloride acid, is added, and the stirring continue for another 10 min at 50°C. A predetermined amount of bioash particles are added to this solution. The resulting mixture, TESPT and bioash in toluene, is stirred for 1 h at 50°C. The mixture is then filtered by vacuum, with usage of filer paper and ceramic funnel, and washed with distilled water following by ethanol to remove the unreacted TESPT.

Finally, the modified bioash is dried in an oven for 24 h at 100°C [41].

The resulted modified bioash is called RAW TESPT:

- **RAW TESPT** → Raw bioash with 7% w/w TESPT

The rubber compounds, created with the addition of RAW TESPT, are the following:

- **STD5-RAW TESPT** → Compound with 5 phr of bioash functionalised by 7% w/w TESPT
- **STD15-RAW TESPT** → Compound with 15 phr of bioash functionalised by 7% w/w TESPT

2.7.5. Compounding with gMAH and with ENR

The polymer is highly customizable thanks to compounding process.

The compounding consists of loading in the mixer of five main class of ingredients: elastomer, filler, protectant, processing aid and curing agent phase.

Elastomer must be selected knowing the overall intended application and the desired physical properties.

Fillers type, for example the carbon black, and their quantities are crucial for the desired properties of final compound.

Protectants like antioxidants and antiozonants determinate the creation of a physical barrier from external environment.

Processing aid, normally an oil, help the compound mixing and processing.

Curing agent is responsible of cross-linking of the rubber, that is why small differences in the amount or ratio of curing agents can drastically change the properties of final rubber compound.

Therefore, it is possible, during compound processing, to add directly one or more materials, such as the bioash and the compatibilizer, to observe changes in the properties of final rubber.

In particular, polyisoprene-graft-maleic anhydride (gMAH) and epoxidized natural rubber (ENR) help to transform the apolar natural rubber in a polar material to allow interaction with polar bioash.

It is important to underline that there is no rubber compound formula that will give all the 'ideal' properties at the same time. Usually, one property will have to be compromised in order to another is made prominent [42].

Simply loading compatibilizer agent during mixing process, different compounds are set, the formulations are available in the chapters § 2.3.3 and § 2.3.4.

3. Results and discussion

3.1. Preliminary studies

First of all, test on the standard rubber compound are performed to have a reference against the compound modified by the bioash.

Secondly, the chemical and physical characterization of the bioash is needed to understand how to convert it from a waste of process to a filler for rubber compound.

The only information in our possession, originally, is related to the provider of the wood and the process of combustion, to give the steam power necessary to the Banbury for rubber mixing, that generate the bioash (§ 1.2).

Finally, effects of raw bioash loading on the properties of final rubber compound are investigated with the aim of developing a process implementation that guarantees a good compound performances.

3.1.1. Features of standard rubber compound

The formula of standard compound without bioash (STD0) is provided by TWS, available at the chapter § 2.3.1.

The materials have been mixed by Brabender mixer (§ 2.4.1).

First test, performed on the crude (not yet cross-linked) compound, is the DMA analysis (§ 2.5.1).

The curve of imaginary part of elastic modulus against time at 151°C is showed in the Figure 3.1. It must be remembered that the DMA machine employs a certain time to reach 151°C, in other words, the test is not completely isothermal, so the test does not include the scorch time (time in which the softening of the rubber happens, the modulus decreases and it is possibility to shape the compound before the irreversible cross-linking).

The main features to describe the DMA curve are the maximum and the minimum value of imaginary shear modulus (G' max & G' min), the vulcanization time to reach complete cross-linked compound (t vulc.) and the percentage of the modulus decadency after 30 minutes from the achievement of its maximum value (ΔG' dec.) [43].

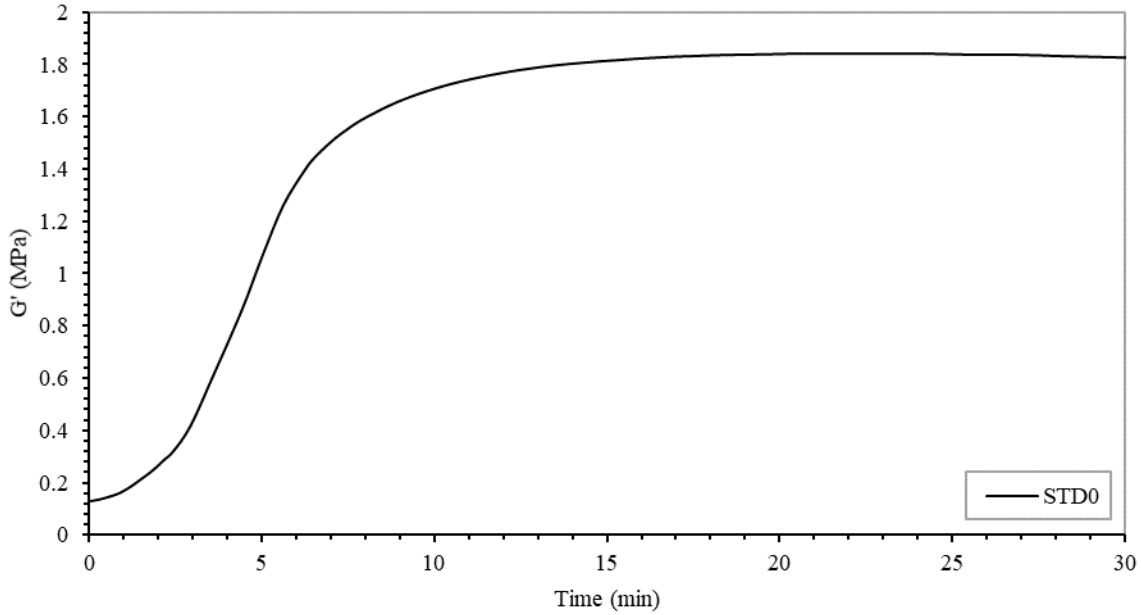

Figure 3.1 DMA curve of STD0, Modulus.

The main data to describe DMA curve are available in the Table 3.1 below.

Moreover, optimum cure time (t 90), time necessary for the compound to achieve optimal properties, is obtained from the curve of tan δ against time (Figure 3.2).

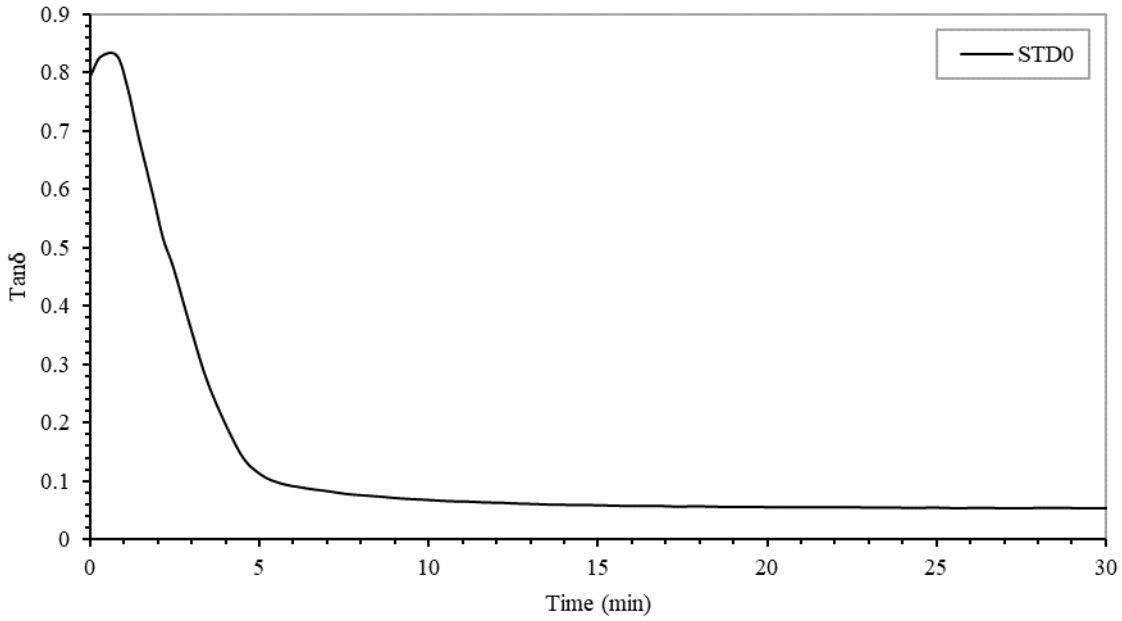

Figure 3.2 DMA curve of STD0, tan δ.

Table 3.1 DMA curve data of STD0.

DMA data	*u.m.*	***STD0***
G' max	MPa	1.84
G' min	MPa	0.13
ΔG' dec.	%	6
t vulc.	min	22
t 90	min	4.8

The vulcanization time is 22 minutes. Since the modulus decadency is low (about 6%) there is not a substantial degradation of rubber, the vulcanized compound can be considered stable. And so, the condition of 30 minutes at 151°C into the press mould to cross-link the rubber, is approved (§ 1.3.3).

The tensile test is performed to investigate the tensile resistance of the reference cross-linked compound (§ 2.5.2), the graph is depicted in the Figure 3.3.

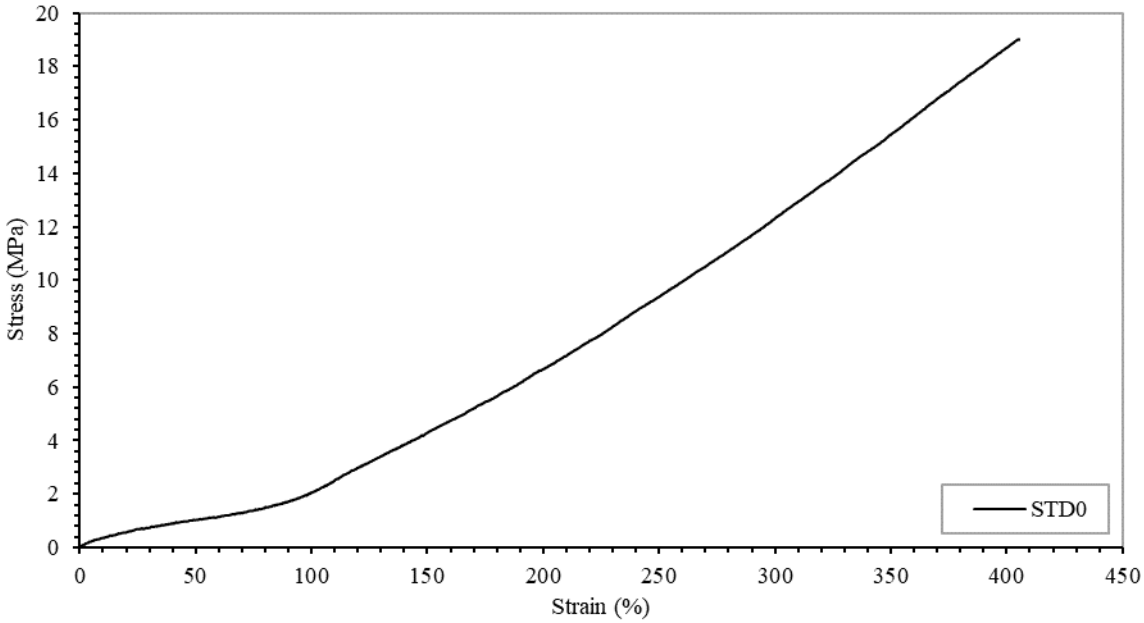

Figure 3.3 Stress-strain curve of STD0.

In the graph is visible a very small section that is related to elastic deformation and the yield point at about 97% of the strain; after that, the slope of the curve drastically changes since strain-induced crystallization of rubber.

To detect clearly the above points is not straightforward, so stresses at different percentages of deformation (M 50%, M 100%, M 200%, M 300%) and values of stress and strain at the break point (σ_b and ε_b) are used as comparison among various compounds, these are summarized in Table 3.2 below.

At the 100% of deformation the modulus is around 2.74 MPa, after this value the curve slope has a sudden increase in strain-hardening region, in fact at 300% of deformation the corresponding modulus is 13.23 MPa: almost five times the previous value.

Table 3.2 Stress-strain curve data of STD0.

Tensile data	*u.m.*	***STD0***
σ_b	MPa	17.80 ±1.94
ε_b	%	378 ±27
M 50%	MPa	1.47 ±0.09
M 100%	MPa	2.74 ±0.34
M 200%	MPa	7.26 ± 0.62
M 300%	MPa	13.23 ±0.85

A clean cut of the cross-linked compound allows the dispersion grade analysis (§ 2.5.4). The image of the surface, elaborated by the software, is shown in the Figure 3.4.

The white spots are the solid filler particles, in this case the carbon black and the bioash grains, dispersed in the rubber matrix: the dark background.

The picture proves the good dispersed since the uniformity of the white spots that are not organized in big aggregates.

A quantitative analysis can be done looking at the Figure 3.5 where the count of particles agglomerates for each certain dimension are graphed. Most of the white spots have a low dimension: the cumulative curve (in orange colour) suggests that more than the half of the aggregates have size under 10 μm.

The grade of dispersion is 93% and the main agglomerate size is 9.7 μm.

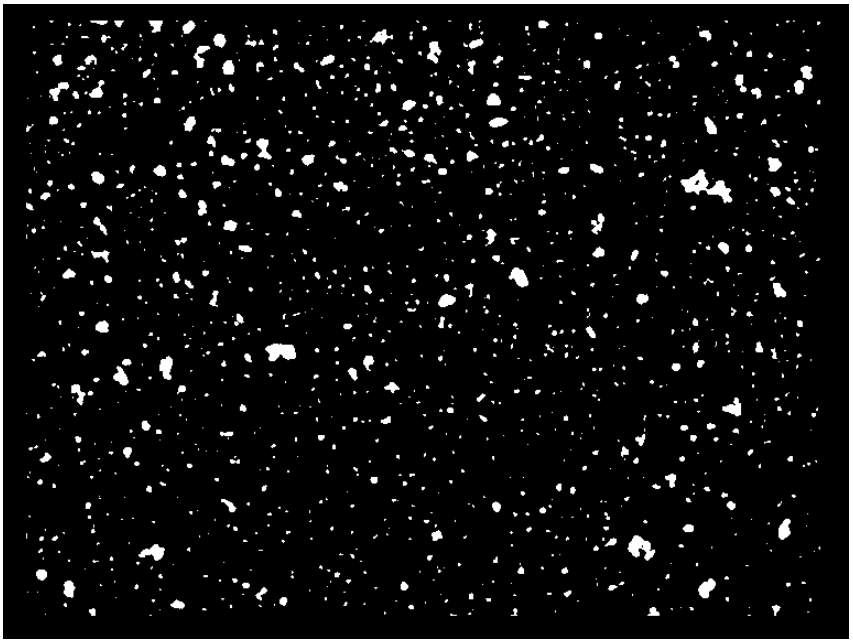

Figure 3.4 Dispersion grade image of STD0.

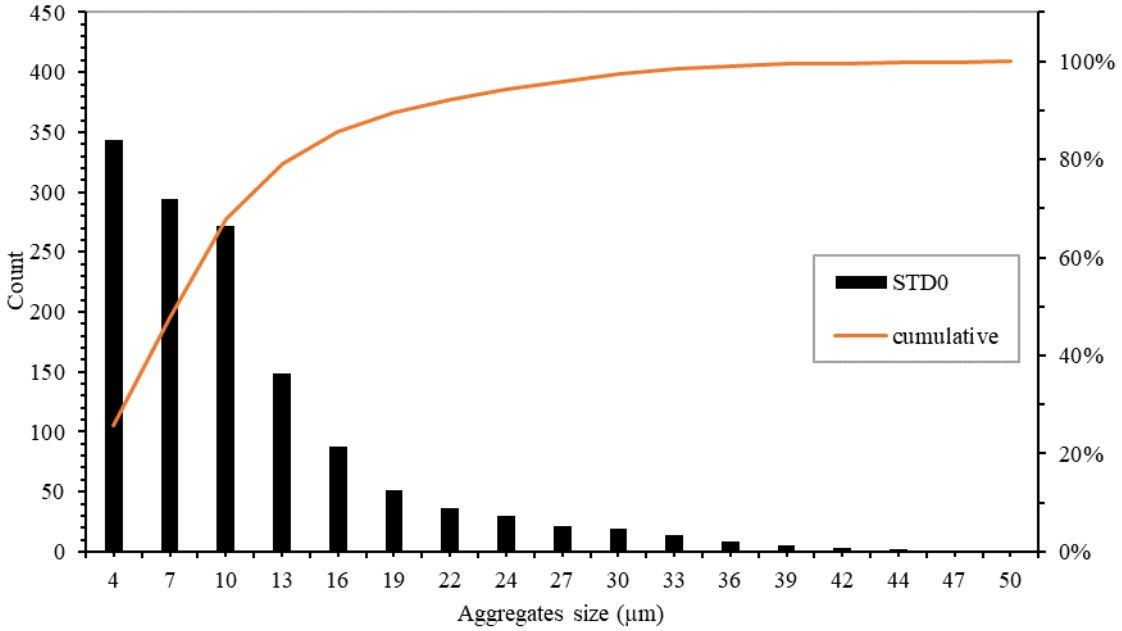

Figure 3.5 Dispersion grade analysis of STD0.

3.1.2. Features of the raw bioash

To understand nature of the waste coming from the steam production, a first chemical analysis has been done on the produced bioash from the trial implant.

The LabAnalysis s.r.l. was tasked with examination of it, provided general information are showed in the Table 3.3.

Table 3.3 General information about raw bioash from trial plant by LabAnalysis s.r.l.

Test	*Standard*	*u.m.*	*Result*
pH	CNR IRSA 1 Q 64 Vol 3 1985		11.80 ±0.17
Apparent Density	UNI EN 13040:2002	g/L	1090
Residue at 105°C	UNI EN 14346:2007 Method A	%	100
Residue at 600°C	CNR IRSA 2 Q 64 Vol 2 1984	%	75.7 ±3.8
Total Organic Carbon	UNI EN 13137:2002 Method A	%	7.2 ±1.5

Moreover, types of elements present in the bioash from the trial plant are investigated, the analysis is based on standard: UNI EN 15309:2007 [44].

Apart from total organic carbon previous analysed, elements found in the bioash with a percentage higher than 10^{-3} are summarized in the following Table 3.4:

Table 3.4 Elements presence, apart from organic carbon, in bioash from trial plant by LabAnalysis s.r.l.

Element	*u.m.*	*Result*	*Tolerance*
Calcium	%	22.0	±2.00
Potassium	%	6.71	±1.50
Silicon	%	6.10	±1.50
Aluminium	%	2.49	±0.60
Magnesium	%	2.21	±0.71
Iron	%	1.05	±0.27
Sodium	%	0.46	±0.13
Sulphur	%	0.45	±0.14
Chlorine	%	0.42	±0.12
Bromine	%	0.002	
Manganese	%	0.082	±0.010
Barium	%	0.044	±0.008
Zinc	%	0.005	

Copper	%	0.003	
Chrome	%	0.001	
Lead	%	0.001	
Nickel	%	0.001	

To deeply understand the chemical composition of the bioash, X-Ray Diffraction (XRD) analysis is needed. It allows to individuate the type of molecules starting from peaks of XRD signal (§ 2.6.1). Heights of peaks gives approximate information on the quantities of such molecule presence.

The resulted graph of XRD signal on the bioash come from the current plant is showed in the Figure 3.6 below, coloured lines are indications from the database on type of molecule corresponding to that peak, as can be read in legend below the graph.

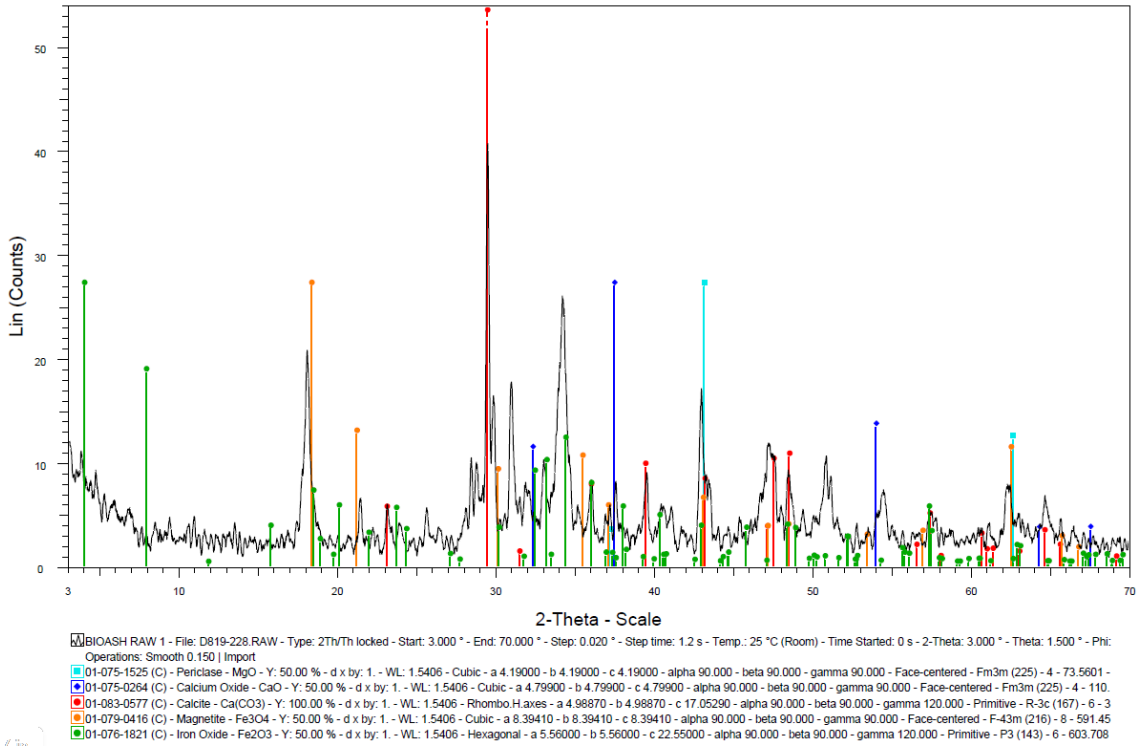

Figure 3.6 XRD analysis on the bioash of current plant.

To investigate the possible differences in the composition between the bioash from the current plant and the bioash from the trial plant, their graphs are compared in the Figure 3.7 and a table with rough data on the percentage presence of the various molecules is built (Table 3.5).

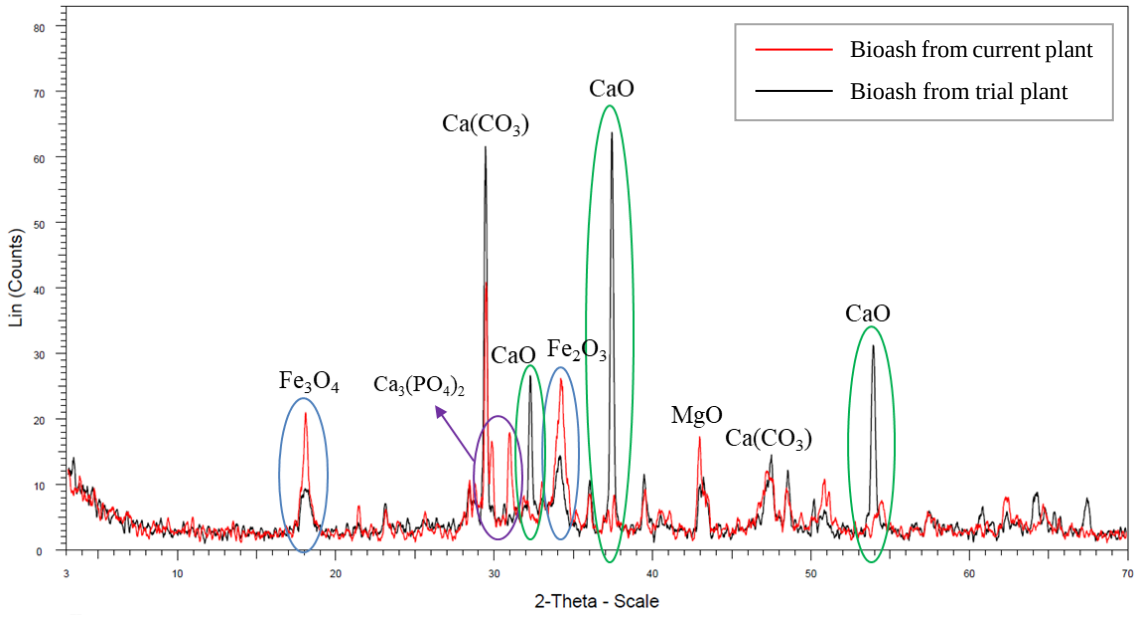

Figure 3.7 XRD analysis, comparison between bioash from current plant and bioash from trial plant.

Table 3.5 XRD analysis, approximate percentages of molecules presence in bioash

Molecule	*Amount in bioash from current plant (%)*	*Amount in bioash from trial plant (%)*
$CaCO_3$	29	33
CaO	6	30
$Ca_3(PO_4)_2$	18	0
Fe_3O_4	20	4
Fe_2O_3	15	16
MgO	9	7

In both types of the bioash the higher presence is represented by Calcite ($Ca(CO_3)$). The main difference to underline is the appearance of a new peak, in the bioash from the current plant, reported to calcium phosphate ($Ca_3(PO_4)_2$), ringed violet in the Figure 3.7, that justifies the lower availability of Calcium Oxide (CaO), ringed green, compared to the bioash come from trial plant.

Moreover, in the bioash of the current plant, Iron is present in higher percentage, ringed in blue, since magnetite (Fe_3O_4) and iron oxide (Fe_2O_3) have peaks higher than the bioash from the trial plant; this can justify its yellowish colour (b) compared to white colour of the bioash from the trial plant (a), as can be seen in picture Figure 3.8.

Figure 3.8 Picture of bioash from trial plant (a) and bioash from current plant (b).

Besides, the presence of Periclase (MgO) occurs in both cases.

In order to understand the type and nature of bonds that link the molecules, FT-IR is performed (§ 2.6.2). The spectrum of the raw bioash shows five distinct groups.

Intense absorption peaks at 1439 cm^{-1} is related to C–O symmetric stretching. The peaks appeared at 525 and 1049 cm^{-1} are attributed to the Si–O bond in $[SiO_4]^{4-}$ tetrahedron of the C-S-H. The bending of S–O in $[SO_4]^{2-}$ is observed at 1119 cm^{-1} and 619 cm^{-1} [45]. However, two sharp peaks in the range of 900–700 cm^{-1} are attributed to bending vibrations of carbonate group. Out of plane and in plane bending vibrations produce the peak located at 876 cm^{-1} and 712 cm^{-1}, respectively. These results are consistent with the data in the literature [46]. The peak located at 3645 cm^{-1} is attributed to the stretching vibration of the hydroxide group (O–H) which is assigned to the water molecules adsorbed on the surface. The graph is consulted in the Figure 3.9 below.

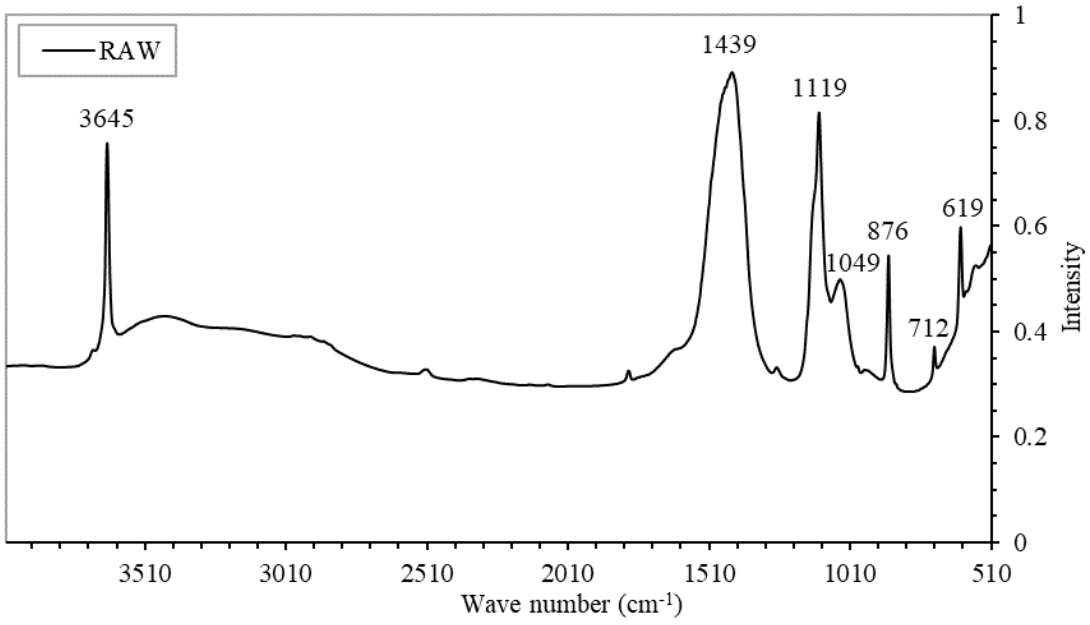

Figure 3.9 FT-IR absorbance spectra of raw bioash.

Another test to measure the thermal stability of the bioash is the TGA analysis (§2.6.4), the result is showed in the graph below (Figure 3.10), in this case we can see a substantial difference between the two types of bioash.

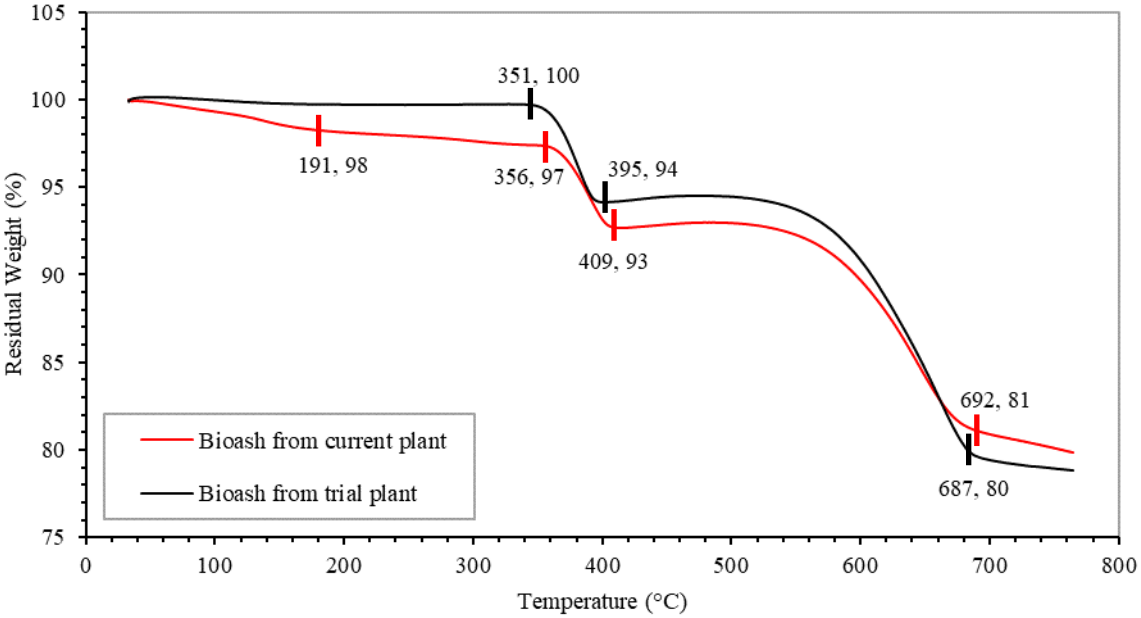

Figure 3.10 TGA curves of raw bioash.

The first difference is notable in the range from 30°C up to about 350°C.

The bioash from the trial plant appears stable while the bioash from the current plant has a percentage of lost weight of 3%: in the first step, the weight loss is associated to removal of physically adsorbed materials on the surface which occurs in the range of 30–200°C. This mass loss of 2% can be assigned to the evaporation of water and solvents. The weight loss of 1% in the second step, which takes place in the range of 200–350°C, can be attributed to the removal of chemically adsorbed material on the surface [47].

The presence of this step demonstrates the presence of a lot of chemicals different from calcite. In fact, the calcite graph is characterized by a single sharp weight loss, starting from 570 °C onward.

In the first high step, in temperature range of 350°C to 410°C, organic components that are chemically adsorbed on the calcite surface are oxidized. The $Ca(OH)_2$ calcination occurs [48].

The higher step of the bioash from the trial plant compared to the bioash from the current plant confirms the major presence of CaO in the bioash from the trial plant as it was concluded by XRD Analysis (Figure 3.7).

The final step of weight loss is due to slow decomposition of calcium carbonates ($CaCO_3$) of calcite into calcium oxide (CaO) and carbon dioxide (CO_2), which occurs above 520 ◦C up to 690°C [39].

The same conclusion can be reached analyzing the derivative of TGA curves (Figure 3.11): the peak at 134°C is absent in the curve of the bioash from the trial plant and the peaks intensity of the bioash from the trial plant peaks are higher; it means that the bioash from the current plant shows presence of water and less amount of adsorbed component. The slightly transition of the peaks of the two bioash means a small change in the composition of the different bioash.

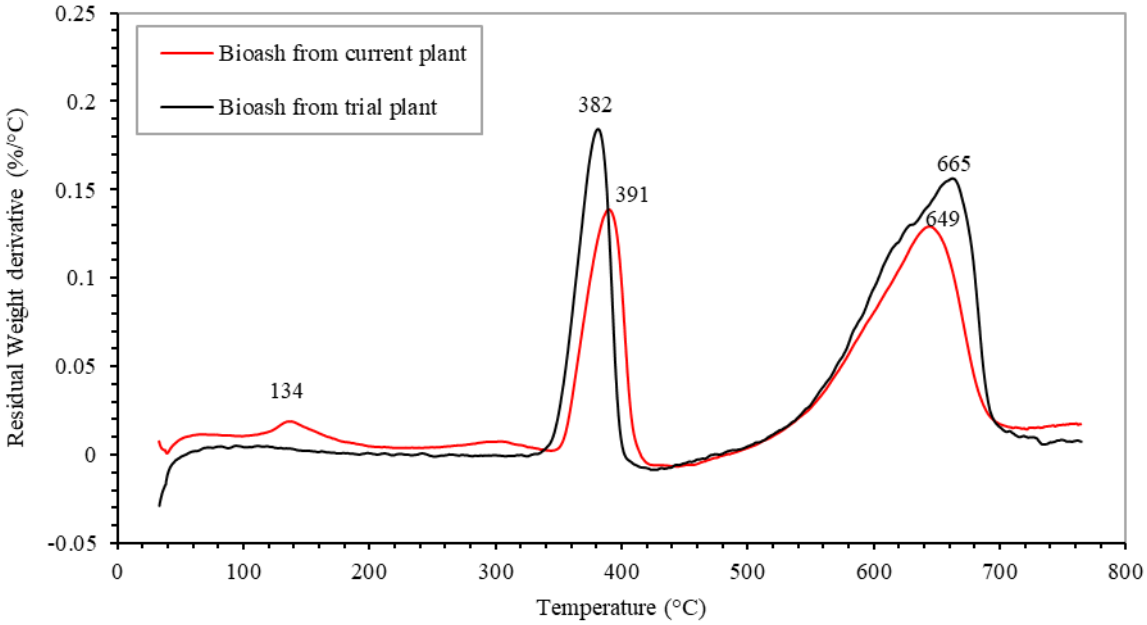

Figure 3.11 Derivates of TGA curves of raw bioash.

Another feature responsible for good mixability of bioash in rubber compound is grains dimension (§ 2.6.5).

The distribution of grains sizes reflects the inhomogeneity of the bioash composition and the higher dimension of the bioash grains than traditional reinforcing fillers.

The result of particles size analysis is shown in Figure 3.12 and the data listed in Table 3.6.

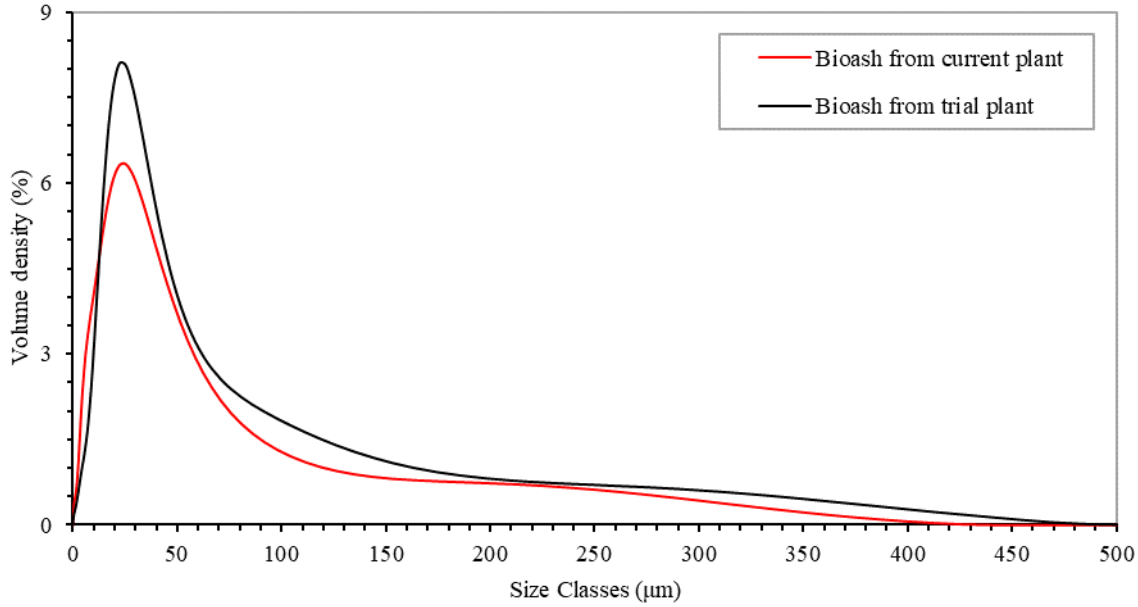

Figure 3.12 Raw bioash particle size analysis.

Table 3.6 Raw bioash particle size analysis.

Particle size analysis	*u.m.*	*Bioash from current plant*	*Bioash from trial plant*
Mode	µm	25.7	22.6
Median	µm	9.2	19.9
D[3/2]	µm	8.0	7.5
Specific Area	m^2/kg	754.5	744.3

There is not significant difference between the size dimension of the two types of bioash. Most of the particles have a diameter higher than 22 µm that is a value too big respect of size of a few µm of traditional reinforcing fillers (§ 1.3.4).

Another way to verify the particle dimension is the SEM microscopy (§ 2.6.1). SEM gives also information on morphology of the bioash grains and it can be used to confirm the nature of molecules detected by XRD. In the Figure 3.13, coming from a zoom of 1'000 times, diverse shapes and dimensions of the bioash grains are visible.

Some particles appear aggregated in irregular way, others organized in solids with linear edges like a crystal structure, as well depicted in Figure 3.14 thanks to a further zoom of 5'000 times.

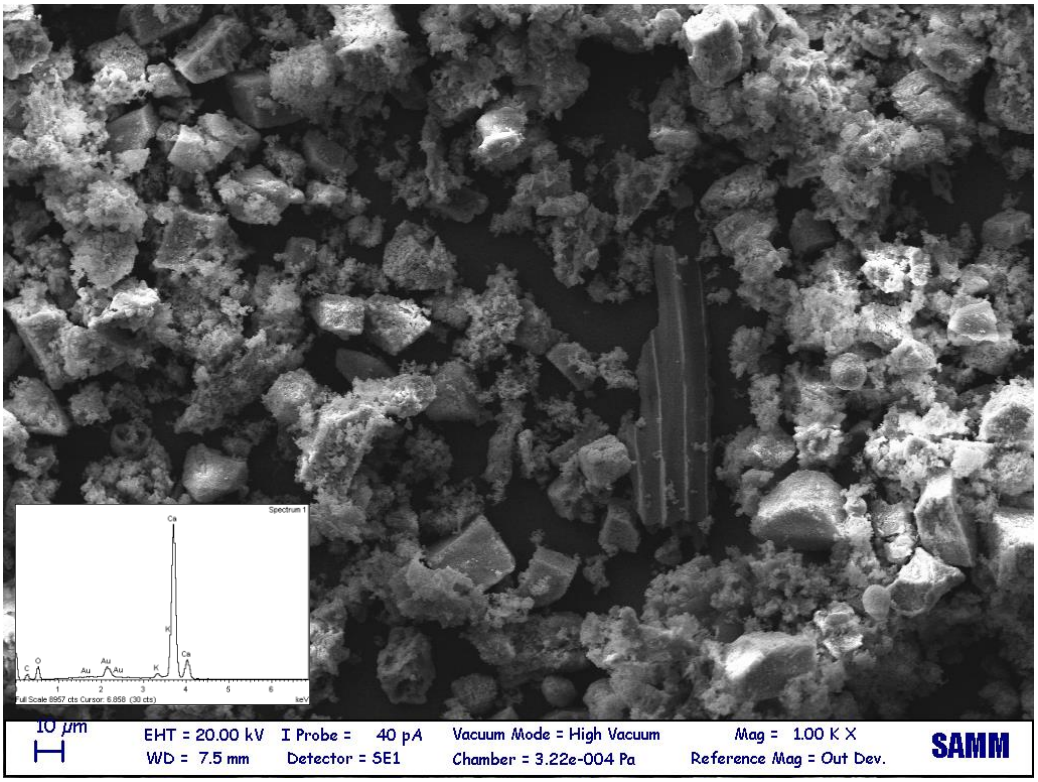

Figure 3.13 SEM micrograph of raw bioash (1'000 X) and relative medium spectrum.

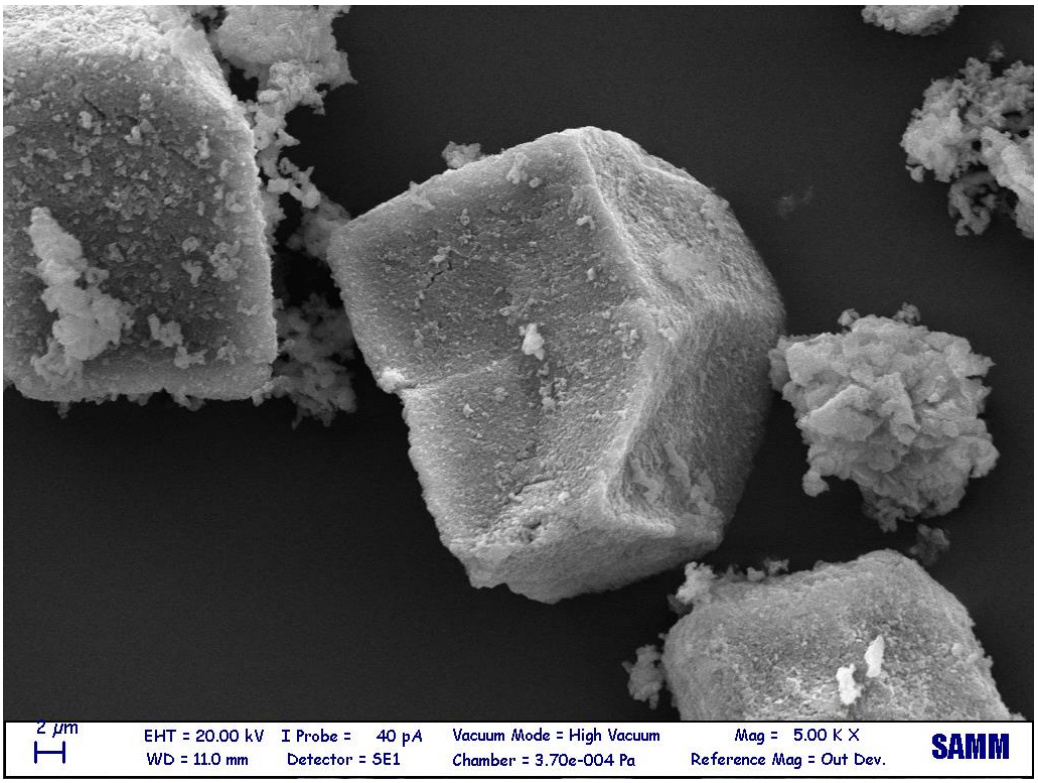

Figure 3.14 SEM micrograph of raw bioash, detail (5'000 X).

To have a reference about the bioash density, the Poured Bulk Density and the Tapped Density have been measured (§ 2.6.7) and result summarized in the Table 3.7 below:

Table 3.7 Density measurement of raw bioash.

Density measurement	*u.m.*	*Poured Bulk Density*	*Tapped Density*
Bioash	g/L	431 ±20	573 ±10

The tapped density has a lower standard deviation since it has less technological limits than poured bulk density and it is easier to reproduce.

The last test to completely characterized the bioash is the OCA (§ 2.6.8).

The raw bioash turns out to be total hydrophilic: it is not possible to measure any angle formed by the water drop since the water is completely absorbed: c.a. 0° (contact angle).

3.1.3. Features of compound with raw bioash

Changes of rubber properties after adding of the raw bioash in the compound are here investigated.

The effects of different percentage of the raw bioash in compounding are studied, so various formulations are tested (§ 2.3.2).

First performed test has been the DMA on the crude compound.

The resulting curve is depicted in Figure 3.15 below and the characteristic values summarized in Table 3.8.

It can be seen that presence of the bioash decreases optimum cure time (t 90) and trends of modulus of the various compounds are not directly proportional to the increasing of the bioash presence into compound.

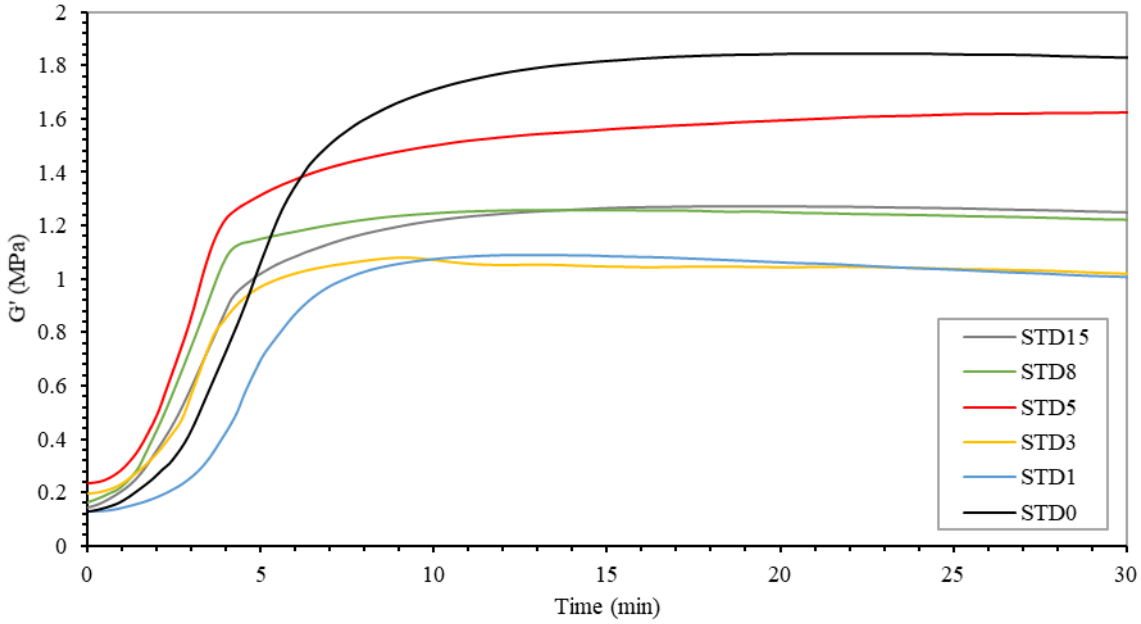

Figure 3.15 DMA curves of not functionalized bioash.

Table 3.8 DMA data of compounds with raw bioash.

DMA data	*u.m.*	***STD0***	***STD1***	***STD3***	***STD5***	***STD8***	***STD15***
G' max	MPa	1.84	1.09	1.08	1.62	1.26	1.27
G' min	MPa	0.13	0.13	0.19	0.23	0.16	0.14
ΔG' dec.	%	6	13	8	0	5	8
t vulc.	min	22	12	9	25	13	20
t 90	min	4.8	4.8	3.6	3.2	2.7	3.2

Since G' max measures the stiffness of rubber, with the bioash loading, the decreasing of G' max means decreasing in stiffness of compounds and increasing of the deformation of the natural rubber molecules.

When the filler loading is increased, more heat is generated due to the additional friction. In general, cure characteristics of rubber compounds also depend on properties of fillers such as surface area, surface activity, particle size, moisture content, and metal oxide content [49].

The enhancement of the cure rate indicates a reduction of activation energy for formation of crosslinks and an accelerating effect attributed to the bioash.

To confirm this phenomenon the same compounds have been produced by TWS and tested by RPA rheometer.

The values of the maximum torque reflect the data of DMA: in both cases, the higher value is attributed to STD0, the compound without bioash.

On the other hand, a great divergence is presented in the case of STD1: in the DMA, its curve reaches a low value while the compound with 1 phr of the bioash produced by TWS has the same curve of STD0. It suggests that 1 phr of bioash is the limit value, after while a clear difference in the properties of final compound can be observed.

The STD3 has the lowest value in both performed test so it can be considering the worst situation since in the dispersion grade analysis the high number of small distinguishable particles all over the matrix is evident and they act as failed initiation sites.

The most relevant value is notable in the case of STD5: its curve is the closer to STD0, while, increasing of the bioash presence in the compound, the curves fall off (STD8 and STD15).

It can be supposed that, in STD5, the particles are organized in agglomerates of medium dimension, so the number of defects is the lowest.

Increasing the quantities of the bioash the modulus decreases again: the number of defects is lower than STD3, but the aggregates have a higher dimension of STD5 and so create a notable effect on the strength of the final compound.

To sum up, it can be concluded that:

- Bioash in STD: phr < 1 → no significant changes compared to STD0
- Bioash in STD: 1 < phr < 3 → great numbers of defects of small size
- Bioash in STD: phr = 5 → low number and low size of defects
- Bioash in STD: 8 < phr < 15 → low number but big size of defects

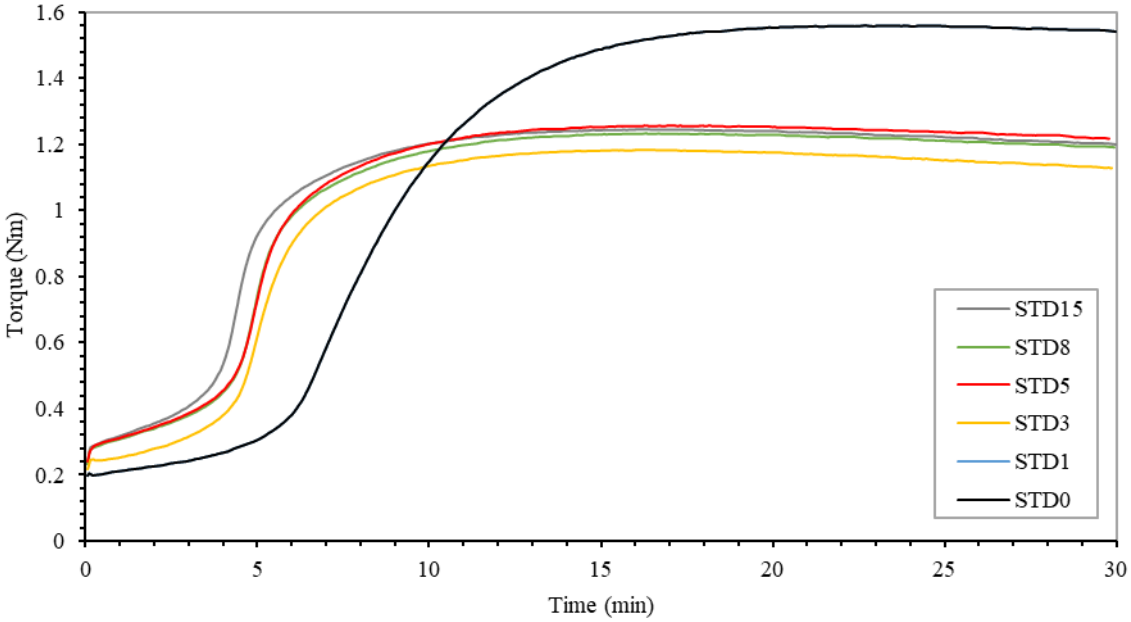

Figure 3.16 RPA curves of compounds with different percentage of raw bioash.

This conclusion can be consolidated with the data of dispersion grade analysis on the discussed compounds (Figure 3.17).

The particles with dimension between 0 and 11 μm are more frequent in STD1 and STD3. Large agglomerates, with dimension from 21 up to 50 μm, are mainly found in STD8 and STD15 compound.

In the middle there is STD5 with agglomerates of dimension between 12 and 20 μm. The grade of dispersion decreases linearly from 93% to 71% adding the bioash in the compound while the mean dimension of agglomerate increase as the bioash presence increases, from 9.7 μm to 14.5 μm. These values are presented in Table 3.9.

Table 3.9 Main data of dispersion grade analysis for compound with raw bioash.

	u.m.	***STD0***	***STD1***	***STD3***	***STD5***	***STD8***	***STD15***
Dispersion grade	%	92.9	93.5	88.3	84.8	80.6	70.5
Agglomerate mean size	µm	9.7	10.o	11.1	12.4	12.8	14.5

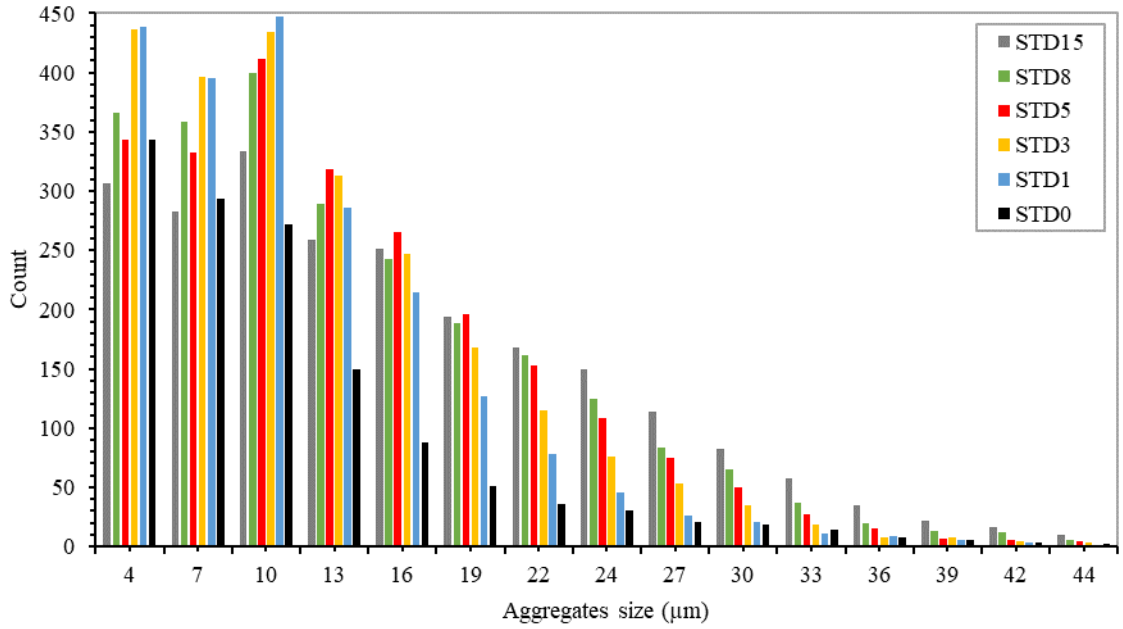

Figure 3.17 Dispersion grade analysis of compounds with different percentage of raw bioash.

To sum up, the bioash agglomerations result in difficult stress transmission from matrix to grains and in disturbance of the continuity of the matrix phase. This leads to a reduction of the tensile strength, as next discussed.

5 phr is the quantity of bioash that seems to give lower problems to compound, the worst performance is given by the compound with low presence of bioash such as STD3 and a medium result can be achieved by STD15.

Of course, in a perspective of circular economy, it is preferable to use as high as possible amount of the bioash in compounding.

The effects on rubber modulus can be better verified by tensile test.

In this test not only, the elastic behaviour is analysed but the viscous effect too, so there may be a mismatch with DMA results due to a complex nature of rubber (§ 1.3.2).

In Figure 3.18 stress-strain curve of compound with different percentage of the bioash is depicted. The first evidence is the slope of the last segment of the curve that decreases gradually with the addition of the bioash in compound. To better understand what happen in each curve a summary of extrapolated data is needed (Table 3.10).

The bioash grain, not strongly bonded to the rubber matrix, represent a defect of different size depends on particles tendency to agglomeration and consequentially the strength of rubber decreases, in fact, in the presence of the bioash the stress at break is lower than the compound without the bioash.

On the other hand, the bioash has an acceleration effect on cross-linking, so, increasing the bioash content, the cross-linking increases. Since cross-linking is responsible of elastic recovery of the rubber, higher bioash presence means gradually higher deformability.

The worst situation is again in the case of STD3 since there is a high number of small defects while STD5 is again the better situation since the aggregates are not excessive in number and dimension as in compound with higher quantities of the bioash.

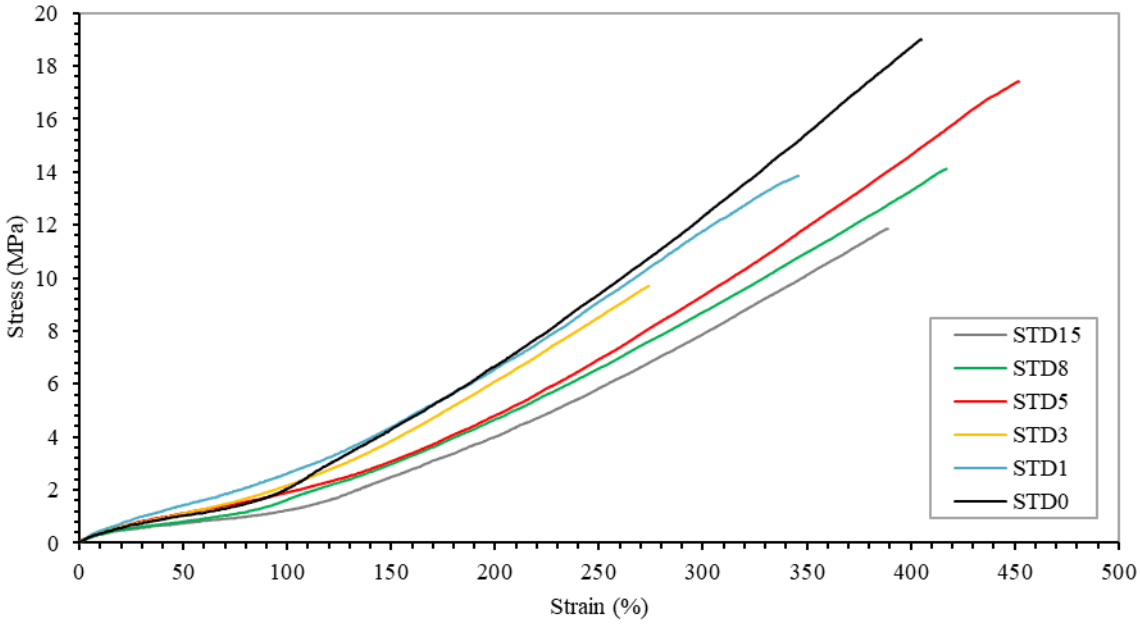

Figure 3.18 Stress-strain curves of compounds with different percentage of raw bioash.

Table 3.10 Data of stress-strain curves of compounds with different percentage of raw bioash.

Tensile data	*u.m.*	***STD0***	***STD1***	***STD3***	***STD5***	***STD8***	***STD15***
σ_b	MPa	17.8 ±1.9	14.5 ±0.5	9.9 ±0.2	16.7 ±1.4	14.0 ±0.2	10.8 ±1.0
ε_b	%	378 ±27	366 ±15	273 ±4	431 ±28	407 ±24	368 ±26
M 50%	MPa	1.47 ±0.09	1.65 ±0.15	1.43 ±0.05	1.29 ±0.16	0.92 ±0.08	0.48 ±0.35
M 100%	MPa	2.74 ±0.34	2.80 ±0.32	2.41 ±0.10	2.21 ±0.18	1.84 ±0.18	0.94 ±0.35
M 200%	MPa	7.26 ±0.62	6.61 ±0.74	6.09 ±0.24	5.33 ±0.36	4.92 ±0.45	3.85 ±0.52
M 300%	MPa	13.23 ±0.85	11.10 ±0.69	///	9.94 ±0.57	9.15 ±0.75	7.81 ±0.80

3.2. Effects of bioash with smaller grains size

The sizes of reinforcing or semi-reinforcing fillers are usually in the range between 1 and 10^{-2} μm (Figure 1.12). The usual dimension of raw bioash grains is about 25 μm and more than 65% of remain bioash grains have bigger size (Table 3.6). To exploit the possible improvement of properties of the compound with bioash after a grain size reduction, different methods to reach the smaller dimension of the grains are investigated.

Small dimension of polar bioash means small dimension of defects in apolar rubber matrix and higher surface area available for possible reaction with compatibilizers.

3.2.1. Size reduction of raw bioash

The first method, that has been investigated to decrease sizes of the bioash from the trial plant (BA), has been the sieves with 50 μm sizes of perforations (BA S). In that way all the particles with dimension higher that 50 μm are almost completely eliminated but this method generates a great number of waste bioash [50]. Moreover, the dimension of the grains is still not enough small to be classified as reinforce filler.

And so, the Ball Milling method has been investigated (BA BM), it is a low-cost process, rapid and easy as reported in many scientific articles.

The conditions are taken in according with literature [51]: ball-to-powder ratio is 10:1 and the time fixed at the least 24 hours to ensure a good result.

The final data is not so better than those obtained by sieve, so the two methods are adopted in sequence: after sieve, the ball milling has been performed (BA S BM); the dimension of grains are lower than in the case of previous method but not yet sufficient.

The inefficiency of the ball milling on the bioash is due to electrical attraction with plastic walls of container that decreases the number of interactions between the particles, so a metallic container has been used, and a certain grade of improvement is observed (BA BMM).

This mean that the obstacle to size reduction by ball milling is the polarity of the bioash, so the wet ball milling is used (BA BMW) [37]; the condition for the wet ball milling is presented in chapter 2.7.1.

The bioash, composed mainly of calcite, in water results in partial dissolution of calcite according to the following equation:

$$CaCO_3 + H_2O \leftrightarrow Ca_2^+ + HCO_3^- + OH^-$$

As a result of partial dissolution of calcite, a primary positive anion (Ca^{2+}) is formed. Moreover, the presence of calcium ions and hydroxide ions (OH^-) in the solution generates the secondary active ion (calcium hydroxide) for chemisorption:

$$Ca^{2+} + OH^- \leftrightarrow CaOH^+$$

Hence, the hydrated calcite surface contains protonated anions of $HCO3^-$ as well as hydroxylated cations of $CaOH^+$ [39]. It improves the dissociation and reactivity of the bioash treated by the ball milling. The wet ball milling results to be the better method to reduce the bioash dimension from an average of 76 μm to 8 μm.

The Figure 3.19 illustrates the distribution of grains dimension measured by Particle Size Analysis (§ 2.6.5) and Table 3.11 summarizes the main data of the analysis.

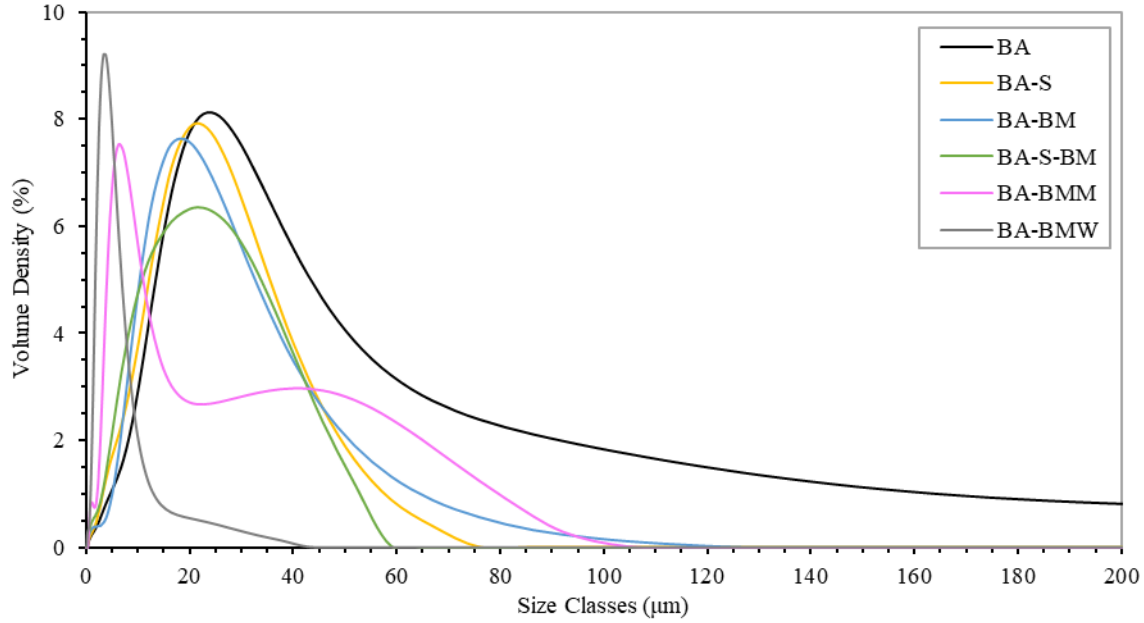

Figure 3.19 Size Dimension Distribution of raw bioash after size reduction methods.

Table 3.11 Size Dimension Analysis of raw bioash after size reduction methods.

	u.m.	*BA*	*BA S*	*BA BM*	*BA S BM*	*BA BMM*	*BA BMW*
Mode	*μm*	22.6	24.1	18.7	24.1	6.3	3.3
Median	*μm*	19.9	5.2	4.6	4.0	7.3	7.2
D[3/2]	*μm*	7.5	7.0	7.1	5.8	4.9	2.2
Specific Area	m^2/kg	744.3	863.7	842.7	1’031.0	1’225.0	2’677.0

It should be noted that the wet ball milling did not have the same effect on the bioash from the current plant (RAW), the difference can be seen in Figure 3.20 and in the values of Table 3.12.

This phenomenon can be explain looking the TGA performed on the both bioash types (Figure 3.10): the bioash from the current plant has a certain amount of water absorbed that is absent in the bioash from the trial plant, this involves that the grains of the dried bioash have higher possibility of interacting one each other thanks to higher efficiency in dissociation by water action.

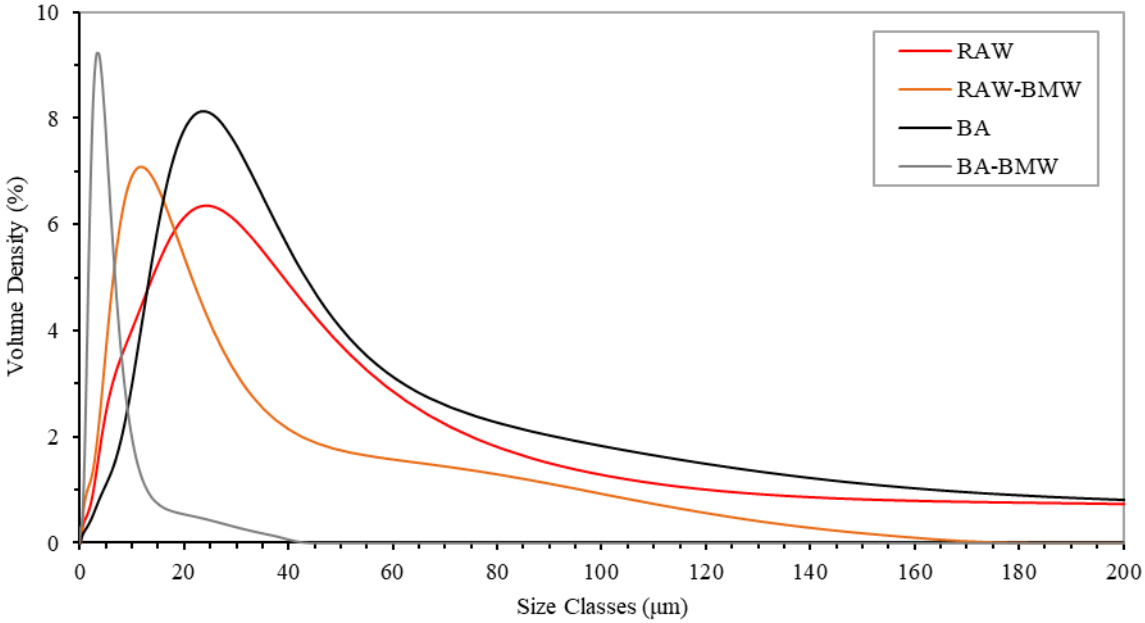

Figure 3.20 Size Dimension Distribution of raw bioash after ball milling wet.

Table 3.12 Size Dimension Analysis of raw bioash after ball milling wet.

	u.m.	*RAW*	*RAW BMW*	*BA*	*BA BMW*
Mode	µm	25.7	8.1	22.6	3.3
Median	µm	9.2	7.2	19.9	7.2
D[3/2]	µm	7.9	4.99	7.5	2.2
Specific Area	m^2/kg	754.5	1’203.0	744.3	2’677.0

3.2.2. Features of compound with wet ball milled bioash

To verify the improvement of rubber compound properties using the bioash with smaller size compared to usage of the raw bioash, the compounds with 5 and 15 phr of the treated bioash are produced. The formulations are presented in the chapter § 2.3.2.

The compound with 5 and 15 phr of the bioash are been chosen since they showed the most significant effects compared to standard rubber compound, see previous chapter.

The DMA graph is depicted in Figure 3.21 below and the main data summarized in Table 3.13.

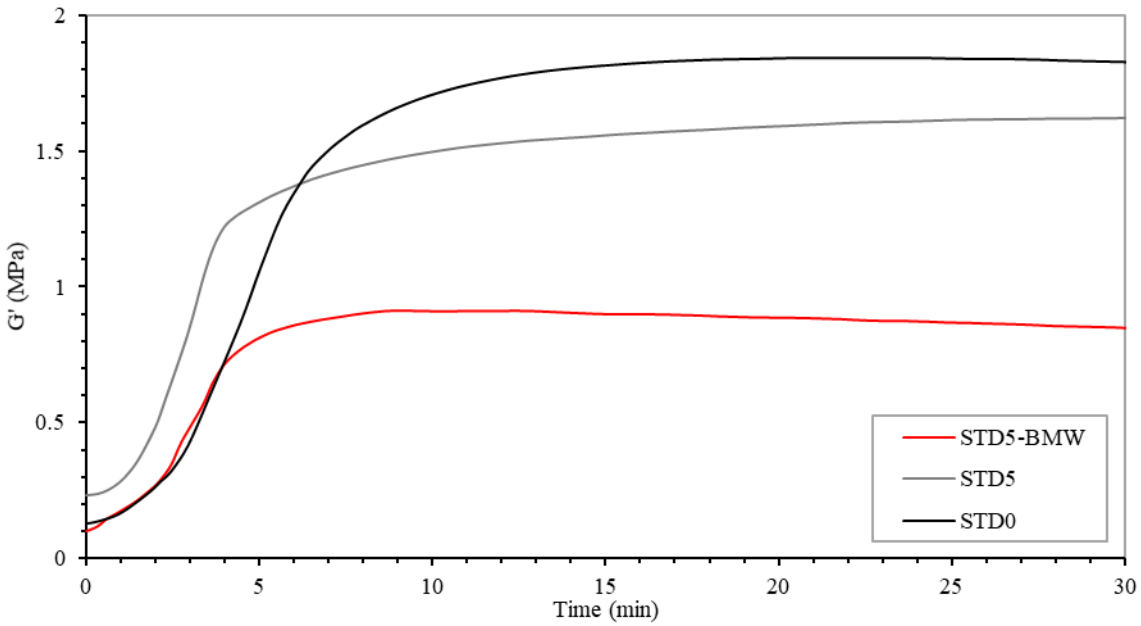

Figure 3.21 DMA curves of compound with 5 phr of bioash with smaller size grains and references.

Table 3.13 DMA data of compound with 5 phr of bioash with smaller size grains and references.

DMA data	*u.m.*	***STD0***	***STD5***	***STD5 BMW***
M' max	MPa	1.84	1.62	0.91
M' min	MPa	0.13	0.23	0.10
ΔM' dec.	%	6	0	11
t vulc.	min	22	25	9
t 90	min	4.8	3.2	3.0

A substantial decrease in vulcanization time is measured; the lower size of grains means higher number and higher available surface area of the particles that have acceleration effect, and so the vulcanization process is concluded in less time than compound with the raw bioash.

The effects in compound mechanical properties can be analysed by stress-strain curve in Figure 3.22, in this case the difference is not so remarkable compared to the compound with the raw bioash. From data in Table 3.14, it can been noted an evident similarity between the values of STD5 and the values of STD5 BMW, considering the standard deviation too.

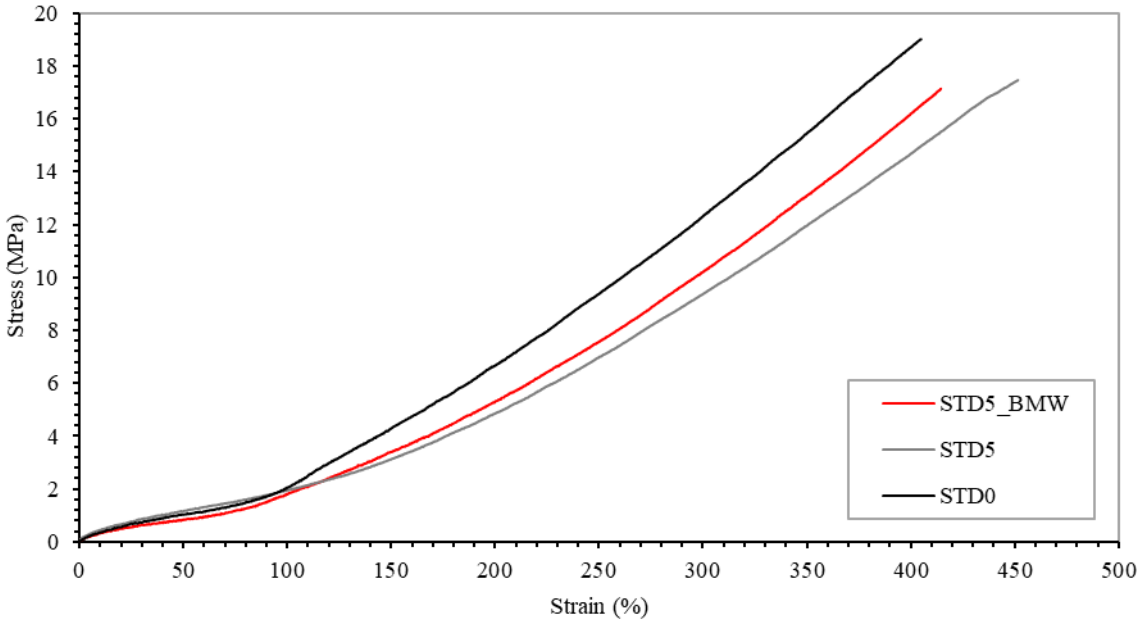

Figure 3.22 Stress-strain curves of compound with 5 phr of bioash with smaller size and references.

Table 3.14 Data of stress-strain curves of compound with 5 phr of bioash with smaller size and references.

Tensile data	*u.m.*	***STD0***	***STD5***	***STD5 BMW***
σ_b	MPa	17.8 ±1.9	16.7 ±1.4	17.3 ±0.6
ε_b	%	378 ±27	431 ±28	409 ±16
M 50%	MPa	1.47 ±0.09	1.29 ±0.16	1.00 ±0.10
M 100%	MPa	2.74 ±0.34	2.21 ±0.18	1.95 ±0.12

M 200%	MPa	7.26 ±0.62	5.33 ±0.36	5.46 ±0.34
M 300%	MPa	13.23 ±0.85	9.94 ±0.57	10.54 ±0.60

Increasing quantities of the treated bioash, effects can be more evident.

In fact, in the Figure 3.23, the graphs of DMA results of STD15-BMW, compared to the reference compound STD15 and STD0, is shown and relative data summarized in Table 3.15.

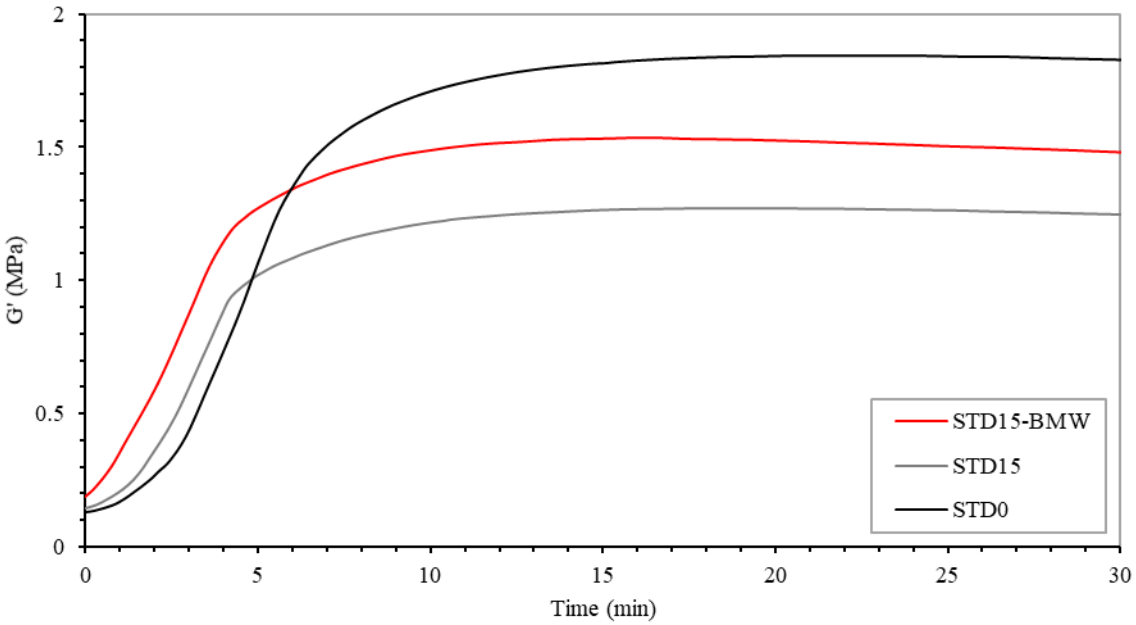

Figure 3.23 DMA curves of compound with 15 phr of bioash with smaller size grains and references.

Table 3.15 DMA data of compound with 15 phr of bioash with smaller size grains and references.

DMA data	*u.m.*	***STD0***	***STD15***	***STD15 BMW***
M' max	MPa	1.84	1.27	1.53
M' min	MPa	0.13	0.14	0.19
ΔM' dec.	%	6	8	1
t vulc.	min	22	20	17
t 90	min	4.8	3.2	3.1

In this case, in fact, data results more coherent with lower size of the bioash: the final modulus is collocated in an intermediate space between the compound without the bioash and the compound with 15 phr of the raw bioash.

The same tendency is notable in the tensile test curve in the Figure 3.24 (main data is summarized in the Table 3.16).

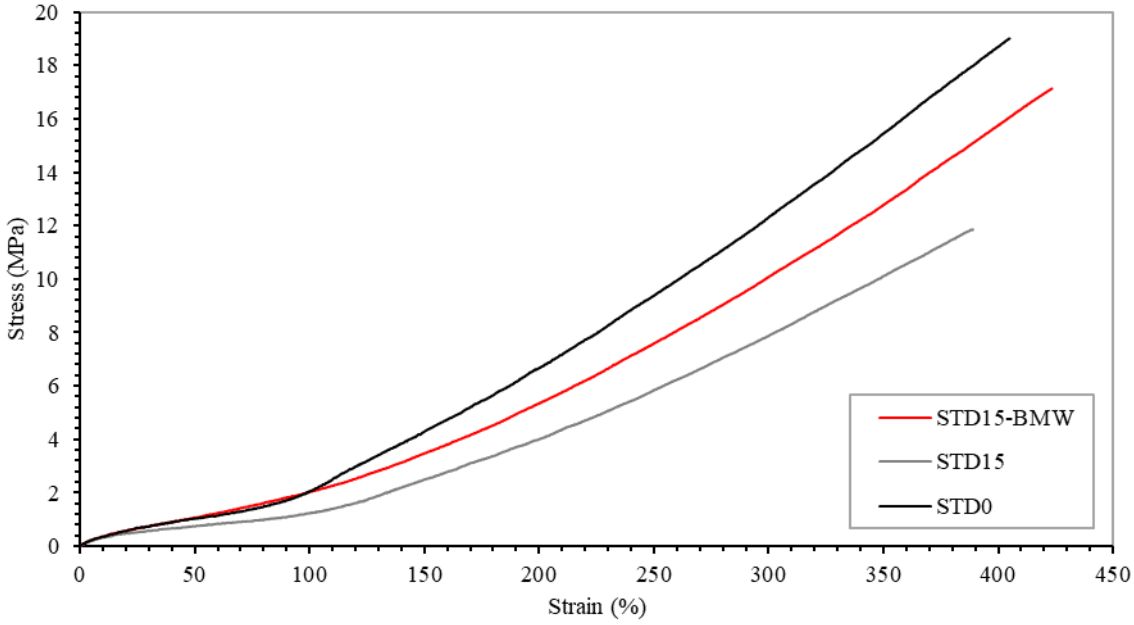

Figure 3.24 Stress-strain curves of compound with 15 phr of bioash with smaller size and references.

Table 3.16 Data of stress-strain curves of compound with 15 phr of bioash with smaller size and references.

Tensile data	*u.m.*	***STD0***	***STD15***	***STD15 BMW***
σ_b	MPa	17.8 ±1.9	10.8 ±1.0	16.4 ±0.9
ε_b	%	378 ±27	368 ±26	418 ±12
M 50%	MPa	1.47 ±0.09	0.48 ±0.35	0.96 ±0.11
M 100%	MPa	2.74 ±0.34	0.94 ±0.35	1.95 ±0.19
M 200%	MPa	7.26 ±0.62	3.85 ±0.52	5.16 ±0.47
M 300%	MPa	13.23 ±0.85	7.81 ±0.80	9.83 ±0.68

The improvement in strength compared to the compounds with the raw bioash is due to anisotropy and higher surface-to-volume ratio of the bioash treated by wet ball milling as can be verify by the dispersion grade analysis (§ 2.5.4).

The result is present in following Figure 3.25.

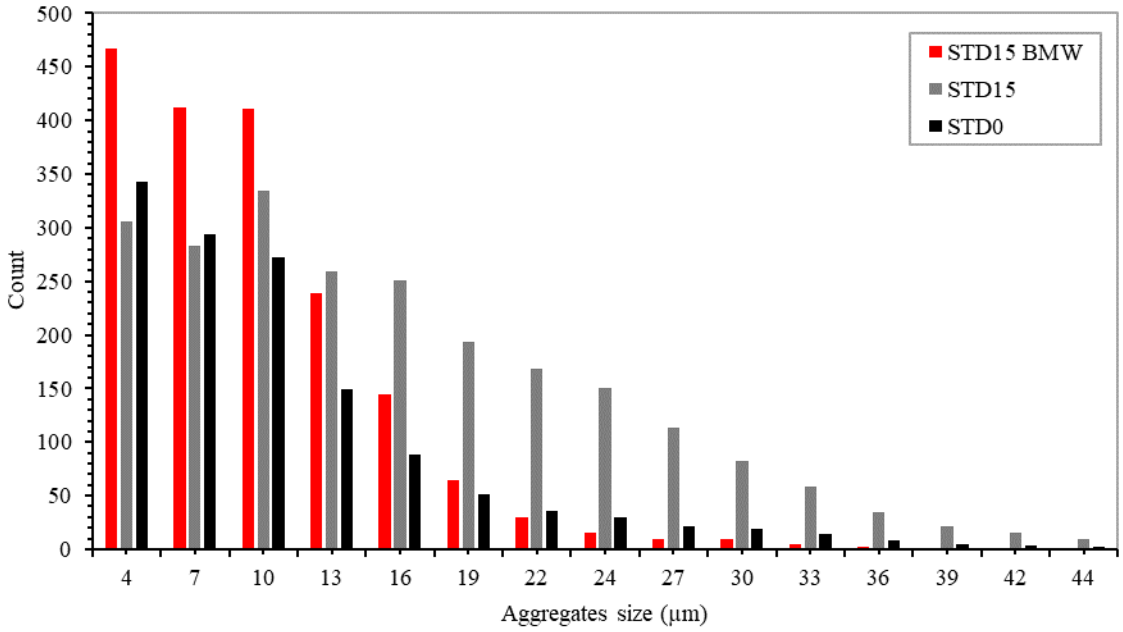

Figure 3.25 Dispersion grade analysis of bioash treated by wet ball milling and references.

The 98% of the agglomerates in STD15-RAW BMW have dimension under 22 µm, while to reach 98% of total agglomerates in SDT15 the size of 33 µm is needed.

In case of STD15-RAW BMW, the grade of dispersion is 97.7% and the main agglomerate size is 8.3 µm.

To sum up, the decrease of size of the bioash gives, to the final product, a small improve in properties but it can be very useful in case of bioash functionalization since the treated bioash has a higher superficial area available for a possible reaction and moreover, small grains dimension improves the dispersion in compounding.

3.3. Effects of bioash functionalized by fatty acid

Many articles present the modification of bioash by fatty acid as the solution for improve the reinforce role of bioash in rubber compound.

The problem to used directly a bioash, constituted prevalently by calcite, is the incompatibility of its high energetic hydrophilic surface with the low-energy surface of hydrophobic polymers. Different studies reveal that dispersion of hydrophobic fillers is more homogeneous than hydrophilic: hydrophobic ash forms a network structure more readily than hydrophilic [52].

The surface treatment can decrease filler-filler interaction and increase adhesion of matrix-filler.

The long chains of fatty acids affect the spatial arrangement of molecules and hence its orientation on the surface. These creates a film as interface between the two phases of the heterogeneous materials.

Moreover, eventually presence of double bond, for example in case of oleic acid, make the acid molecule more polar, reactive and less hydrophobic.

It is well known that when fatty acids are adsorbed onto calcium carbonate surface, they initially form a monolayered array of alkyl chains oriented so that the carboxylic groups are adjacent to the mineral surface. If excess of acid is used, additional acid molecules may be physiosorbed in a second layer, with chains-oriented tail-to-tail to the first molecular layer.

For the practical application, if the amount of fatty acid is low, the desired effect is not achieved, while use of excessive amount of organic phase leads to processing problems, inferior mechanical properties and increased price. Thus, the optimal amount of fatty acid used for treatment of calcium carbonate surface is both a technical and an economical issue, and so different amounts of fatty acid are studied in this chapter.

Effects of modified bioash by fatty acids into compound are following discussed.

3.3.1. Feature of bioash modified by stearic acid (RAW AS)

Stearic acid is a substance already used in rubber compound, so it is immediately available in rubber processing industry (§ 2.1.6) .

The functionalization process by ball milling is discussed in the chapter 2.7.2. Different amounts of stearic acid have been used to modify bioash and many tests to characterize the material has been done to find the correct amount of stearic acid to use.

After the bioash functionalization, FT-IR is performed, and the resulted spectra is illustrated in the Figure 3.26 below:

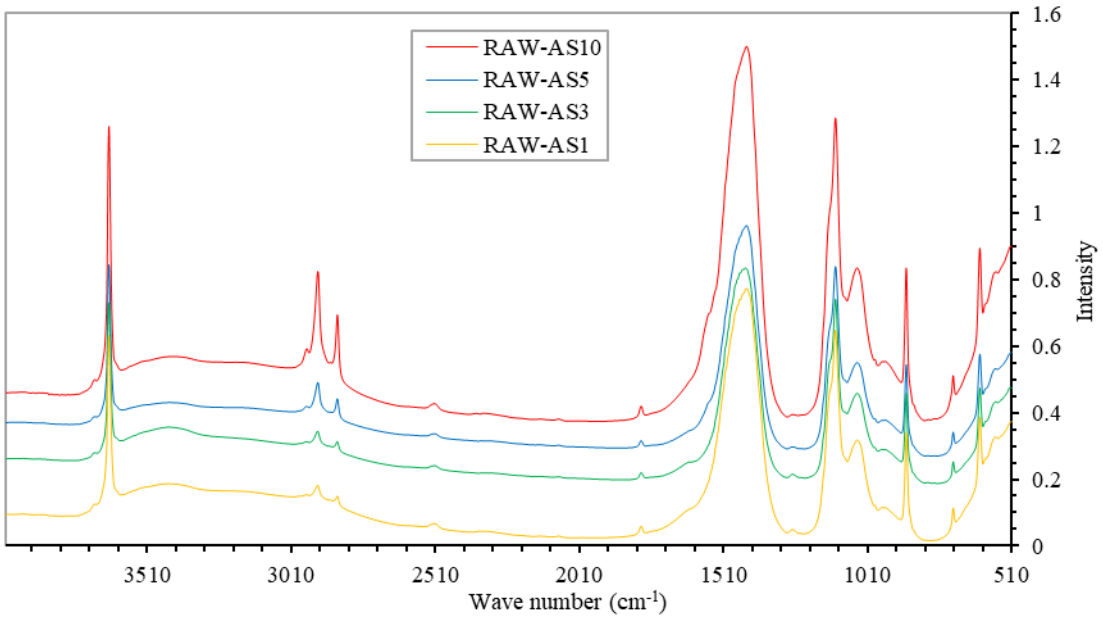

Figure 3.26 FT-IR spectra of raw bioash treated with different percentage by weight of stearic acid.

The shape of spectra is the same for the bioash treated with different percentages of stearic acid (RAW AS), the intensity of peaks increases, increasing stearic acid content.

To better understand the difference with the FT-IR spectra of raw bioash, the RAW AS10 is compared to spectra of raw bioash in the Figure 3.27.

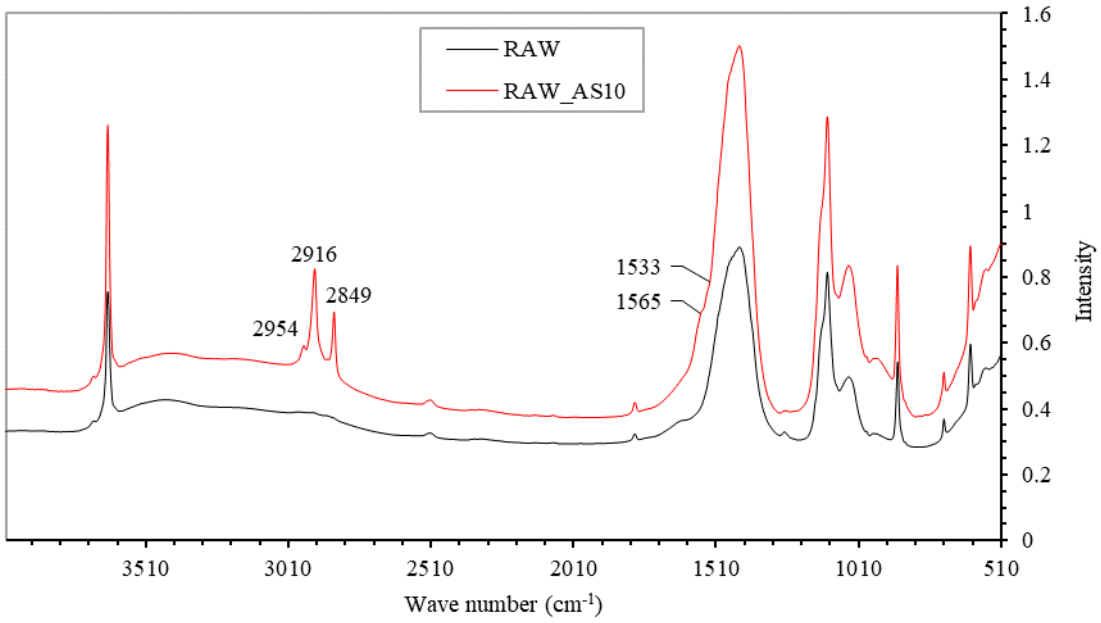

Figure 3.27 FT-IR spectra of raw bioash and bioash treated with 10% by weight of stearic acid.

FT-IR spectrum of the bioash (main calcite) surface treated with stearic acid shows several absorption bands appear in the spectrum compared to that of raw bioash which reveals adsorption of stearate on the surface of calcite after functionalization.

Two small sharp peaks located at 1565 and 1533 cm^{-1} are related to a symmetric stretch vibration of C–O bonds in carboxylate group. In addition, two bands centred at 2916 and 2849 cm^{-1} reflect methylene (–CH2–) asymmetric stretching of C–H and methylene (–CH2–) symmetric stretching vibrations, respectively, they are characteristic feature of the stearic acid spectra.

In addition, the band located at 2954 cm^{-1} is assigned to methyl (CH_3) asymmetric C–H stretching vibration which indicates strong adsorption of stearic acid on the bioash surface. This difference may refer to different amount of adsorbed carboxylate on the surface. Although, FTIR result reveals adsorption of stearic acid on the bioash surface, it only presents a qualitative analysis [39].

Thermogravimetric analysis (§ 2.6.4) has been used to quantify the amount of adsorbance on the bioash surfaces (Figure 3.28).

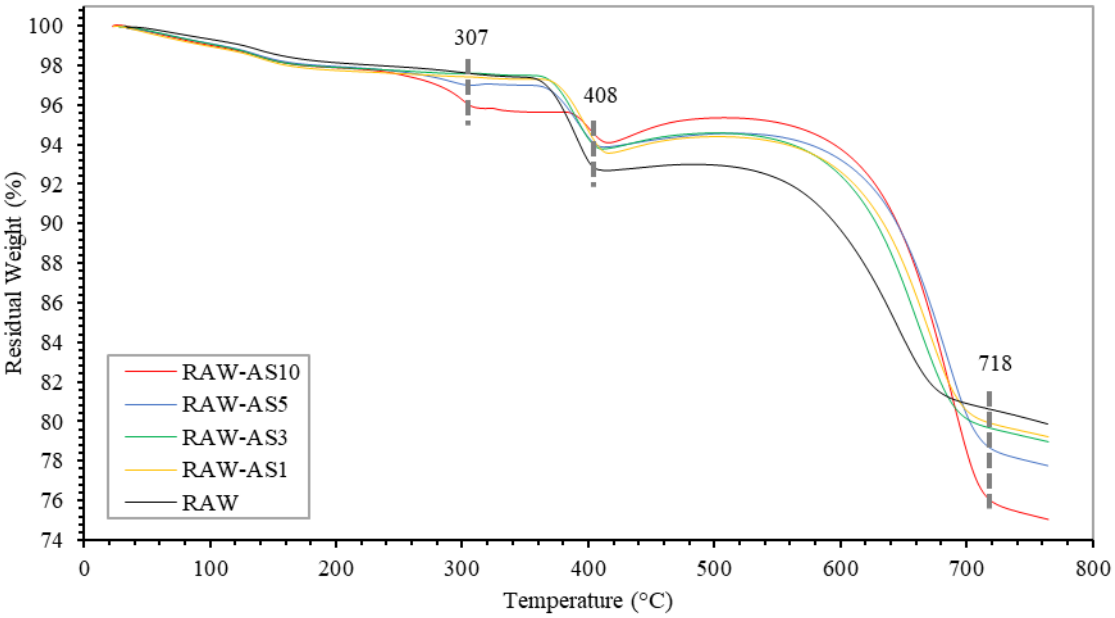

Figure 3.28 TGA graph of bioash treated by different percentages of stearic acid.

In the case of RAW AS5 and RAW AS10, a percentage of weight lost is notable in the range between 200 and 310°C, it is associated to absorbed material. This decadency is absent in the case of lower percentage of bioash, it suggests that the weight lost is associated to physical absorption of stearic acid on surface. In particular, at 307°C, for RAW AS10 the percentage of weight lost is 1.7%, for RAW AS5 is 0.6% and for the last two is under 0.3%. And so, the optimal amount of stearic acid needed to cover the bioash surface with a monolayer of organic molecules lies lower than 5% in weight of bioash, in accordance to literature [53] .

In fact, when fatty acids are adsorbed onto calcium carbonate surface, they initially form a monolayered array of alkyl chains oriented so that the carboxylic groups are adjacent to the mineral surface. If excess of acid is used, additional acid molecules then may be physiosorbed in a second layer, with their chains-oriented tail-to-tail to the first molecular layer [40].

The second step is around 408°C and it is due to oxidation of carbide, the lower weight lost for treated bioash respect raw bioash suggests that a part of calcite bounded with stearic acid is prevented by oxidation at this temperature.

Since the molecules of stearic acid are burned down completely at temperature higher than 720°C, by subtracting the weight loss of the raw bioash from the modified ash beads, the amount of stearic acid on bioash beads was calculated to be 4.8 weight % of total

weight for RAW AS10 considering the physic absorption too, 2.1% in case of RAW AS5, 0.9% for RAW AS3 and 0.6% for RAW AS.

The result of 4.8% of weight lost from RAW AS10 compared to RAW, is in accordance with Kumagawa extraction result (§ 2.6.3).

In fact, the efficiency of extraction is 54.5%, it means that of the 10% in weight of stearic acid only 54.5% is strongly bounded to bioash.

For example, 100 grams of bioash is functionalized by 10 grams of stearic acid; from the TGA result the bounded acid is 4.8% so 5.3 grams that is about 53% of used acid, considering the test errors, it is in accordance with extraction efficiency.

The effect of intermediate layer between the hydrophobic polymer and hydrophilic is reflected in the Size Dimension Analysis of bioash treated with stearic acid by ball milling (§ 2.7.2), two samples: RAW AS3 and RAW AS10 are analysed as references. The graph is available in the Figure 3.29 and shows the positive effect of stearic acid on the bioash size reduction, in fact, the main dimension from 25 µm becomes 4-5 µm (Table 3.17) and as the percentage in weight of stearic acid is higher, as the effect on size reduction is better.

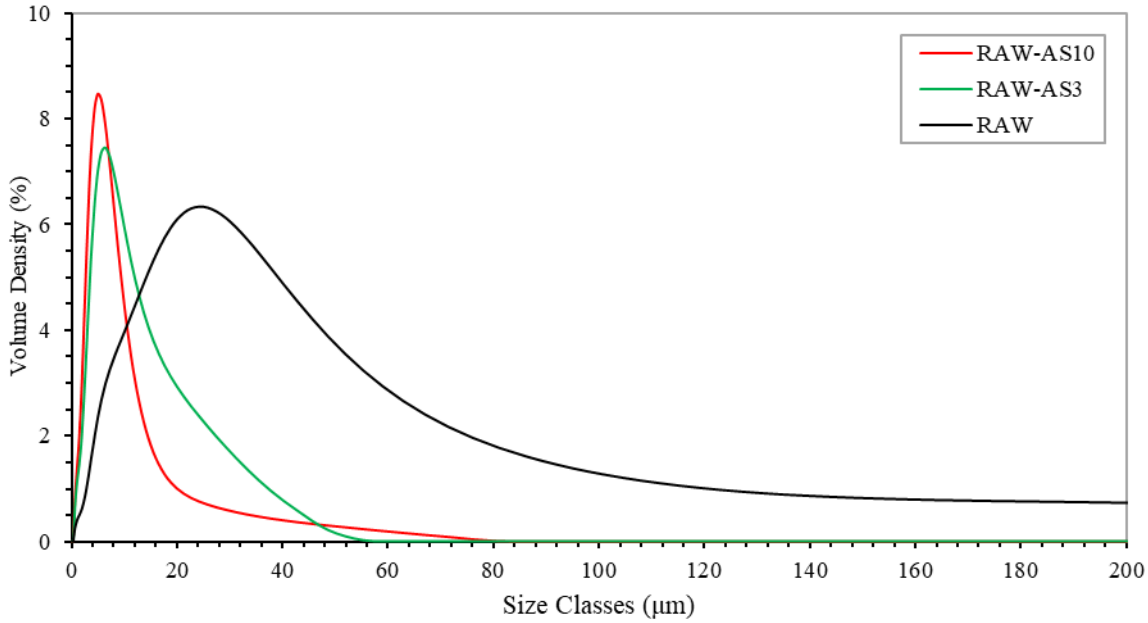

Figure 3.29 Size Dimension Analysis graph of bioash treated by stearic acid.

Table 3.17 Size Dimension Analysis data of bioash treated by stearic acid.

	u.m.	*RAW*	*RAW AS3*	*RAW AS10*
Mode	µm	25.7	6.3	4.9
Median	µm	9.2	3.8	4.3
D[3/2]	µm	7.9	3.4	2.5
Specific Area	m^2/kg	755	1’759	2’410

The difference in the dimension of grains is also clearly visible by SEM (§ 2.6.6). The Figure 3.30 can be compared with Figure 3.13.

Both figures have a 1’000 x scale, the lower dimension of grains is evident.

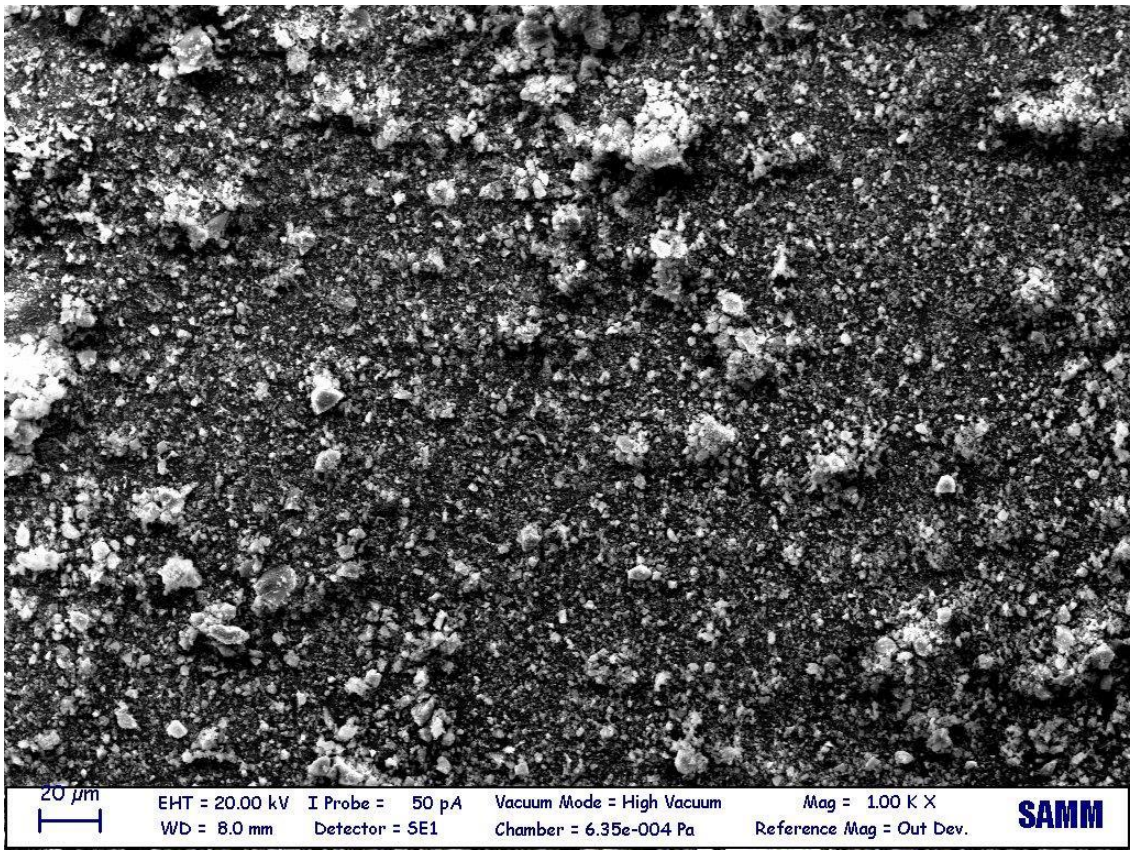

Figure 3.30 SEM micrograph of raw bioash treated by stearic acid (1’000 X).

Another feature to underline is changing of density of the bioash, adding stearic acid.

Stearic acid has a higher density than bioash (§ 2.1.6) but the main characteristic, that permits increasing of density of the functionalized bioash, is the lower dimension of grains that allows a better compaction of the grains.

As the quantity of the steric acid added to the bioash increases, the main size of grains decreases (Figure 3.29).

This is evident in values of tapped density that increase adding stearic acid, the measurements are available in the Table 3.18 below.

Table 3.18 Tapped density of bioash treated by different percentage of stearic acid.

	u.m.	*RAW*	*RAW AS1*	*RAW AS3*	*RAW AS5*	*RAW AS10*
Tapped Density	g/L	573 ±10	855 ±10	944 ±10	1010 ±10	1053 ±10

The last test to characterize the functionalized bioash is the Optical Contact Angle (OCA § 2.6.8). It is known the total hydrophilicity of the raw bioash, in fact, the contact angle with a drop of water is zero (§ 3.1.2).

With the adding of 1% by weight of stearic acid the hydrophilicity decreases, and the contact angle becomes 85°.

In the case of RAW AS3, RAW AS5, RAW AS10 the total hydrophobicity is reached, and the contact angle is about 90°.

This effect can be seen with naked eyes too in Figure 3.31.

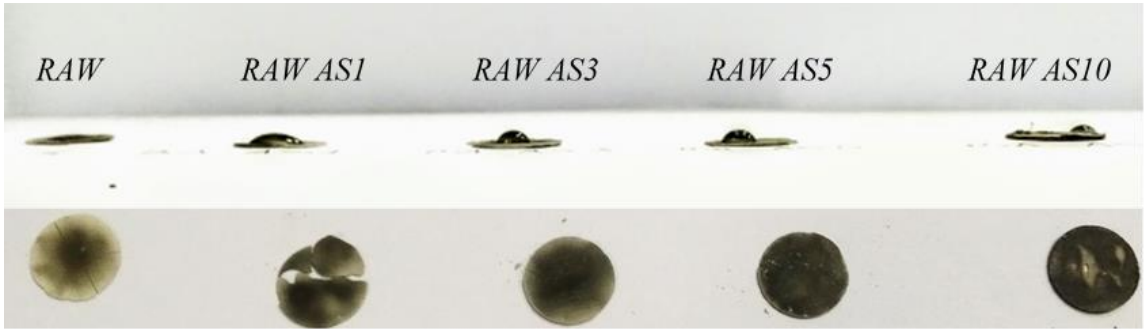

Figure 3.31 OCA of bioash modified by stearic acid.

3.3.2. Features of compound with bioash modified by stearic acid

The effects of bioash modified by different percentage of stearic acid into compound are discussed in this sub-chapter. The quantities of functionalised bioash added at the standard compound are 5 and 15 phr, formulations are available in the chapter § 2.3.3. The Dynamic Mechanical Analysis (DMA) at 151°C (§ 2.5.1) is performed. The imaginary part of elastic modulus against time is plotted in Figure 3.32 below and the main data summarized the Table 3.19 for compound with 5 phr of bioash and a percentage of stearic acid of 1, 3, 5 and 10% (respectively STD-RAW AS1, STD-RAW AS3, STD-RAW AS5, STD-RAW AS10), compound with 5 phr of raw bioash (STD5) and compound without bioash (STD0).

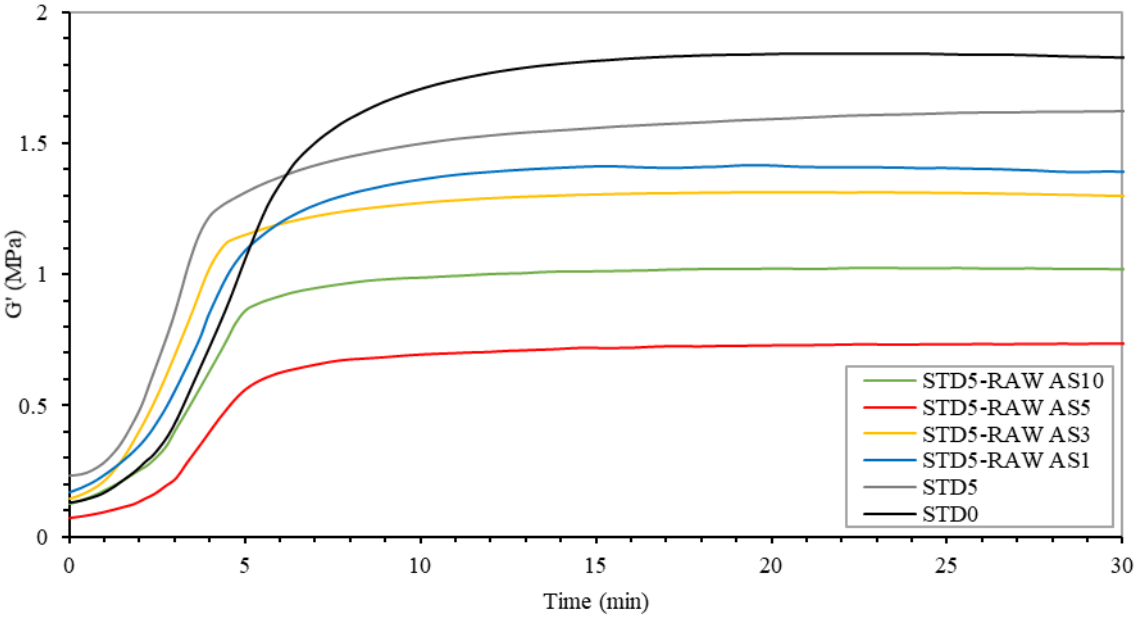

Figure 3.32 DMA curves of compound with 5 phr of bioash modified by stearic acid.

Table 3.19 Data of DMA curves of compound with 5 phr of bioash modified by stearic acid.

DMA data	*u.m.*	***STD0***	***STD5***	***STD5-RAW AS1***	***STD5-RAW AS3***	***STD5-RAW AS5***	***STD5-RAW AS10***
G' max	MPa	1.84	1.62	1.41	1.31	0.74	1.02
G' min	MPa	0.13	0.23	0.17	0.14	0.07	0.13
ΔG' dec.	%	6	0	8	4	0	3
t vulc.	min	22	25	20	21	25	23
t 90	min	4.8	3.2	4.0	3.0	4.0	3.9

The first conclusion is that the modification by stearic acid has a low impact on the rate of vulcanization time. Moreover, it is notable that the STD5-RAW AS1 and STD5-RAW AS3 curves are close to STD5 curve, it is due to the low quantities of stearic acid adding in percentage compared to already low bioash presence of 5 phr.

The decrease of finale imaginary part of elastic modulus has been observable in the samples STD5-RAW AS5 and STD5-RAW AS10. The great effect of STD5-RAW AS5 is notable also in the stress-strain curve (Figure 3.33), it has the higher value of deformation at fixed stress (Table 3.20).

The other samples do not show improvement compared to the raw bioash in the standard compound.

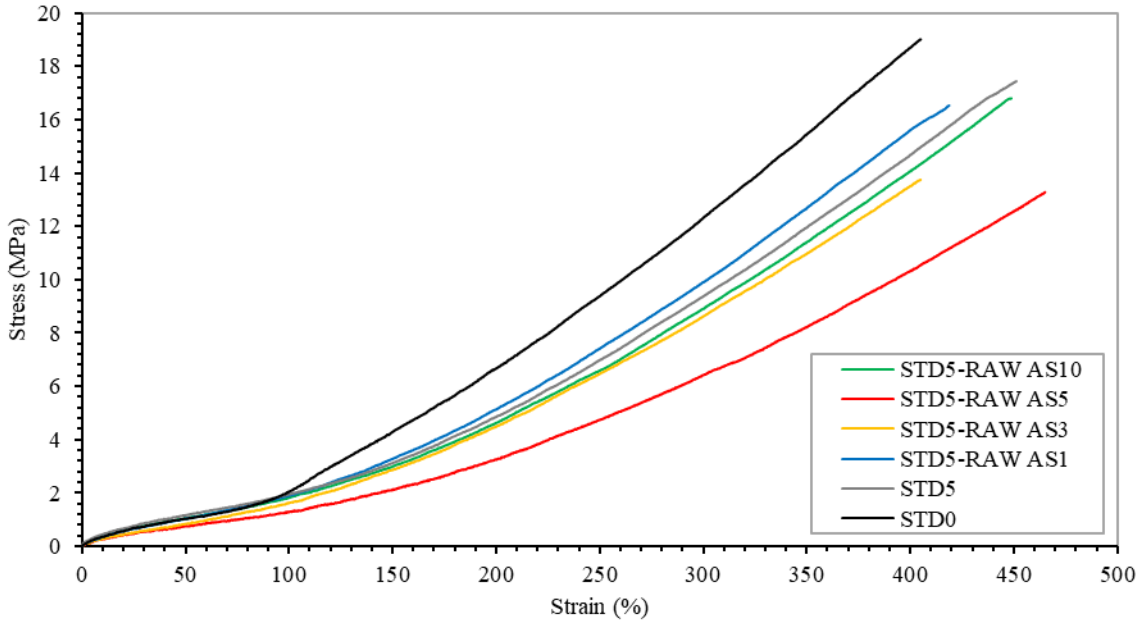

Figure 3.33 Stress-strain curve of compound with 5 phr of bioash modified by stearic acid.

Table 3.20 Data of stress-strain curve of compound with 5 phr of bioash modified by stearic acid.

Tensile data	*u.m.*	***STD0***	***STD5***	***STD5-RAW AS1***	***STD5-RAW AS3***	***STD5-RAW AS5***	***STD5-RAW AS10***
σ_b	MPa	17.8 ±1.9	16.7 ±1.4	16.8 ±0.4	14.3 ±1.3	12.8 ±0.30	15.5 ±2.0
ε_b	%	378 ±27	431 ±28	426 ±5	401 ±43	477 ±8	441 ±22
M 50%	MPa	1.47 ±0.09	1.29 ±0.16	1.11 ±0.03	1.02 ±0.07	0.14 ±0.10	0.45 ±0.10
M 100%	MPa	2.74 ±0.34	2.21 ±0.18	1.93 ±0.09	1.91 ±0.50	0.65 ±0.10	1.25 ±0.11

M 200%	MPa	7.26 ±0.62	5.33 ±0.36	4.95 ±0.30	5.42 ±1.38	2.45 ±0.25	4.02 ±0.30
M 300%	MPa	13.23 ±0.85	9.94 ±0.57	9.39 ±0.57	9.38 ±1.33	5.40 ±0.49	8.27 ±0.56

In the compound STD15, with 15 phr of bioash, if modification of the bioash by different percentages of stearic acid is done, the quantities of absolute stearic acid in the compound are higher than in compound with 5 phr of the bioash modified by stearic acid, so a different result is expected.

The DMA graph of STD15 with functionalised bioash is illustrated in Figure 3.34 below, and the main data summarised in Table 3.21.

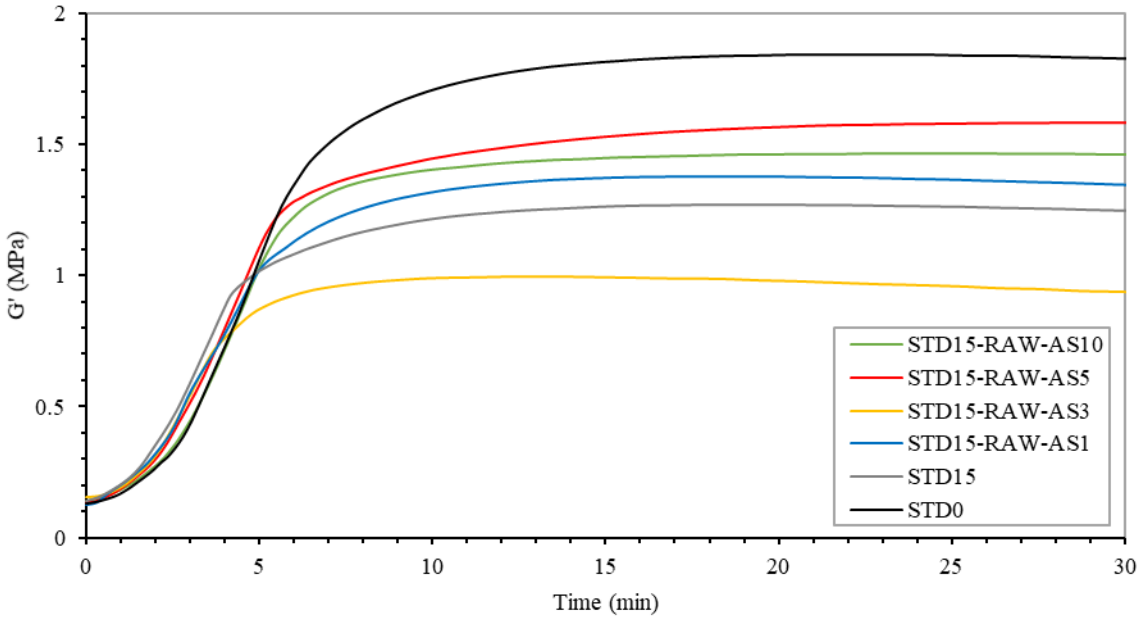

Figure 3.34 DMA curves of compound with 15 phr of bioash modified by stearic acid.

Table 3.21 Data of DMA curves of compound with 15 phr of bioash modified by stearic acid.

DMA data	*u.m.*	***STD0***	***STD15***	***STD15-RAW AS1***	***STD15-RAW AS3***	***STD15-RAW AS5***	***STD15-RAW AS10***
G' max	MPa	1.84	1.27	1.38	1.00	1.58	1.46
G' min	MPa	0.13	0.14	0.13	0.16	0.14	0.14
ΔG' dec.	%	6	8	9	12	1	2
t vulc.	min	22	20	19	14	24	24
t 90	min	4.8	3.2	3.8	3.3	4.4	4.1

In this case, 1% of stearic acid seems not resulting in a big difference respect its absence but yet with 3% of stearic acid, final modulus changes drastically becoming lower.

With 5 and 10% of stearic acid in 15 phr of bioash in compounding there is an increase of modulus that comes close to the compound without bioash.

The rate of vulcanization also is closer to value of standard compound.

The improvement of the compound with modified bioash respect to the compound with raw bioash is remarkable in the tensile test too, the curves are presented in the Figure 3.35 below and the main feature summarized in the Table 3.32.

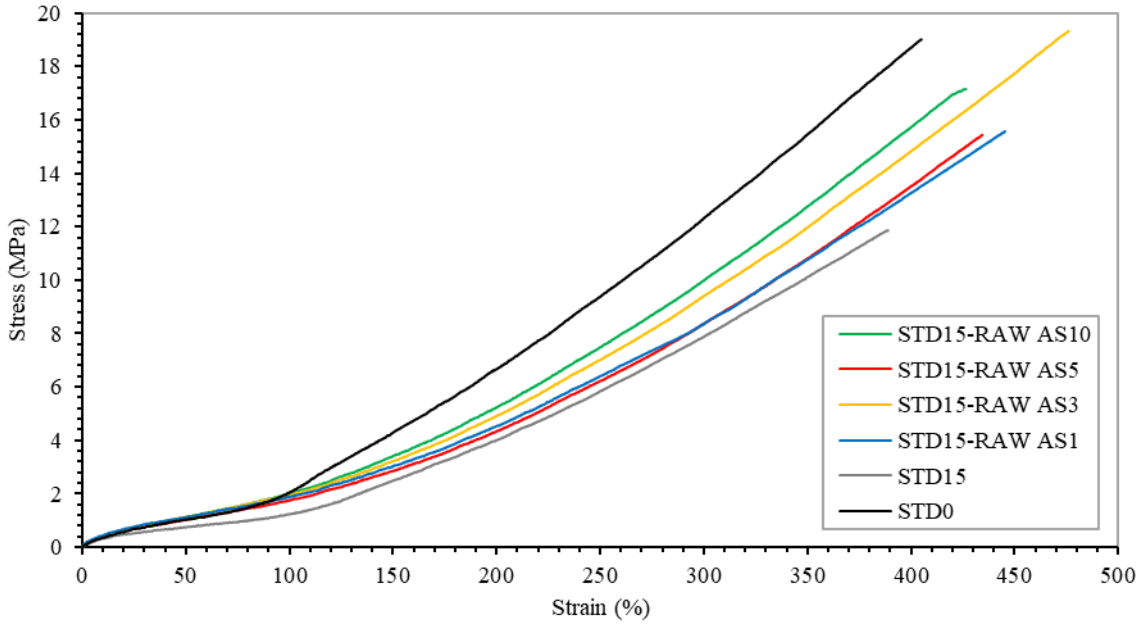

Figure 3.35 Stress-strain curve of compound with 15 phr of bioash modified by stearic acid

Table 3.22 Data of stress-Strain curve of compound with 5 phr of bioash modified by stearic acid.

Tensile data	*u.m.*	***STD0***	***STD15***	***STD15-RAW AS1***	***STD15-RAW AS3***	***STD15-RAW AS5***	***STD15-RAW AS10***
σ_b	MPa	17.8 ±1.9	10.8 ±1.0	15.6 ±2.0	17.8 ±0.7	16.1 ±1.3	14.8 ±1.1
ε_b	%	378 ±27	368 ±26	432 ±14	459 ±10	443 ±25	409 ±16
M 50%	MPa	1.47 ±0.09	0.48 ±0.35	0.48 ±0.07	0.58 ±0.09	0.56 ±0.06	0.80 ±0.27
M 100%	MPa	2.74 ±0.34	0.94 ±0.35	1.30 ±0.13	1.45 ±0.11	1.38 ±0.10	1.73 ±0.34

M 200%	MPa	7.26 ±0.62	3.85 ±0.52	4.16 ±0.39	4.43 ±0.26	4.20 ±0.37	4.96 ±0.56
M 300%	MPa	13.23 ±0.85	7.81 ±0.80	8.46 ±0.85	8.99 ±0.37	8.42 ±0.68	9.69 ±0.76

To sum up, the compound with 5phr of the modified bioash is not significative to observe a modification in the final product compared to compound with raw bioash.

Increasing the presence of bioash up to 15phr, an improvement on the effects of the modified bioash, compared to usage of untreated bioash, can be monitored.

However, both in case of 5 and 15 phr of the modified bioash, the stress resistance is lower than standard compound.

In fact, the complete $CaCO_3$ hydrophilization using stearic acid surface treatment is still a distant goal, this can result in the formation of voids and void coalescence which is one of the most common defects in the compound with the bioash.

The presence of voids, even at a very low volume fraction, can significantly damage the material properties.

Very fine $CaCO_3$ particles were to be used to minimise the negative effects of void coalescence, but these particles have a strong tendency to agglomerate [54].

In fact, the dispersion grade analysis shows that the lower particle of RAW AS10, resulting from size dimensional analysis (Table 3.17), does not overlap with the compound with smaller size of agglomerates as can be seen in the Figure 3.36.

The presence of particles with size up to 24 µm is consistence in the STD15-RAW AS10.

The grade of dispersion increases compared to the compound with the raw bioash but, on the other hand, the agglomerate dimension is higher.

The details are available in the Table 3.23.

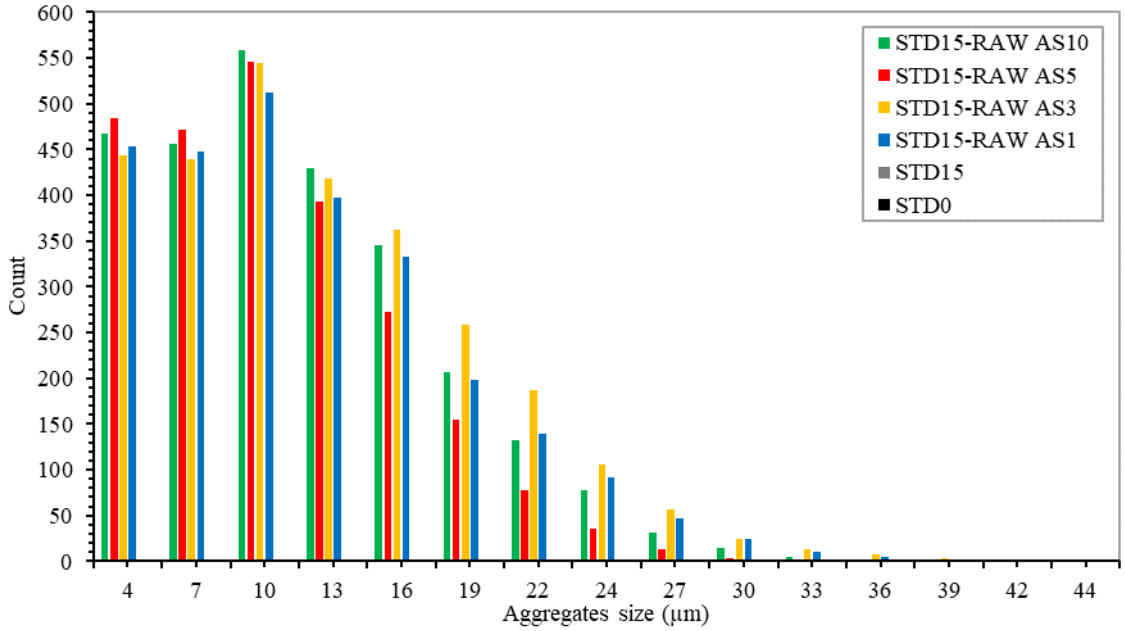

Figure 3.36 Dispersion grade analysis of compound with bioash modified by different percentages of AS.

Table 3.23 Data of dispersion grade analysis of compound with bioash modified by different percentages of AS.

	u.m.	***STD15-RAW AS1***	***STD15-RAW AS3***	***STD15-RAW AS5***	***STD15-RAW AS10***
Dispersion grade	%	93.6	92.0	98.5	96.0
Agglomerate mean size	µm	10.8	11.3	9.4	10.4

To sum up, the optimum amount of stearic acid to use with 15 phr of bioash, seems to be 3% by weight of bioash.

Even if, the final properties of the compound with the modified bioash are not the same of the compound without bioash, there is an improvement using bioash modified by a low percentage of stearic acid: around 3%.

3.3.3. Feature of bioash modified by oleic acid (RAW AO)

The addition in the compound of bioash modified by stearic acid results in better rubber properties than the case of the compound with raw bioash but it is not yet comparable to the properties of compound without bioash.

And so, effects of another similar agent are investigated: oleic acid.

The oleic acid differs from stearic acid for the presence of a double bond along the long organic chain, between C_9 and C_{10}, that makes the acid molecule more reactive but less hydrophobic and bulkier. The literature suggests the usage of oleic acid percentage of oleic acid 7% by weight of bioash [55].

To be sure of the right amount of needed oleic acid and to do a comparison to the data of bioash modified by stearic acid, bioash treated by 5 and 10% by weight of oleic acid is discussed in this study, the process of functionalization is presented in the chapter § 2.7.3. FT-IR spectra of the modified bioash shows adsorption of oleic acid on the bioash surface (Figure 3.37).

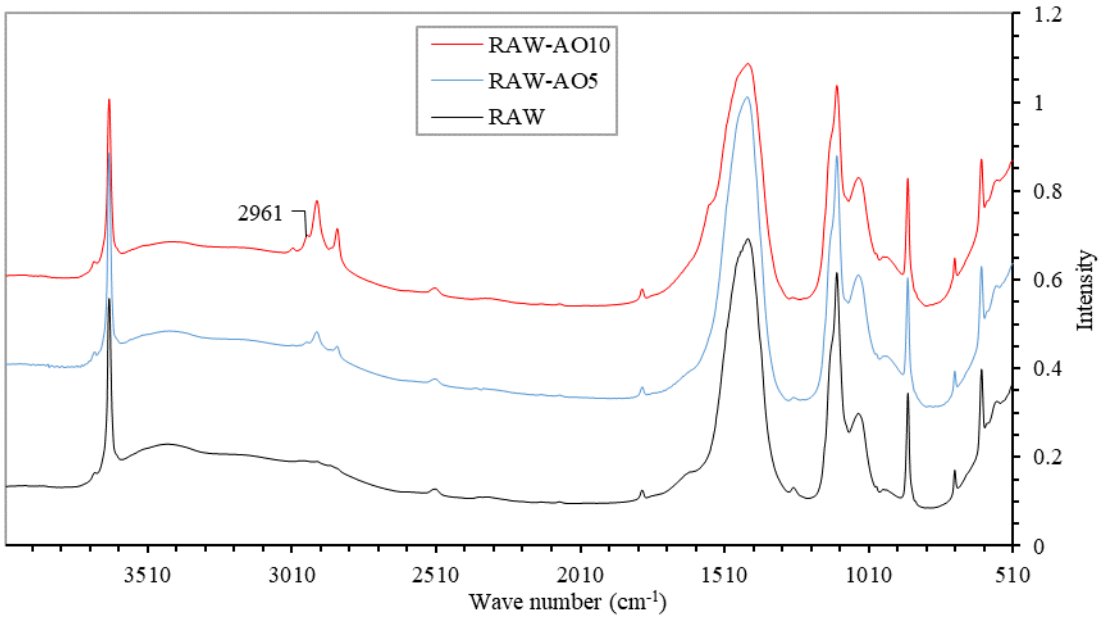

Figure 3.37 FT-IR spectra of raw bioash treated with 5 and 10% in weight of oleic acid and referment

Shape of the spectra is the same for bioash treated with 5 and 10 percentage of oleic acid (RAW AO), the intensity of the peaks increases, increasing oleic acid content.

To better understand the difference with the FT-IR of untreated bioash, the RAW AO graphs are compared to the spectra of the raw bioash.

The spectra of the bioash modified by oleic acid does not differ much from the spectra of the bioash treated by stearic acid (Figure 3.27), except for a small peak appeared at 2961 cm^{-1}, which is referred to asymmetrical stretching of methylene group ($–CH_2–$).

The typical peaks of oleic acid are located at 2930 and 2850 cm^{-1} and they refer to stretching vibrations of C–H bond in the $–CH_3$ and $–CH_2$ groups [56].

Stretching vibrations of C=C usually appear at 1667-1640 cm^{-1}; however, due to low amount of acid adsorption on the surface, C=C stretching vibrations was not detected in the FTIR spectrum of the modified bioash [57].

Comparison of the FTIR spectra of the bioash modified by stearic and oleic acids shows that stearic acid has more interactions with the bioash surface which resulted in higher adsorption. This observation is in line with the higher hydrophilicity of stearic acid than oleic acid, previously discussed [39].

The lower adsorption of oleic acid molecules than steric acid, can be related to their structure: the presence of double bond in hydrocarbon tail, tends to lie the acid in a nonlinear fashion reducing the interaction between hydrocarbon chains. Thus, the oleic acid occupies larger surface area on the bioash surface compared to stearic acid, reducing its capabilities to be adsorbed (Figure 2.28). This means that the dissociation and the acidity strength of stearic acid is higher than oleic acid. All these parameters facilitate higher adsorption of stearic acid than oleic acid on the bioash surface and this resulted in higher wettability alteration in the case of bioash modified by stearic acid [58].

Size Dimension Analysis results are in line with FTIR results: the effect of stearic acid on calcite is more pronounced compared with oleic acid.

By thermogravimetric analysis (TGA § 2.6.4), the right quantity to create a monolayer of oleic acid on bioash surface can be investigate, the graph is shown in the Figure 3.38.

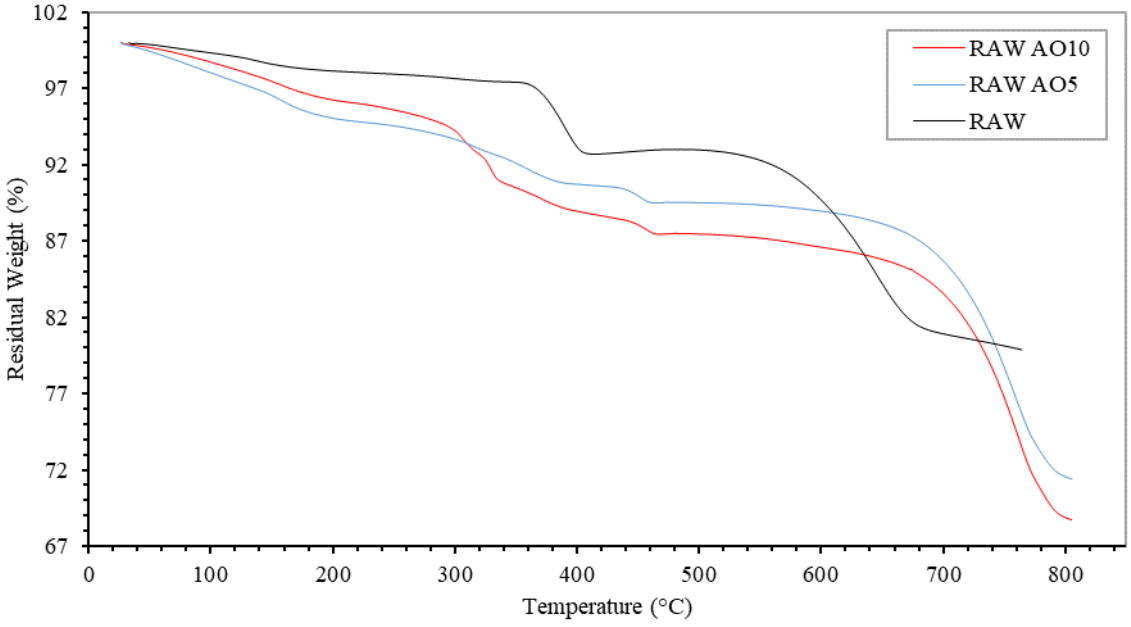

Figure 3.38 TGA curves of bioash modified by 10 and 5% of oleic acid and curve of raw bioash.

Continuous weight loss can be observed over the entire temperature range, and two exothermic peaks appear at 340 and 670°C on the cure of derivate of lost weight. The exothermic peak at 340°C can be attributed to the desorption or combustion of oleic acid molecules, whereas the exothermic peak at 670°C can be attributed to chemical changes of the dehydration of the –OH groups.

In the case of bioash modified by 10% of oleic acid (RAW AO10), a higher percentage of weight lost is notable in the range between 300 and 500°C than bioash modified by 5% of oleic acid, it is associated to higher quantities of physical absorbed material. This excessive presence of oleic acid in RAW AO10, weakly bounded to bioash surface, suggests that the optimal amount of oleic acid needed to cover the bioash surface with a monolayer of organic molecules lies lower than 10% by weight of bioash, in accordance to literature that indicate 7.21 % w/w as the optimum amount of oleic acid to use for bioash modification [55].

The use of excess acid leads to multilayer adsorption in which only a monolayer is chemisorbed, while the others are physiosorbed in a tail-to-tail arrangement.

The use of an optimal amount of functionalizer is not only of economic importance but has also technically advantageous because excessive amounts of surfactant lead to processing problems and inferior mechanical properties as can be also verify from tensile test result in the next sub-chapter [59].

The effect of intermediate layer of oleic acid is reflected in Size Dimension Analysis of the modified bioash. The graph is available in Figure 3.39 and shows the positive effect of oleic acid on the bioash size reduction: the main dimension from 25 μm becomes 2-3 μm (Table 3.24), smaller of about 3 μm than case of stearic acid (Table 3.17), and again the presence of fatty acid increases as well as the main grain dimension decreases. On the other hand, the median values are higher than the case of stearic acid.

It means that the good efficiency in size reduction affects a lower number of grains, it may be due to not homogeneity of functionalization since the consistency of oleic acid is like a gel, so its processability is more difficult and due to the lower adsorption of oleic acid molecules discussed in FT-IR analysis: the presence of double bond, in hydrocarbon tail, tends to lie the acid in a nonlinear fashion reducing the available space for the interaction.

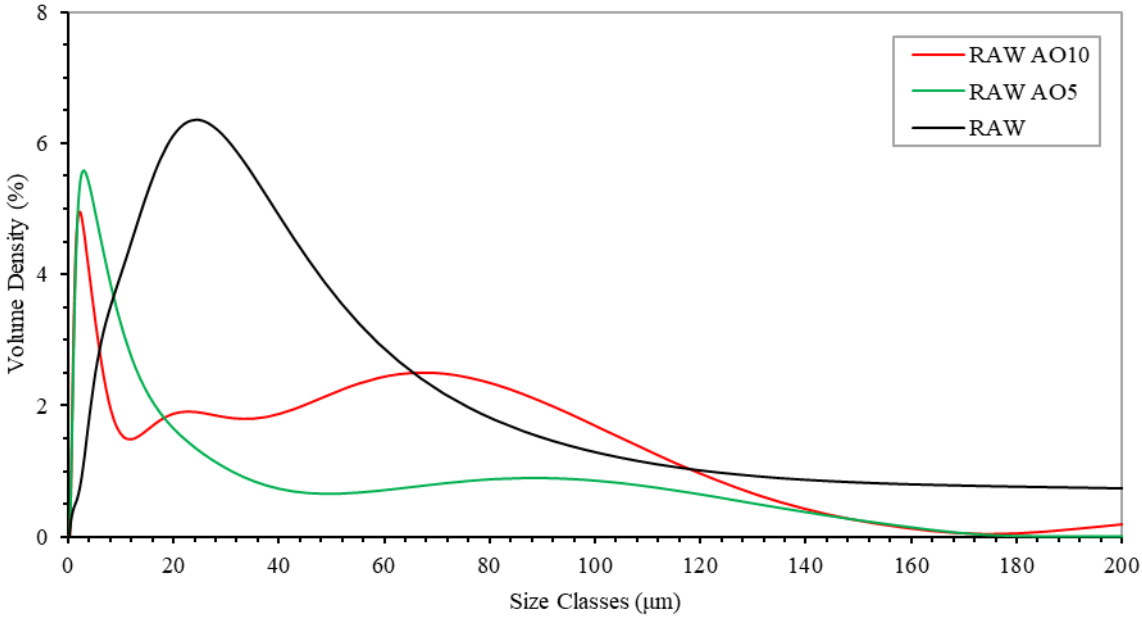

Figure 3.39 Size Dimension Analysis graph of bioash modified by oleic acid.

Table 3.24 Size Dimension Analysis data of bioash modified by oleic acid.

	u.m.	*RAW*	*RAW AO5*	*RAW AO10*
Mode	µm	25.7	2.9	2.3
Median	µm	9.2	7.2	13.6
D[3/2]	µm	7.9	2.5	2.7
Specific Area	m^2/kg	755	2'372	2'214

To sum up, the ability of oleic acid to interact with the bioash surface is less compared to stearic acid but the presence of double bonds gives to oleic acid a higher reactivity that can be verify by the properties of rubber compound, discussed in the next sub-chapter.

3.3.4. Features of compound with bioash modified by oleic acid

The effects of bioash modified by oleic acid on the properties of the rubber compound are discussed in this sub-chapter.

Again, the quantities of functionalised bioash adding at the standard compound is 5 and 15 phr, the formulation is available in the chapter § 2.3.2.

The Dynamic Mechanical Analysis (DMA) at 151°C (§ 2.5.1) is performed. The imaginary part of elastic modulus against time is plotted in the Figure 3.40 below and the main data of the curves summarized in the Table 3.25 for compound with 5 phr of modified bioash (STD5-RAW AO), compound with 5 phr of raw bioash (STD5) and compound without bioash (STD0).

The percentage of oleic acid used to functionalise bioash is 5 and 10% by weight of 5 phr of bioash (respectively STD5-RAW AO5 and STD5-RAW AO10).

The quantities of oleic acid and the functionalization process are presented in chapter § 2.7.3.

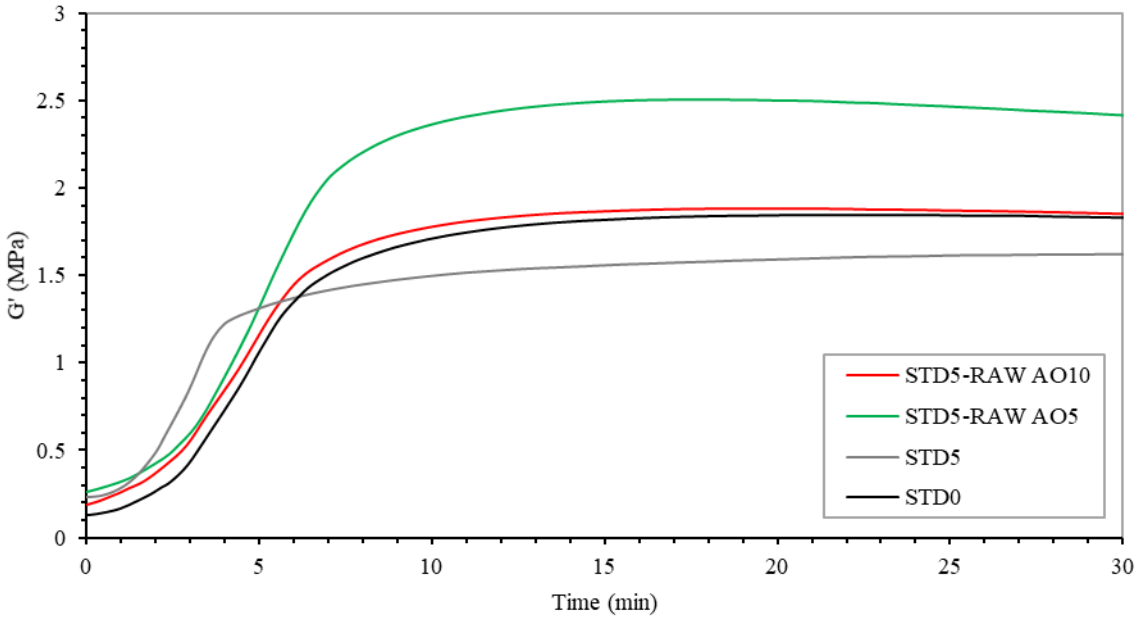

Figure 3.40 DMA curves of compounds with 5 phr of bioash modified by 5 and 10% oleic acid and references.

Table 3.25 Data of DMA curves of compounds with 5 phr of bioash modified by 5 and 10% oleic acid and references.

DMA data	*u.m.*	***STD0***	***STD5***	***STD5-RAW AO5***	***STD5-RAW AO10***
G' max	MPa	1.84	1.62	2.50	1.88
G' min	MPa	0.13	0.23	0.26	0.19
ΔG' dec.	%	6	0	11	6
t vulc.	min	22	25	17	20
t 90	min	4.8	3.2	5.0	4.8

In this case the maximum value of modulus of the compound with the modified bioash is higher than compound with the raw bioash, especially for low percentage of oleic acid (STD5-RAW AO5).

The compound with the bioash modified by higher percentage of oleic acid (STD5-RAW AO10) has a curve more similar at the curve of the compound with the raw bioash.

It is to remember that the low value of modulus for the compound with 5 phr of the raw bioash is due to grains aggregation (§ 3.1.3), in the case of functionalization by oleic acid, it can be supposed that the agglomeration does not occur since the surface of bioash becomes more hydrophobic.

The rate of vulcanization is slightly decreased for the compound with the modified bioash, it suggests a lower grade of cross-linking.

It can be verified by tensile stress, the stress-strain curve is illustrated in the Figure 3.41 below and the main data summarized in Table 3.26.

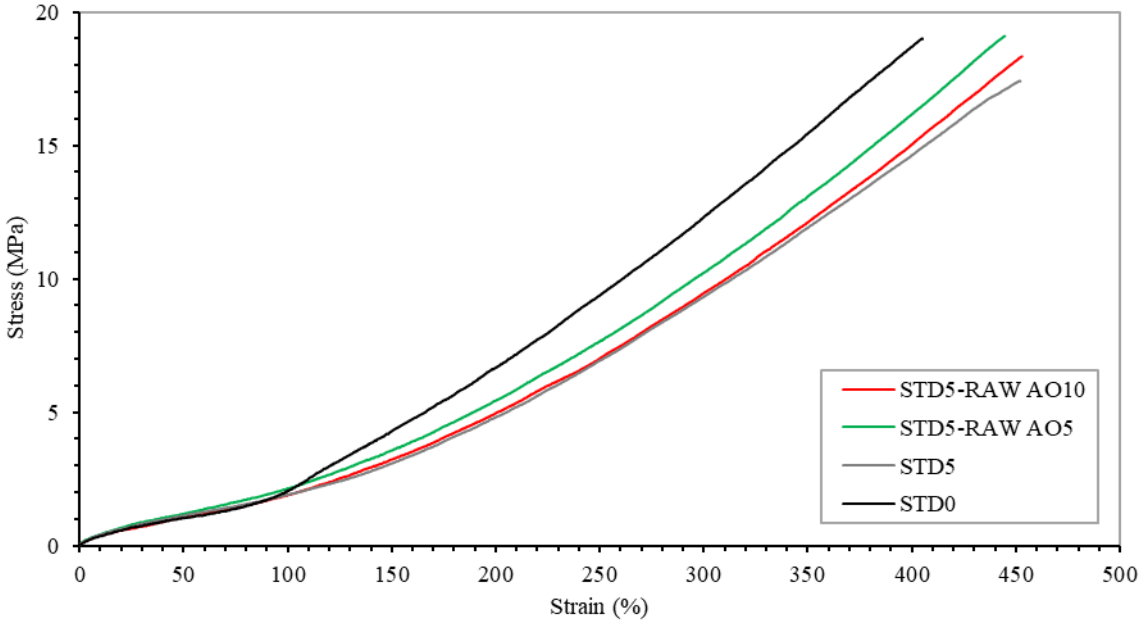

Figure 3.41 Stress-strain curve of compounds with 5 phr of bioash modified by oleic acid and references.

Table 3.26 Data of Stress-stain curves of compounds with 5 phr of bioash modified by oleic acid and references.

Tensile data	*u.m.*	***STD0***	***STD5***	***STD5-RAW AO5***	***STD5-RAW AO10***
σ_b	MPa	17.8 ±1.9	16.7 ±1.4	18.8 ±0.4	18.1 ±0.6
ε_b	%	378 ±27	431 ±28	448 ±5	455 ±7
M 50%	MPa	1.47 ±0.09	1.29 ±0.16	1.11 ±0.02	0.97 ±0.05
M 100%	MPa	2.74 ±0.34	2.21 ±0.18	2.05 ±0.03	1.78 ±0.07
M 200%	MPa	7.26 ±0.62	5.33 ±0.36	5.30 ±0.07	4.75 ±0.18
M 300%	MPa	13.23 ±0.85	9.94 ±0.57	9.93 ±0.19	9.14 ±0.34

Since the oleic acid quantities of 5 and 10% by weight of 5 phr of bioash correspond to a small amount of oleic acid into compound, effects on the properties of the rubber are not so evident.

It can be underlined a slight improvement in the stress resistance of the compound with the modified bioash and a slight increase of deformation at break.

As in the result of DMA, also in the tensile test, the 5% of oleic acid has a higher effort than 10%. It is due to the monolayer formed in case of oleic acid presence under 7.2%, a higher presence of fatty acid decreases the compound properties [55].

Higher presence of modified bioash means higher presence of oleic acid in compound too. And so, the DMA and tensile test are performed in the case of compound with 15 phr of modified bioash by 5 and 10% of oleic acid (respectively STD15-AO5 and STD15-AO10).

The DMA result is illustrated in Figure 3.42 and the main data summarized in Table 3.27.

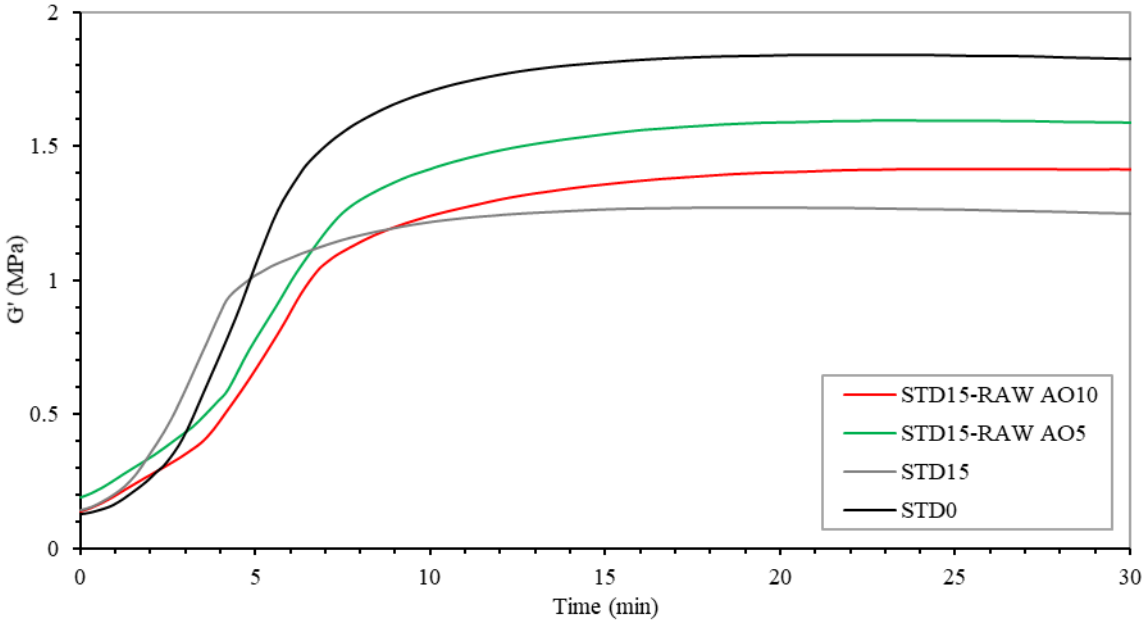

Figure 3.42 DMA curves of compound with 15 phr of bioash modified by 5 and 10% of oleic acid and references.

Table 3.27 Data of DMA curves of compound with 15 phr of bioash modified by 5 and 10% of oleic acid and references.

DMA data	*u.m.*	***STD0***	***STD15***	***STD15-RAW AO5***	***STD15-RAW AO10***
G' max	MPa	1.84	1.27	1.59	1.41
G' min	MPa	0.13	0.14	0.19	0.14
ΔG' dec.	%	6	8	4	3
t vulc.	min	22	20	24	25
t 90	min	4.8	3.2	5.8	5.4

The bioash modification, for compound with 15 phr of bioash, shifts the DMA curve close to the compound without bioash.

Again, the use of 5% of oleic acid results in higher final value of imaginary part of modulus, near to value of standard compound so the better properties of the compound with bioash treated by 5% of oleic acid compared to 10% is verified.

The introduction of oleic acid delays vulcanization reaction as confirmed by an increase in the cure times. This effect is attributed to interaction between the double bonds and the acid OH groups present on the bioash and to the different components of the cure system.

To verify this property tensile test is performed. The graph is depicted in the Figure 3.43 and the main data summarized in the Table 3.28.

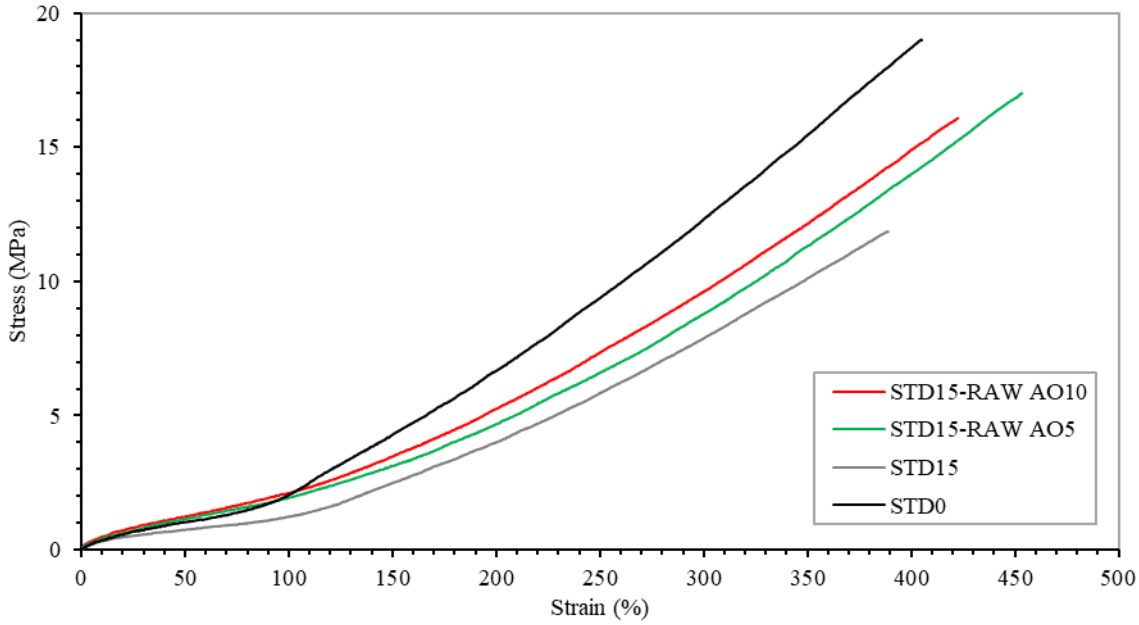

Figure 3.43 Stress-strain curves of compounds with 15 phr of bioash modified by oleic acid and references.

Table 3.28 Data of stress-strain curves of compounds with 15 phr of bioash modified by oleic acid and references.

Tensile data	*u.m.*	***STD0***	***STD15***	***STD15-RAW AO5***	***STD15-RAW AO10***
σ_b	MPa	17.8 ±1.9	10.8 ±1.0	17.0 ±0.3	16.3 ±0.8
ε_b	%	378 ±27	368 ±26	455 ±28	412 ±13
M 50%	MPa	1.47 ±0.09	0.48 ±0.35	1.07 ±0.09	1.10 ±0.06
M 100%	MPa	2.74 ±0.34	0.94 ±0.35	1.93 ±0.14	2.04 ±0.12
M 200%	MPa	7.26 ±0.62	3.85 ±0.52	4.88 ±0.35	5.33 ±0.31
M 300%	MPa	13.23 ±0.85	7.81 ±0.80	9.12 ±0.57	10.01 ±0.58

The stress resistance is higher than in the case of bioash modified by stearic acid as well as the deformation at the break point (Table 3.22), it may be due to higher reactivity of oleic acid compared to stearic acid.

The stress resistance of the compound with the bioash treated by 5% of oleic acid is better than 10% since the percentage of 5% permits the formation of one monolayer of fatty acid on the bioash surface.

The dispersion grade analysis confirms that the better effect on the lower size of agglomeration is reached by STD15-RAW AO5. The improvement is evident especially for particles with dimension higher than 25 µm (Figure 3.44).

The grade of dispersion is 98.4% and the main agglomerate size is 9 µm while for the STD15-RAW AO10 the grade of dispersion is 95.1% and the main agglomerate 9.7 µm.

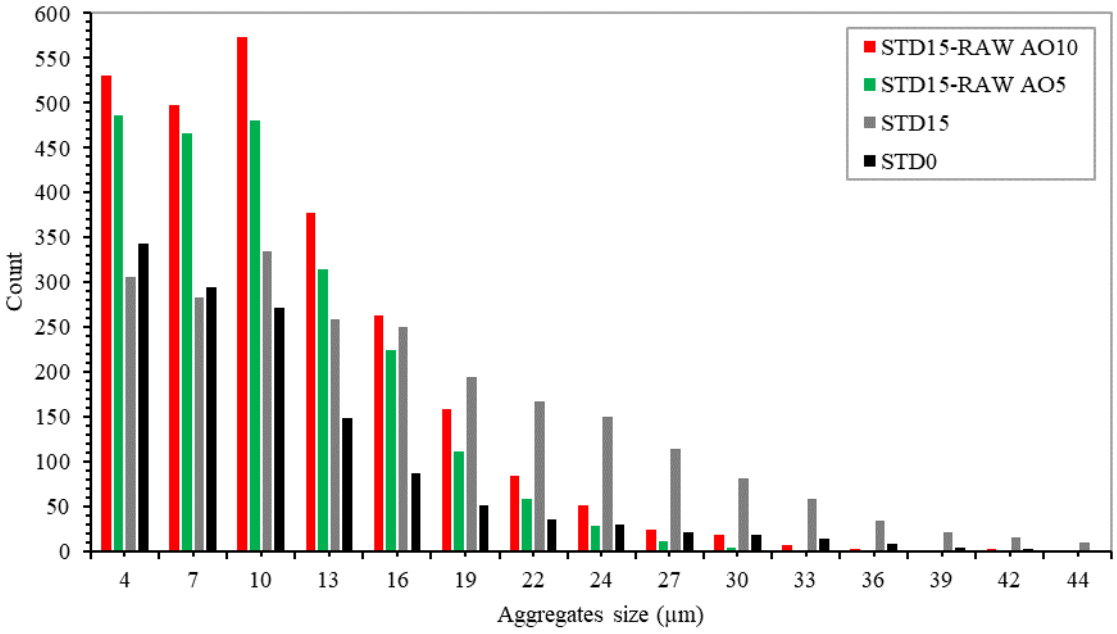

Figure 3.44 Dispersion grade analysis of compound with 15 phr of bioash modified by oleic acid.

To sum up, the optimum quantities of oleic acid to functionalize the bioash is under 10%, the oleic acid is less adsorbed by bioash since its bulky structure, but it is more reactive due to the presence of double bond along its organic chain.

The same tensile properties of the rubber with bioash modified by 5% of oleic acid can be reached used bioash modified by 3% of stearic acid.

Moreover, the process of functionalization by stearic acid is easier since the oleic acid consistence is like a gel and so a reaction in solution is needed (§ 2.7.3) while the stearic acid can be loaded directly in ball mill (§ 2.7.2).

Anyway, the rubber properties are improved compared to the compound with the raw bioash, but the same properties of the standard compound have not been reached yet.

3.4. Effects of bioash modified by silane coupling agent

The presence of calcite and similar in the bioash have suggested the reaction with fatty acid, instead, the presence of iron and silica in the bioash from the current plant suggests the possible reaction with silanes.

The presence of silica in the rubber offers different advantages. These include improvement in tear strength, reduction in heat build-up, and increase in compound adhesion in multi-component products such as tyres. The adverse effect of silica on the curing mechanism of sulphur in NR and SBR can be corrected through the use of silane coupling agents.

An essential prerequisite for a coupling agent is that the molecule must be bi-functional, capable of reacting chemically with both the silica and either directly or indirectly with the polymer chains via participation in the vulcanization reaction or sulphur crosslinking process [60].

The literature implies, as coupling agent, the bis-3-triethoxysilylpropyl (TESPT) (chap. § 2.2.3); since the indication is clear, the only percentage of TESPT that has been studied is 7% by weight of the bioash [41].

The process of this reaction is more complex than in the case of fatty acid since the presence of solvent and catalyst is needed, and so it is more difficult in terms of possible industry application. The steps of bioash functionalization by TESPT is outlined in the chapter § 2.7.4.

Despite the presence of silica in the bioash is low, test results of compound with TESPT can be interesting, so the study is carried out and the outcomes are discussed in this chapter.

3.4.1. Feature of bioash modified by TESPT (RAW TESPT)

The bioash modified by TESPT is characterized.

The first test to understand the occurrence of reaction has been the FR-IT (§ 2.6.2); the result is depicted in the Figure 3.45.

The spectra of modified bioash by TESPT (RAW TESPT) is compared to the spectra of the raw bioash (RAW).

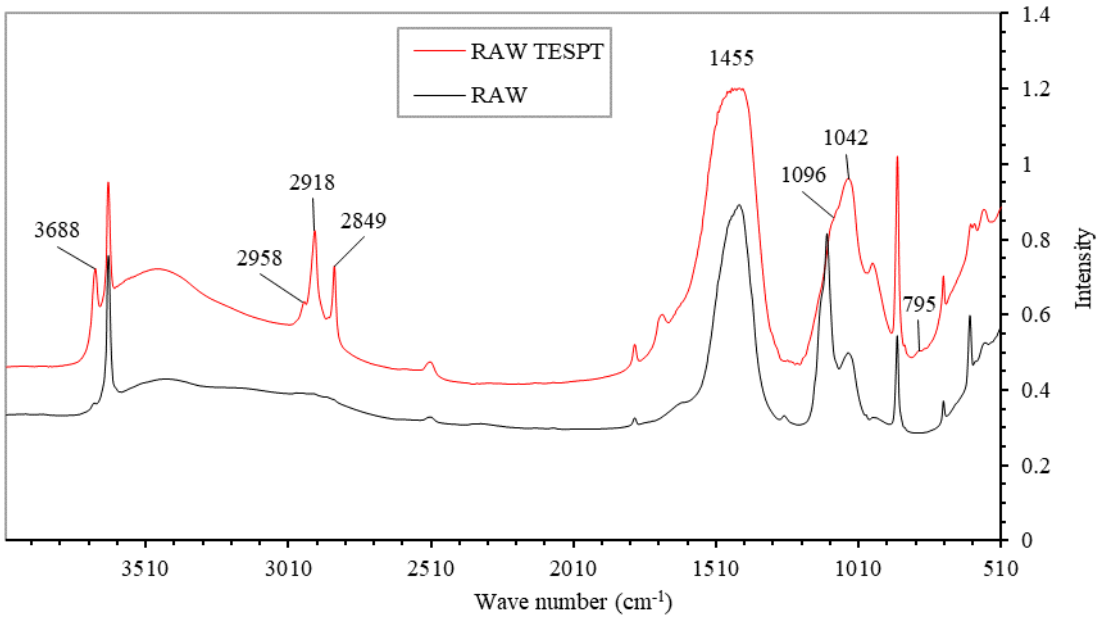

Figure 3.45 FT-IR absorbance spectra of bioash modified by TESPT and raw bioash.

Starting from the left of RAW TESPT spectra, the increase of the peak at 3688 cm^{-1} denotes an increase of OH band. The new peaks at 2958, 2918 and 2849 cm^{-1} in the modified bioash indicate the presence of TESTP, in fact, these groups are also depicted in the spectra of the pure TESPT (Figure A.3).

At 1096 and 795 cm^{-1}, the spectra of RAW TESPT shows significant stretching vibrations, which corresponds to Si=O=Si bond absent in the case of raw bioash [41].

The bioash treated by TESPT demonstrates a much more intense band at 1042 cm^{-1} attributing to C–S–C stretching vibration, while the counterpart from the untreated is observed at 1052 cm^{-1}. The shift of wave number and increase of intensity may be attributed to the introduced Si–O–C bonds in TESPT and the C–S linkages formed between the silane and the rubber matrix.

It was worth noting that the diagnostic characteristic of TESPT, i.e. Si–O–C stretching at approximately 1100 cm^{-1} and 1072 cm^{-1}, is not clearly found in the spectrum, which should have overlapped with the band of C–S–C stretching after being incorporated into the composite [61].

The high presence of peaks between 1500 and 1450 cm^{-1} is due to overlap of raw bioash peak refers to C=O bond with characteristic shape of TESPT spectra.

The spectra of RAW TESPT clearly shows the decrease of the absorption peaks of the methyl groups at 1455 cm^{-1}. This suggests that TESPT reacts by condensation [62].

The appearance of new peaks in the spectra of the bioash modified means that TESPT is chemically bonded with bioash and the total disappearance of some peaks present in the raw bioash spectra indicates that the particles surface is completely covered with the adsorbed TESPT.

The chemical modification of the bioash grains can also be supported from the thermogravimetric analysis (TGA § 2.6.4).

The TGA graph is shown in the Figure 3.46 below.

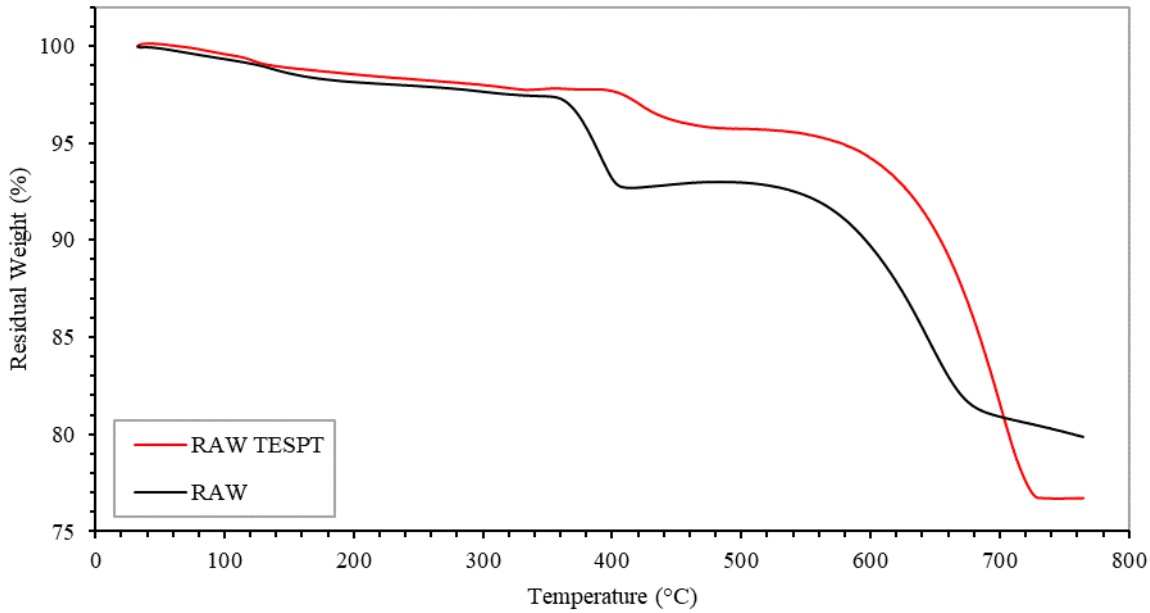

Figure 3.46 TGA graph of the bioash modified by TESPT and raw bioash.

The first observation to do is about the step starting at 370°C in the curve of the raw bioash, absent in the case of the modified bioash, it means that TESPT stabilizes the treated bioash: the TESPT bonds the -OH- groups of bioash and so it hinders the calcination of $Ca(OH)_2$.

The last step of RAW TESPT is higher than RAW, as can be clearly seen in the graph of the derivate of lost weight in the Figure 3.47 at a temperature of 701°C.

The percentage of the final residual weight of the raw bioash is 79.9% while for the modified bioash it is 76.7%. It means that 3.2% of the weight refers to effective TESPT presence in modified bioash.

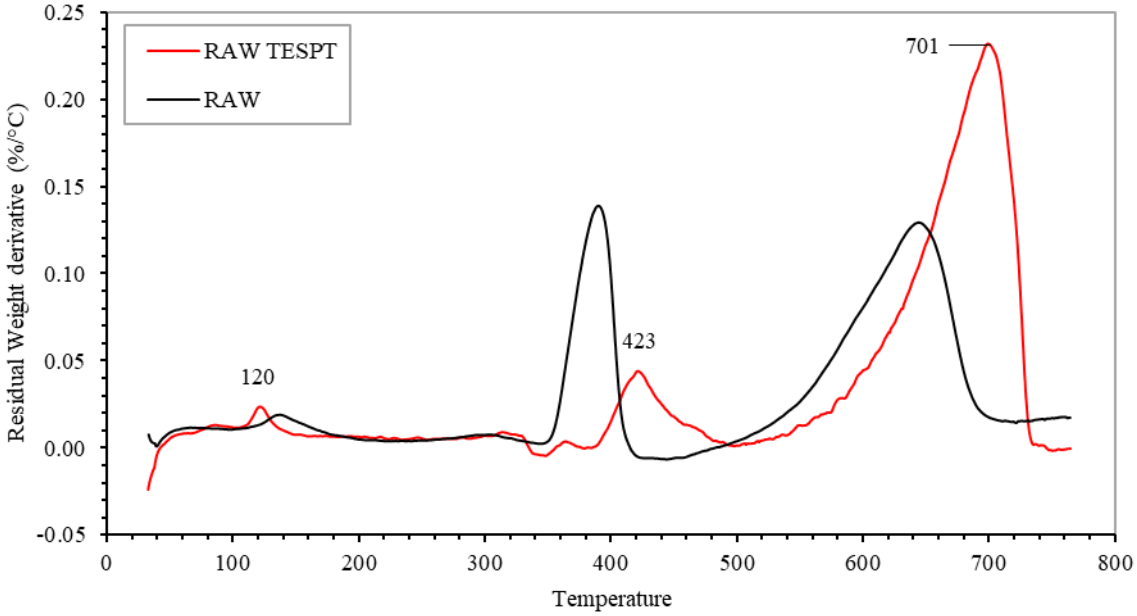

Figure 3.47 Derivates of TGA curves of bioash modified by TESPT and raw bioash.

This great discrepancy, between the temperature ad intensity of peaks in the curves of derivates of weight lost for the raw bioash and the bioash modified by TEST (Figure 3.47), shows that functionalized agent is chemically bonded to the hydroxyl groups of the bioash, rather than a mere physical adsorption.

To verify a possible effect on grains dimension too, the particle size analysis (§ 2.6.5) has been performed. The result is shown in the Figure 3.48 and the main data summarized in the Table 3.29.

The values of the mode and the median of the bioash modified by TESPT are lower than the respective values of the raw bioash but they are not lower that the case of the bioash modified by fatty acid, especially for the presence of many grains with size over 40 μm, almost absent in the bioash treated by fatty acid.

The treatment helps the physical modification of the bioash agglomeration creating fine particles that combine together to form a porous structure [41].

This dissertation justifies the presence of big size particles in granulometry analysis (Figure 3.48).

Effects on the rubber compound are discussed in the next sub-chapter.

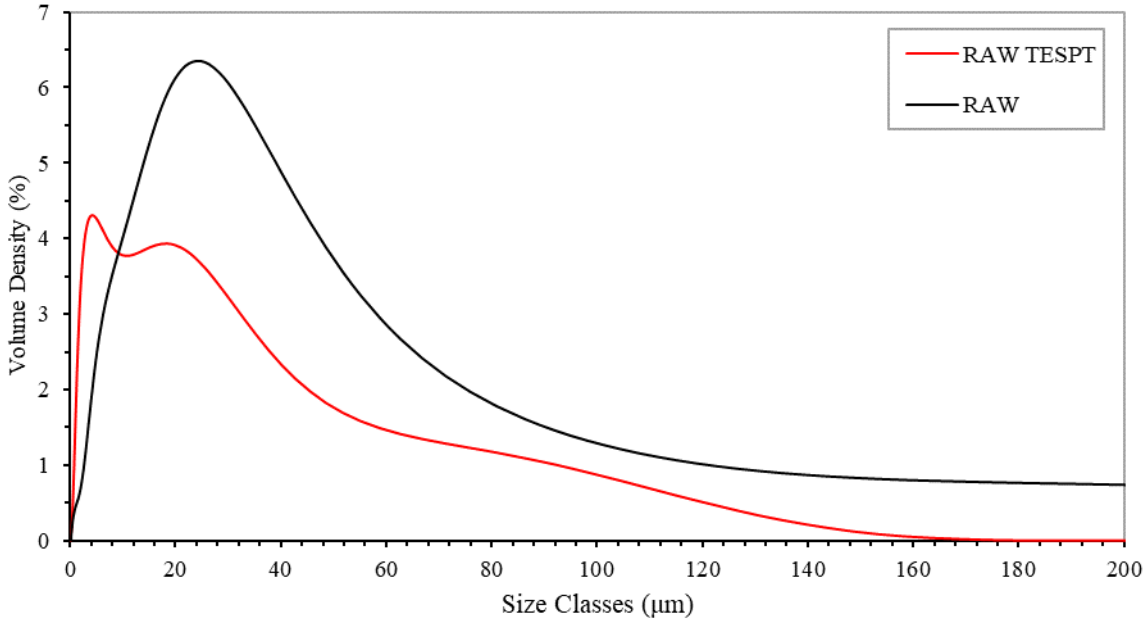

Figure 3.48 Dimension Analysis graph of bioash modified by TESPT and of raw bioash.

Table 3.29 Dimension Analysis data of bioash modified by TESPT and of raw bioash.

Particle size analysis	*u.m.*	*RAW*	*RAW TESPT*
Mode	µm	25.7	4.3
Median	µm	9.2	7.2
D[3/2]	µm	7.9	3.6
Specific Area	m^2/kg	755	1’665

3.4.2. Features of compound with bioash modified by TESPT

The effect of addition in compouding of bioash modified by TESPT on the properties of the final rubber compound are discussed in this sub-chapter.

Again, the quantities of functionalised bioash added at the standard compound are 5 and 15 phr, the formulations are available in the chapter 2.3.2.

The Dynamic Mechanical Analysis (DMA) at 151°C (§ 2.5.1) is performed. The imaginary part of elastic modulus against time is plotted in the Figure 3.49 and the main data of the curves summarized in the Table 3.30 for compound with 5 phr of modified bioash (STD5-RAW TESPT), compound with 5 phr of raw bioash (STD5) and compound without bioash (STD0).

The percentage of TESPT used to functionalise bioash is 7% in weight of 5 phr of bioash as suggested in literature [41].

The functionalization process is presented in chapter 2.7.4.

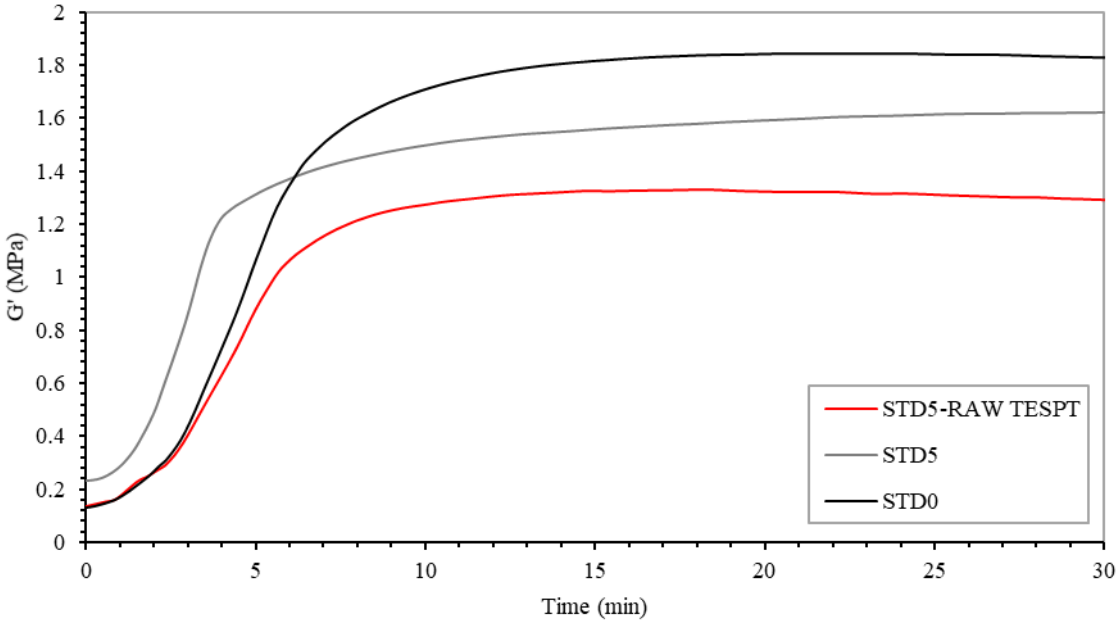

Figure 3.49 DMA curves of compound with 5 phr of bioash modified by 7% of TESPT and references.

Table 3.30 Data of DMA curves of compound with 5 phr of bioash modified by 7% of TESPT and references.

DMA data	*u.m.*	***STD0***	***STD5***	***STD5-RAW TESPT***
G' max	MPa	1.84	1.62	1.33
G' min	MPa	0.13	0.23	0.14
ΔG' dec.	%	6	0	9
t vulc.	min	22	25	18
t 90	min	4.8	3.2	4.40

The effect of the adding of 5 phr of bioash modified by TESPT is a slightly decrease of the final value of the imaginary part of modulus and a small acceleration of the vulcanization time. The result of the tensile test is shown in the Figure 3.50 and the main data summarized in the Table 3.31.

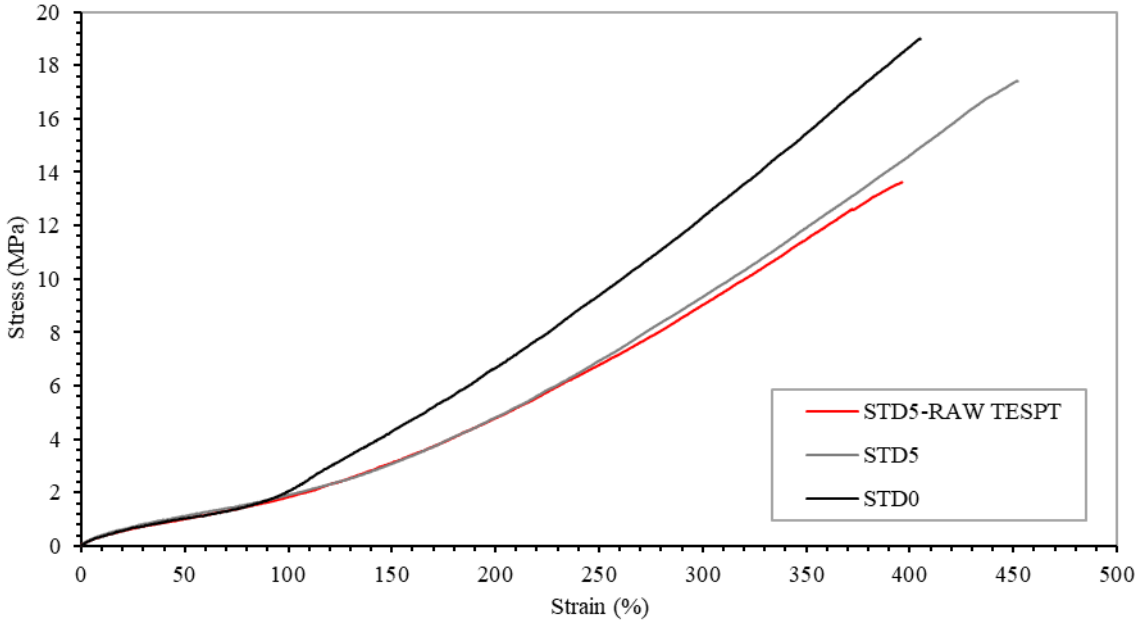

Figure 3.50 Stress-strain curves of compounds with 5 phr of bioash modified by 7% of TESPT and references.

Table 3.31 Data of Stress-Strain curves of compounds with 5 phr of bioash modified by 7% of TESPT and references.

Tensile data	*u.m.*	***STD0***	***STD5***	***STD5-RAW TESPT***
σ_b	MPa	17.8 ±1.9	16.7 ±1.4	14.3 ±0.8
ε_b	%	378 ±27	431 ±28	418 ±17
M 50%	MPa	1.47 ±0.09	1.29 ±0.16	0.48 ±0.05
M 100%	MPa	2.74 ±0.34	2.21 ±0.18	1.28 ±0.09
M 200%	MPa	7.26 ±0.62	5.33 ±0.36	4.19 ±0.27
M 300%	MPa	13.23 ±0.85	9.94 ±0.57	8.43 ±0.48

The result of tensile test shows a very little decreasing in the modulus compared to untreated bioash and a substantial lower stress resistance.

It means that the functionalization of the bioash, with 7% by weight of TESPT, that has been added in the compound results in a very small deviation of the stress-strain curve and in a smaller resistance compared to the case with untreated bioash.

It must be taken in consideration that the press mounding in this case has not been very good: the final product has shown bubbles that become defects in samples for tensile test, and so the worsening of stress resistance can be caused by this inconvenience too.

Since effects have not been so evident, the compound with 15 phr of modified bioash (STD15-RAW TESPT) is tested. The DMA curve is shown in the Figure 3.51 below and the main data summarized in the Table 3.32.

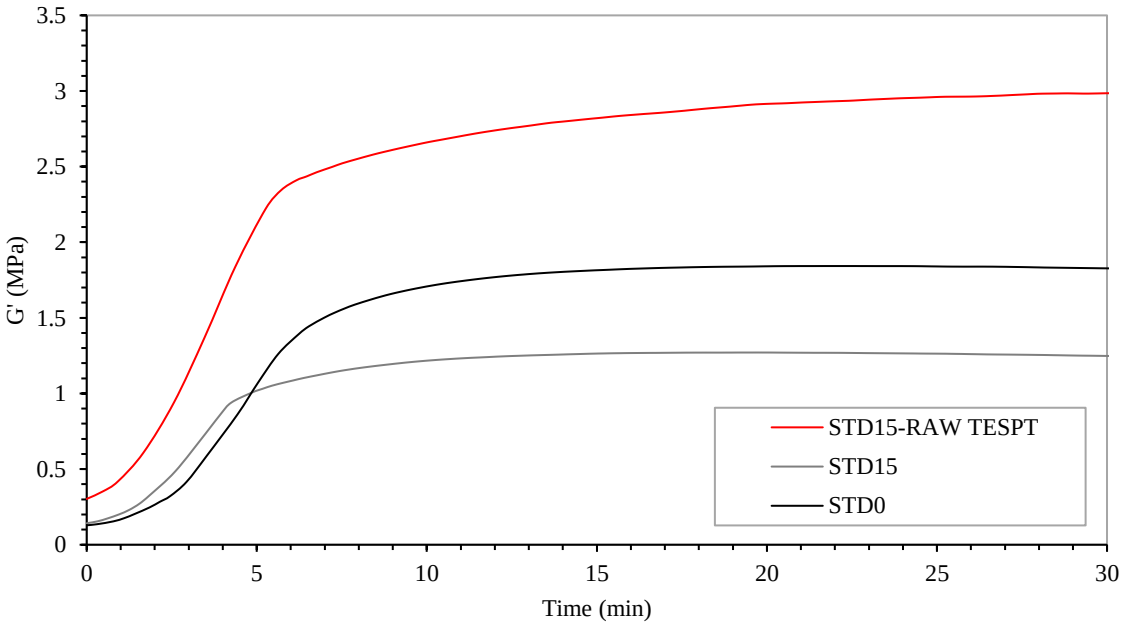

Figure 3.51 DMA curves of compound with 15 phr of bioash modified by 7% of TESPT and references.

Table 3.32 Data of DMA curves of compound with 5 phr of bioash modified by 7% of TESPT and references.

DMA data	*u.m.*	***STD0***	***STD15***	***STD15-RAW TESPT***
G' max	MPa	1.84	1.27	2.99
G' min	MPa	0.13	0.14	0.30
ΔG' dec.	%	6	8	0
t vulc.	min	22	20	22
t 90	min	4.8	3.2	3.8

In this case the imaginary part of modulus increases, differently from the case with 5 phr, maybe due to the higher presence of silane in the compound.

This behaviour is observed in literature too, it shows that a silane coupling agent can be used to improve the processability of the composites particularly at higher filler loading [63]. The vulcanization time is not so different from the case without TESPT.

To verify the more evident effects of the higher presence of the TESPT in the rubber compound the tensile test is performed. The stress-strain curve is depicted in Figure 3.52 while the main data summarized in Table 3.33.

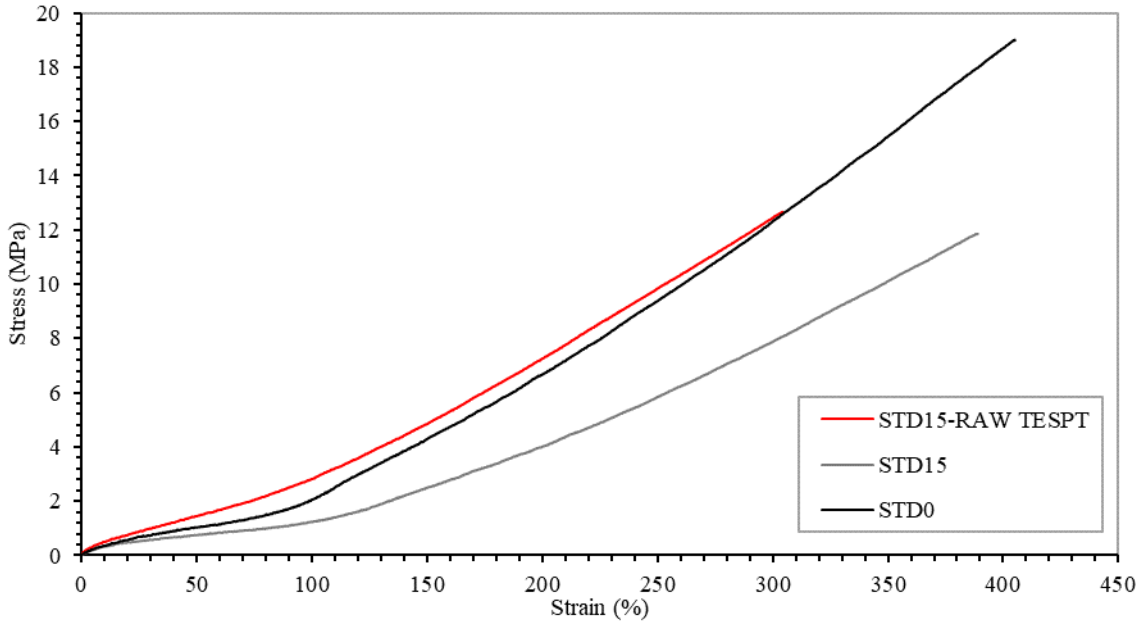

Figure 3.52 Stress-strain curves of compounds with 15 phr of bioash modified by 7% of TESPT and references.

Table 3.33 Data of Stress-strain curves of compounds with 15 phr of bioash modified by 7% of TESPT and references.

Tensile data	*u.m.*	***STD0***	***STD15***	***STD15-RAW TESPT***
σ_b	MPa	17.8 ±1.9	10.8 ±1.0	13.7 ±1.3
ε_b	%	378 ±27	368 ±26	318 ±19
M 50%	MPa	1.47 ±0.09	0.48 ±0.35	1.62 ±0.07
M 100%	MPa	2.74 ±0.34	0.94 ±0.35	3.03 ±0.15
M 200%	MPa	7.26 ±0.62	3.85 ±0.52	7.53 ±0.28
M 300%	MPa	13.23 ±0.85	7.81 ±0.80	12.90 ±0.37

In the case of STD15-RAW TESPT, result is better than the case with 5 phr, in fact the modulus value is similar to the case of compound without bioash, but also the bad stress resistance is verified: the break happens by 4 MPa less compared to the case of the standard compound.

In fact, the reduction in surface energy helps the filler dispersion in the compound by reducing silica agglomerations, but it weakens adhesion between the rubber and the filler and hence reduces the reinforcing capability of the filler [64].

The decrease of elasticity indicates the segmental immobility of the macromolecules after the treatment, in fact, chemical crosslinking occurs between the dissociated TESPT and the rubber molecules [61].

In general, silane coupling agent such as bis-3-triethoxysilyl-propyl-tetrasulfide (TESPT) is used to improve the silica dispersion as well as to prevent adsorption of curatives on the silica surface. The silane coupling agent reacts with silanol on the silica surface and then a siloxane bond is formed. The silane molecule is bound to the silica surface. TESPT makes bound rubber formation of carbon black-filled and silica-filled rubber compounds enhance, especially in silica-filled rubber compounds.

In the present study the surface to modify is the bioash surface that contain silica, but in a small quantity. The higher presence of the bioash corresponds to higher possible presence of silica and it can explain the better results in mechanical properties of the compound with 15 phr of bioash than the compound with 5 phr of bioash [65].

On the other hand, the TESPT that is not bounded to bioash can be bound to carbon black and natural rubber (§ 2.2.3).

The interaction of TESPT with silane of bioash, carbon black and natural rubber should be result in a good dispersion in the compound.

In fact, the dispersion grade analysis shows higher presence of small particles, up to 15 µm, respect to the bigger agglomerates (Figure 3.53).

The dispersion grade is 97.3 %, while the mean dimension of agglomerate is 9.2 µm.

The silane coupling agent improves the dispersion of bioash in the rubber matrix and the interfacial adhesion between the bioash particles and the rubber chains was enhanced as a result of the sulphur atom of TESPT participating in the vulcanization reaction, in accordance with literature [66].

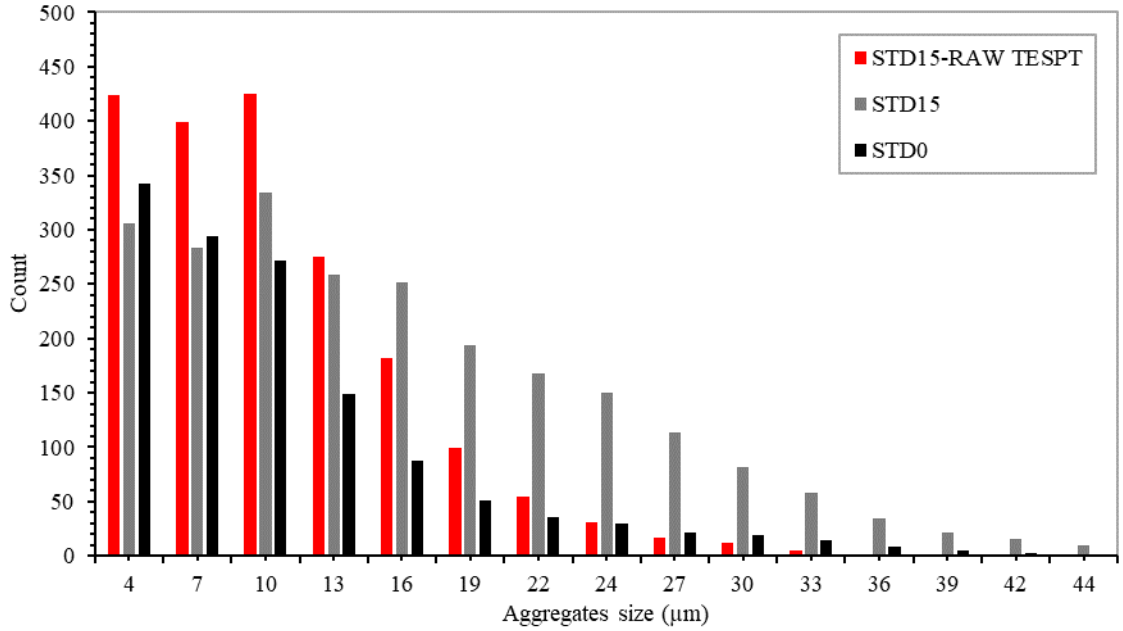

Figure 3.53 Dispersion grade analysis of compound with 15 phr of bioash modified by TESPT and references.

To sum up 15 phr of bioash modified by TESPT can be used to have the same mechanical properties of the compound without bioash but only for low stress since the stress resistance of compound with bioash modified by TESPT is lower than stress resistance of the standard compound.

3.5. Effects of gMAH compatibilizer

The modification of bioash by functionalized agent has given better results in mechanical properties of the final compound than the compound with the raw bioash but the properties are not yet the same of the standard compound.

And so, a directly action on compounding process has been tried. Following the literature information, the polyisoprene-graft-maleic anhydride (gMAH) is added in the compound formulations.

Maleic anhydride is grafted on the double bond of the rubber hydrocarbon. Farmer and Wheeler patented the method of modifying rubber with the maleic anhydride [67].

The reaction of gMAH with bioash in toluene solution has been tried but since the results have been the same of directly loading during compounding and the process is more difficult and longer, this way has not further investigated.

The gMAH has a gel consistence and a structure similar at the natural rubber structure but with a pentacycle with three oxygen atoms that can react with the bioash (§ 2.2.4).

The gMAH acts like a bridge between bioash and natural rubber (NR) matrix.

The improved interfacial adhesion between the bioash and natural rubber matrix may occur via the formation of miscible blends between the NR segments of gMAH and the bulk NR and the formation of hydrogen bonds between the polar part of gMAH and the hydroxyl groups of the bioash in the interfacial region.

3.5.1. Features of compound with the addition of bioash and gMAH

The effects of the introduction of polyisoprene-graft-maleic anhydride (gMAH), during the compound process, on the properties of the final rubber compound are discussed in this sub-chapter.

Again, the quantities of functionalised bioash added at the standard compound are 5 and 15 phr, formulations are available in the chapter 2.3.3.

The details about compounding process in presence of gMAH are presented in chapter 2.7.5.

The Dynamic Mechanical Analysis (DMA) at 151°C (§ 2.5.1) is performed. The imaginary part of elastic modulus against time is plotted in the Figure 3.54 and the main data of the curves summarized in the Table 3.34 for compound with 5 phr of bioash and

double parts of gMAH (STD5-gMAH), compound with 5 phr of raw bioash (STD5) and compound without bioash (STD0).

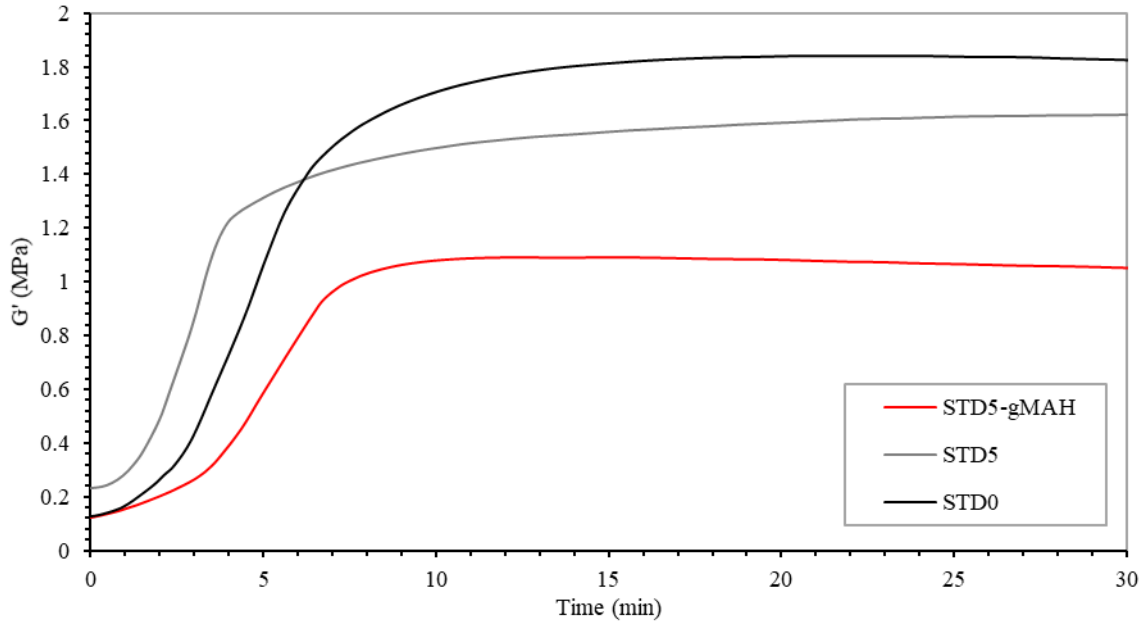

Figure 3.54 DMA curves of compounds with 5 phr of bioash and gMAH compatibilizer, and references.

Table 3.34 DMA data of compounds with 5 phr of bioash and gMAH compatibilizer, and references.

DMA data	*u.m.*	***STD0***	***STD5***	***STD5-gMAH***
G' max	MPa	1.84	1.62	1.09
G' min	MPa	0.13	0.23	0.12
ΔG' dec.	%	6	0	6
t vulc.	min	22	25	13
t 90	min	4.8	3.2	5.1

The effects of the addition of 5 phr of bioash at the compound are a decrease of the final value of the imaginary part of modulus and an acceleration of the vulcanization time.

Probably, the lower value of modulus is due to the lower dispersion of energy at filler-matrix interaction due to stronger interfacial bonds created by compatibilizer.

The mechanical properties is measured by tensile test, the curve is depicted in the Figure 3.55 and the main data summarized in the Table 3.35.

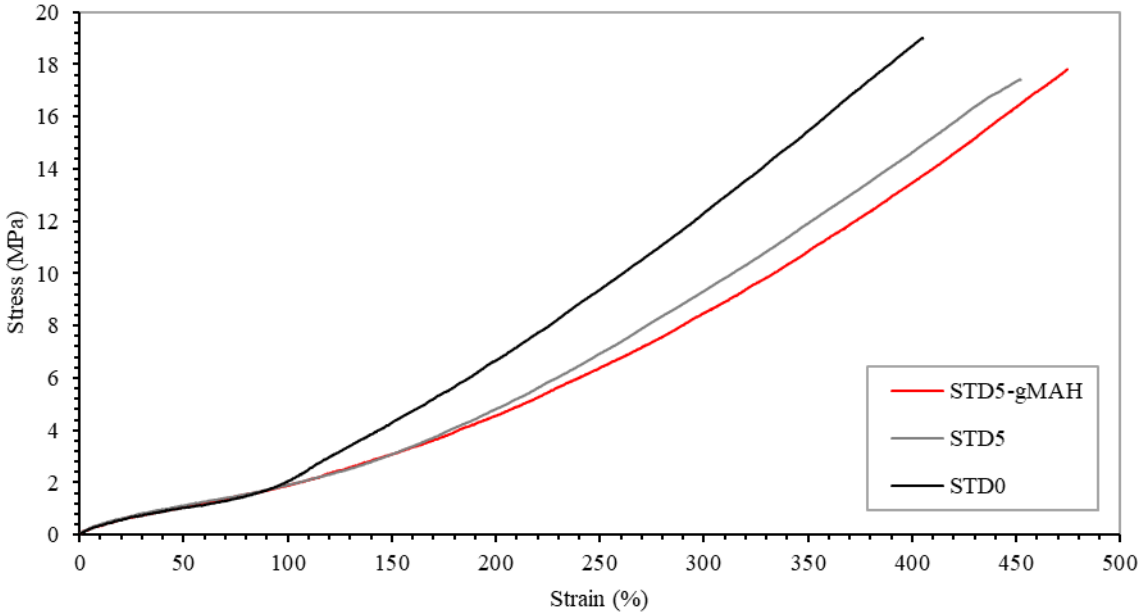

Figure 3.55 Stress-strain curve of compounds with 5 phr of bioash and gMAH compatibilizer, and references.

Table 3.35 Data of the stress-strain curve of compounds with 5 phr of bioash and gMAH compatibilizer, and references.

Tensile data	*u.m.*	***STD0***	***STD5***	***STD5-gMAH***
σ_b	MPa	17.8 ±1.9	16.7 ±1.4	17.9 ±1.7
ε_b	%	378 ±27	431 ±28	470 ±17
M 50%	MPa	1.47 ±0.09	1.29 ±0.16	1.16 ±0.13
M 100%	MPa	2.74 ±0.34	2.21 ±0.18	2.01 ±0.12
M 200%	MPa	7.26 ±0.62	5.33 ±0.36	4.68 ±0.22
M 300%	MPa	13.23 ±0.85	9.94 ±0.57	8.50 ±0.34

The result of stress resistance is quite good, in fact, the value is the same of compound without bioash. This may be attributed to the good compound processability due to the improved polar–polar interaction between the blend components and the filler particles.

On the other hand, in accordance with DMA, the elastic modulus is lower and so the final deformation higher than reference compounds.

To see a bigger effects, the quantities of external agents in the compound are increased. The same test have been done with the compound with 15 phr of the bioash and 30 phr of the gMAH (STD15-gMAH) and compared to compound with 15 phr of the raw bioash (STD15) and the compound without bioash (STD0). The graph of DMA is depicted in the Figure 3.56 below and the main value summarized in the Table 3.36.

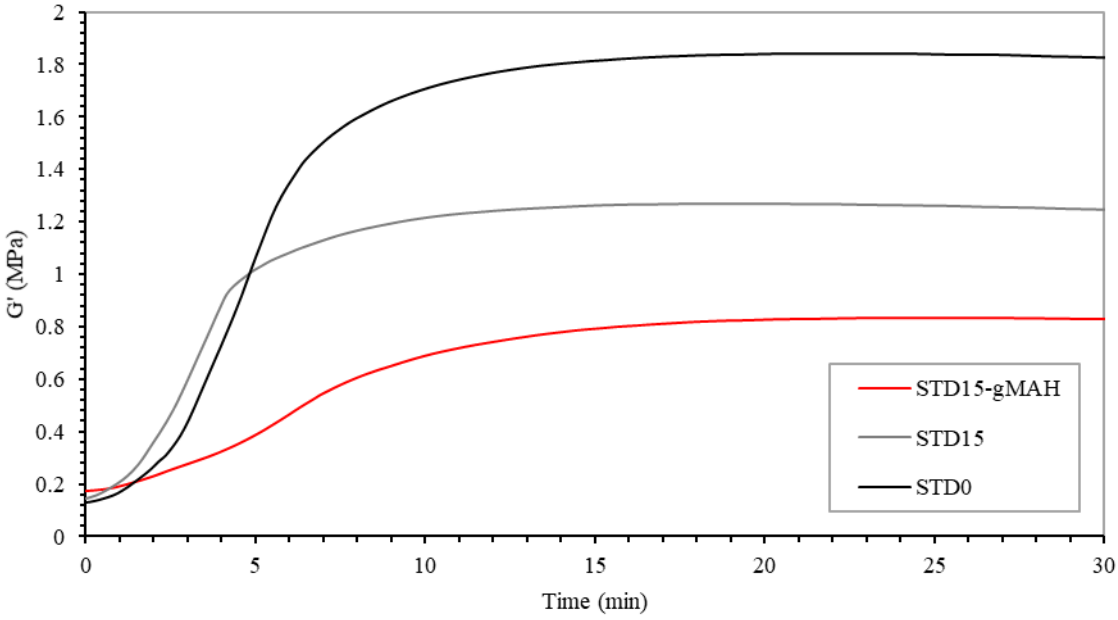

Figure 3.56 DMA curves of compounds with 15 phr of bioash and gMAH compatibilizer, and references.

Table 3.36 Data of DMA curves of compounds with 15 phr of bioash and gMAH compatibilizer, and references.

DMA data	*u.m.*	***STD0***	***STD15***	***STD15-gMAH***
G' max	MPa	1.84	1.27	0.83
G' min	MPa	0.13	0.14	0.18
ΔG' dec.	%	6	8	6
t vulc.	min	22	20	25
t 90	min	4.8	3.2	3.8

As the previous compound, the final imaginary part of the elastic modulus is lower than references, in this case lower than STD5-gMAH too.

On the other hand, the shape of curve is different from the case with 5 phr of bioash: the vulcanization time is increased. This may be attributed to the fact that the

consistence grafting introduces anhydride group on to the rubber compound and anhydrides are known cure retarders. The anhydride not only delay onset of cure reaction they also reduce the cure resulting in hither cure times [68].

The tensile test is performed to explore the mechanical properties of compound. The result is depicted in Figure 3.57 and data summarized in Table 3.37.

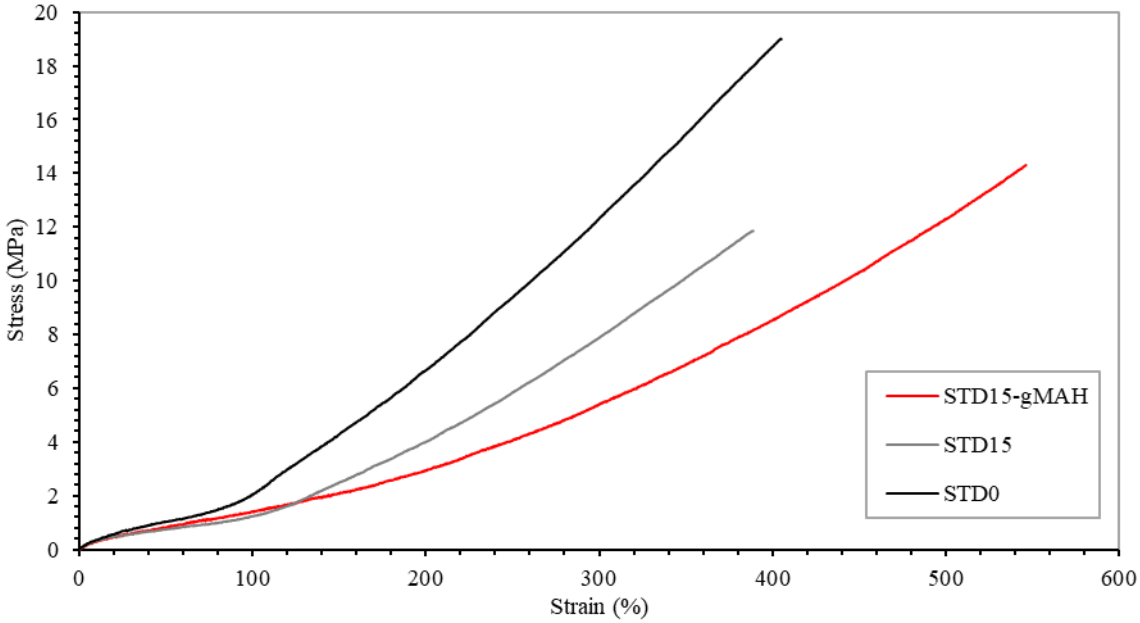

Figure 3.57 Stress-strain curve of compounds with 15 phr of bioash and gMAH compatibilizer, and references.

Table 3.37 Data of stress-Strain curve of compounds with 15 phr of bioash and gMAH compatibilizer, and references.

Tensile data	*u.m.*	***STD0***	***STD15***	***STD15-gMAH***
σ_b	MPa	17.8 ±1.9	10.8 ±1.0	14.4 ±0.8
ε_b	%	378 ±27	368 ±26	559 ±13
M 50%	MPa	1.47 ±0.09	0.48 ±0.35	0.74 ±0.04
M 100%	MPa	2.74 ±0.34	0.94 ±0.35	1.34 ±0.05
M 200%	MPa	7.26 ±0.62	3.85 ±0.52	2.87 ±0.05
M 300%	MPa	13.23 ±0.85	7.81 ±0.80	5.27 ±0.10

The stress resistance is improved compared to the compound with raw bioash but not so much to be similar at properties of the standard compound.

Moreover, the deformation is much higher than reference compounds.

To sum up, the use of gMAH can be a solution to improve the compound the properties of the compound with the raw bioash, considering a decrease of modulus and so a higher deformation but it is not a good solution to reach the result of compound without bioash.

Additionally, the quantities of needed gMAH is quite high and the handling difficult due to its gel like consistence.

The dispersion of particles in compound is not so better that case with untreated bioash as shown in the Figure 3.58 below come from Dispersion Testing Analysis (§ 2.5.4).

The dispersion grade is 95%, while the mean dimension of agglomerate is 9.7 µm.

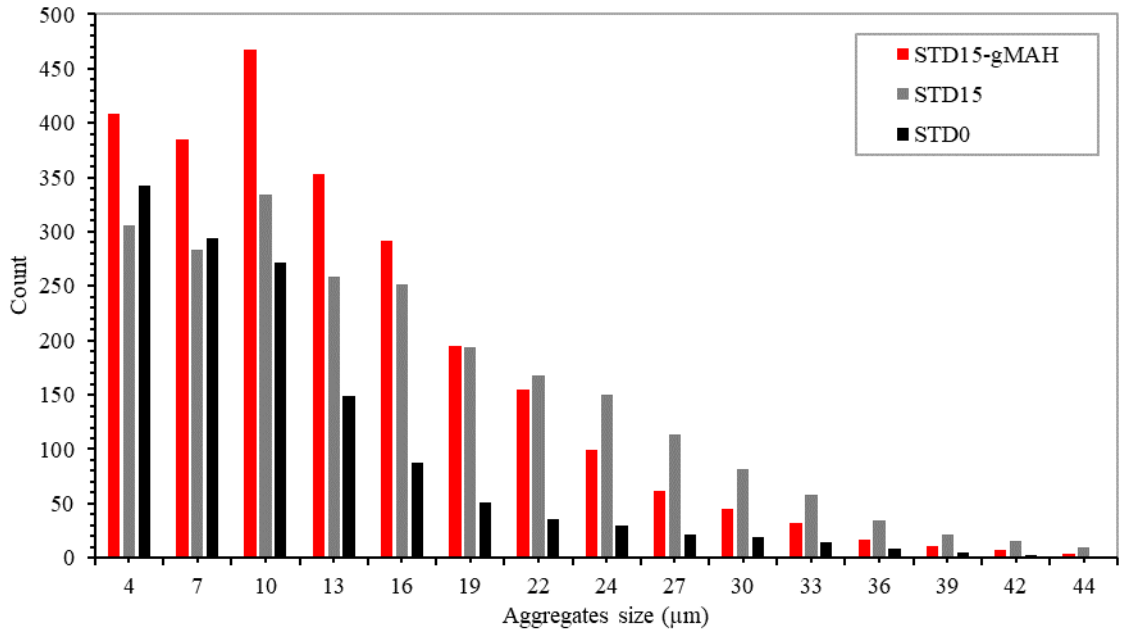

Figure 3.58 Dispersion grade analysis of compounds with 15 phr of bioash and gMAH compatibilizer and references.

3.6. Effects of ENR compatibilizer

To improve the properties of final compound with a compatibilizer directly added during compounding, another solution is investigated: Epoxidized natural rubber 50 (ENR). It is chosen since natural rubber does not contain polar groups in its structure,

The grade 50 of epoxidation is chosen since it is indicated as a better compatibilizer than epoxidation grade 25 (ENR25) [69].

The ENR has a synthetic rubber consistence and a structure similar at the natural rubber but with hydrophilic group along the isoprene backbone (§ 2.2.5).

ENR50 has unique properties such as good oil resistance, low gas permeability, improved wet grip and rolling resistance, coupled with high strength.

However, the market and applications for ENR50 was found to be limited [70].

When the degree of epoxidation is increased, the rubber becomes more polar. This makes ENR more compatible to natural rubber (NR). When the ENR is added in compounding, hydrogen bond between the polar epoxy group of ENR and the polar hydroxyl group of the bioash is formed, while the NR part of ENR forms miscible blend with NR. The improvement of interfacial adhesion between the bioash and the natural rubber can increase the mechanical properties of the final compound as discussed in this chapter.

3.6.1. Features of compound with the addition of bioash and ENR

The effects of the introduction of the epoxidized natural rubber 50 (ENR), during the compound process, on the properties of the final rubber compound are discussed in this sub-chapter.

Again, the quantities of functionalised bioash added at the compound are 5 and 15 phr, formulations are available in the chapter 2.3.4.

The details about compounding process in presence of ENR are presented in chapter 2.7.5.

The Dynamic Mechanical Analysis (DMA) at 151°C (chap. § 2.5.1) is performed. The imaginary part of elastic modulus against time is plotted in the Figure 3.59 and the main data of the curves summarized in the Table 3.38, for compound with 5 phr of bioash and 5 phr of ENR (STD5-ENR), compound with 5 phr of raw bioash (STD5) and compound without bioash (STD0).

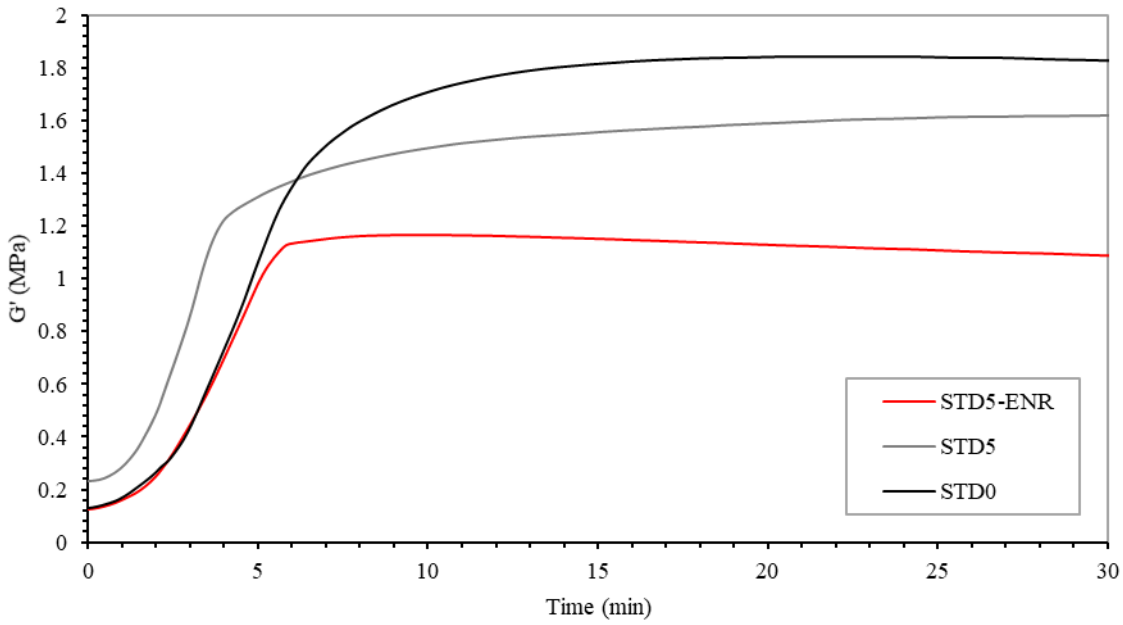

Figure 3.59 DMA curves of compounds with 5 phr of bioash and ENR compatibilizer, and references.

Table 3.38 Data of DMA curves of compounds with 5 phr of bioash and ENR compatibilizer, and references.

DMA data	*u.m.*	***STD0***	***STD5***	***STD5-ENR***
G' max	MPa	1.84	1.62	1.17
G' min	MPa	0.13	0.23	0.13
ΔG' dec.	%	6	0	10
t vulc.	min	22	25	10
t 90	min	4.8	3.2	4.0

As the previous compound with gMAH, the final imaginary part of modulus is lower than references and the vulcanization time decreases.

In fact, the polar functional groups could form hydrogen bonds towards each other resulting in acceleration of the vulcanization process, in accordance with literature [71].

Another notable value is the quite high modulus decadency that suggests a low stability of the compound.

To verify the mechanical properties, the tensile test has been performed.

The resultant graph is shown in the Figure 3.60 and the main data summarized in the Table 3.39

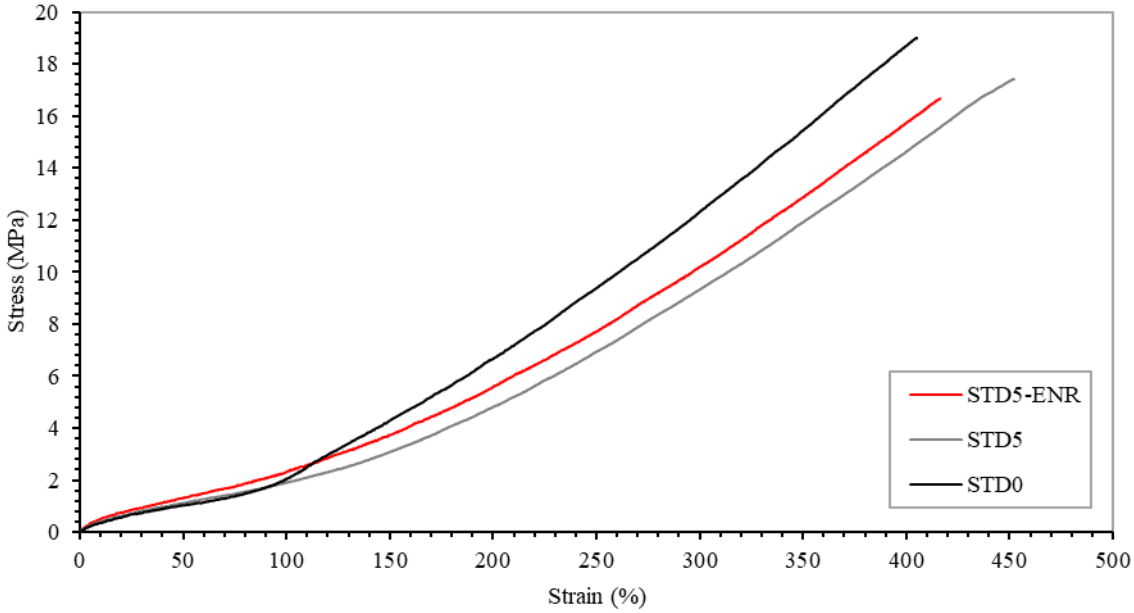

Figure 3.60 Stress-strain curves of compounds with 5 phr of bioash and ENR compatibilizer, and references.

Table 3.39 Data of stress-strain curves of compounds with 5 phr of bioash and ENR compatibilizer, and references.

Tensile data	*u.m.*	***STD0***	***STD5***	***STD5-ENR***
σ_b	MPa	17.8 ±1.9	16.7 ±1.4	16.8 ±0.1
ε_b	%	378 ±27	431 ±28	416 ±5
M 50%	MPa	1.47 ±0.09	1.29 ±0.16	1.32 ±0.06
M 100%	MPa	2.74 ±0.34	2.21 ±0.18	2.30 ±0.10
M 200%	MPa	7.26 ±0.62	5.33 ±0.36	5.55 ±0.16
M 300%	MPa	13.23 ±0.85	9.94 ±0.57	10.14 ±0.23

With the addition of 5 phr of ENR, there is not a big difference with the case of compound with untreated bioash, even if a slightly increase of the deformation at break.

The reinforcing effect, in the first stage of curve, tends to decrease as the strain increases. It occur for high ENR-bioash ratio.

This behaviour can be attributed to formation of chemical bonding between the ENR functional groups and the bioash. That is, during vulcanization process the epoxy groups interact chemically with the hydroxyl groups of the filler surface [72].

A major effect can be appreciated by the addition of 5 phr of ENR at the compound with the presence of 15 phr of bioash (STD15-ENR).

The DMA result is depicted in Figure 3.61 and main value summarized in the Table 3.40.

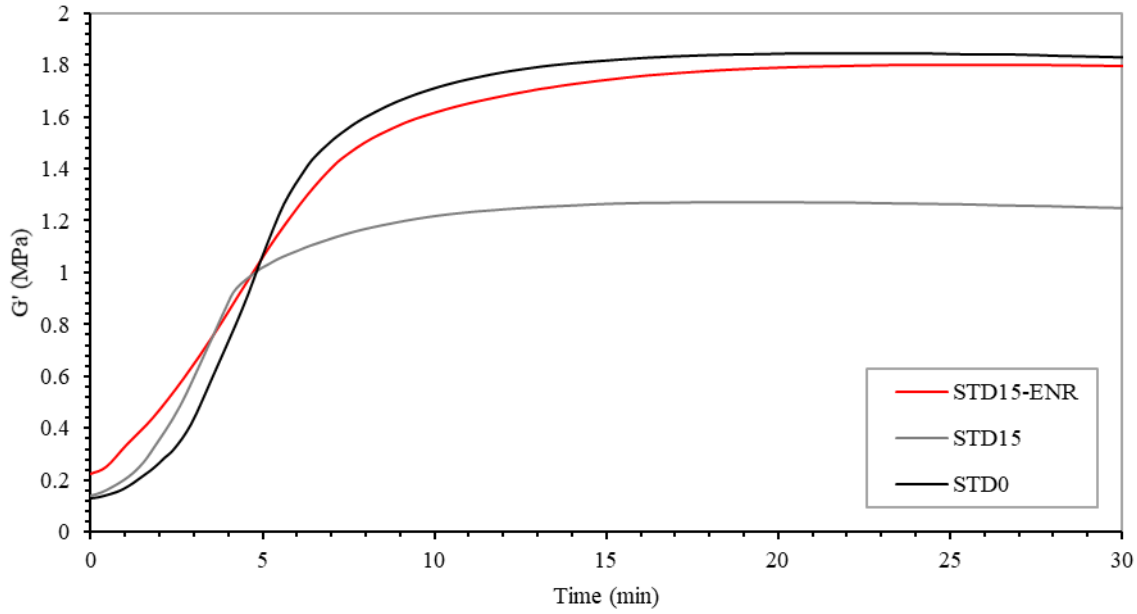

Figure 3.61 DMA curves of compounds with 15 phr of bioash and ENR compatibilizer, and references.

Table 3.40 Data of DMA curves of compounds with 15 phr of bioash and ENR compatibilizer, and references.

DMA data	*u.m.*	***STD0***	***STD15***	***STD15-ENR***
G' max	MPa	1.84	1.27	1.80
G' min	MPa	0.13	0.14	0.22
ΔG' dec.	%	6	8	3
t vulc.	min	22	20	26
t 90	min	4.8	3.2	5.5

The similarity with standard compound (STD0) is evident just from the graph.

The final imaginary part of elastic modulus is similar to the compound without bioash (STD0) and the vulcanization time is slightly higher than STD0.

G' max and G' min values increase with the addition of 5 phr of the ENR in compound formulation modified by 15 phr of bioash. These results suggest that in the presence of ENR, additional crosslinks are formed, giving rise to a sensible increase of the modulus and the crosslinking density compared to previous compounds [73].

Moreover, the modulus decadency shows a lower value, it means a higher thermal stability in accordance with literature [74]; even so, thermal stability of the material can be deeply observed from a shift of the decomposition temperatures in the curve of Thermal Gravimetric Analysis (TGA) or Differential thermal analysis (DTG), not performed in this study.

To appreciate the improvement of the presence of epoxidized natural rubber, the tensile test has been performed. The graph is depicted in Figure 3.62 and the main data summarize in the Table 3.41.

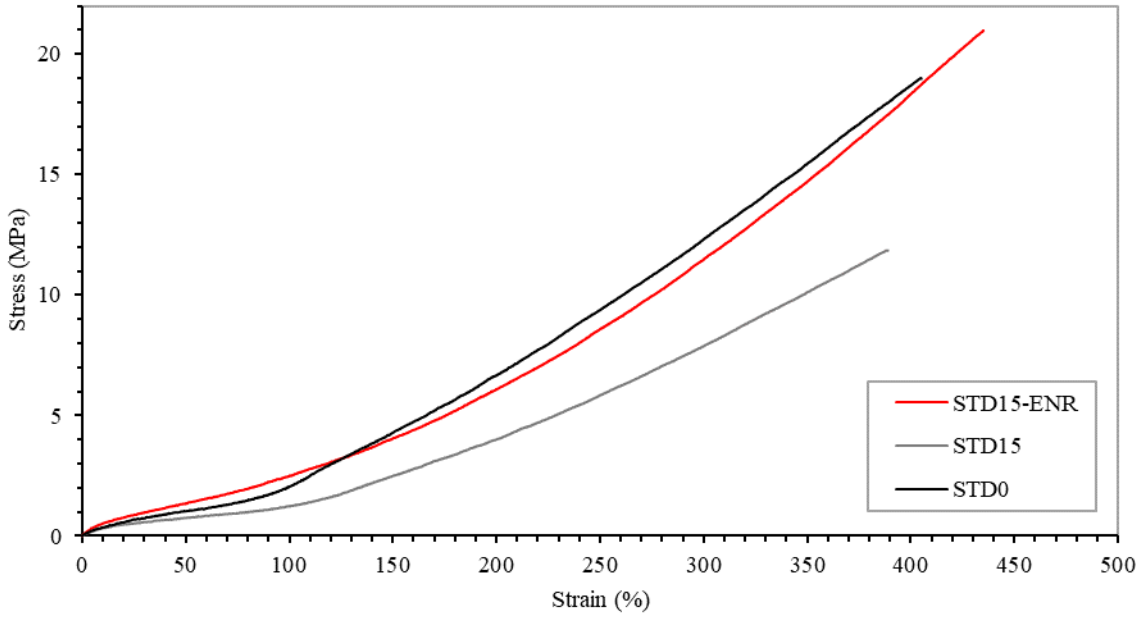

Figure 3.62 Stress-Strain curves of compounds with 15 phr of bioash and ENR compatibilizer, and references.

Table 3.41 Data of stress-Strain curves of compounds with 15 phr of bioash and ENR compatibilizer, and references.

Tensile data	*u.m.*	***STD0***	***STD15***	***STD15-ENR***
σ_b	MPa	17.8 ±1.9	10.8 ±1.0	19.9 ±1.5
ε_b	%	378 ±27	368 ±26	427 ±5
M 50%	MPa	1.47 ±0.09	0.48 ±0.35	1.39 ±0.11
M 100%	MPa	2.74 ±0.34	0.94 ±0.35	2.49 ±0.25
M 200%	MPa	7.26 ±0.62	3.85 ±0.52	6.17 ±0.25
M 300%	MPa	13.23 ±0.85	7.81 ±0.80	11.4 ±0.88

In this case there is a relevant improvement of stress resistance.

Moreover, in contrast with all the previous compounds, this increased strength takes place with a very low loose in the elongation at break of the final product.

This result shows a substantial improvement of mechanical properties of the compound with 15 phr of bioash and 5 phr of ENR compared to the case with untreated bioash.

It is due to improvement in the bioash-rubber compatibility that causes a better dispersion of the bioash particles in the rubber matrix with an increase of interphase, but also due to a decrease of the agglomeration tendency of filler particles as can be seen in the Figure 3.63. According to all these factors, an increment in the final viscosity is expected [75].

An increasing of agglomeration with dimension in the range between 4 and 15 μm is observed in case of the compound with the addition of ENR as compatibilizer.

Moreover, it is evident a decreasing of agglomerates with size higher than 16 μm compared to the case of the compound with the same quantities of bioash but without epoxidized natural rubber.

The dispersion grade is 93.6%, while the mean dimension of agglomerate is 10.3 μm.

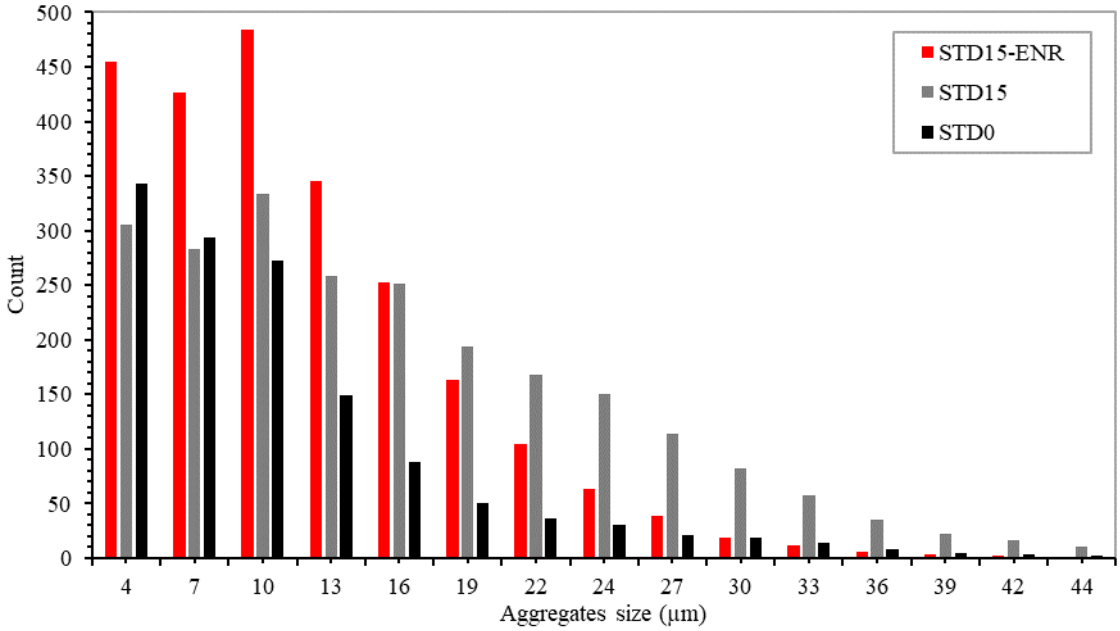

Figure 3.63 Dispersion grade analysis of compounds with 15 phr of bioash and ENR compatibilizer and references.

It is the best result among the possibilities explored in this study.

Moreover, the process is easy and fast: it does not need implementation of new sector in industry production plant since the external agent is added directly during the compounding process.

Finally, 15 phr of bioash is a high quantity to implement its recycling and 5 phr of compatibilizer agent is a quite low quantity of a low-cost material.

4. Conclusions and future developments

4.1. Conclusions

It is possible uses the discarded bioash as filler in rubber compounding to decrease the quantity of bioash that currently needs to be disposed, this also saves money by decreasing the need of standard materials traditionally used for the compound.

This is a case of circular economy that guarantees the optimization of the consumption of raw materials in plant and it is environment friendly.

Higher is the quantities of bioash loaded in the compound, higher will be the positive impact on environment and company economy.

The money saving is about 7% compared to standard rubber compound.

So, in this summary, the results are referred to the upper limit quantity of bioash discussed in this study: 15 parts for hundred of rubber (STD15). All these data are summarized in theTable 4.1.

Table 4.1 Data summary of rubber compound filled with 15phr of bioash.

	STD0	***STD15***	***STD15 BMW***	***STD15-RAW AS3***	***STD15-RAW AO5***	***STD15-RAW TESPT***	***STD15-gMAH***	***STD15-ENR***
G' max (MPa)	1.8	1.3	1.5	1.0	1.6	3.0	0.8	1.8
t 90 (min)	4.8	3.2	3.1	3.3	5.8	3.8	3.8	5.5
σ_b *(MPa)*	18	11	16	18	17	14	14	20
ε_b *(%)*	378	368	418	459	455	318	559	427
E 300 (%)	13	8	10	9	9	13	8	11
Agglomerate (μm)	9.7	14.5	8.3	11.3	9.0	9.2	9.7	10.3

From literature, it is known that the compound, mainly based on natural rubber, is a hydrophobic material while the bioash, from preliminary analysis, results as a highly hydrophilic material.

And so, a good mixing between the rubber and the bioash is difficult to achieve.

The bioash presence in the compound causes a decrease of properties of the final product such as lower vulcanization time, since the bioash acts as an accelerant agent, lower value of shear storage modulus and lower Young modulus at 300% of strain, resulting in higher deformation and higher tendency at formation of big agglomerates of average size 14.5 μm, that decrease the rubber stiffness and so decrease the stress value at the break point compared to unfilled standard rubber compound (STD0) with agglomerates mean size of 9.7 μm.

Firstly, to improve the dispersion of fillers in compound, it's possible reduce the bioash grains dimension, from a mode of 26 μm to 8 μm, by wet ball milling (STD15 BMW).

This method has a positive effect on the value of the tensile strength and a lower effect on modulus that causes the slightly decrease the compound deformation.

To avoid the loss of standard rubber compound properties, the bioash can be chemically modified by a functionalizer or by a compatibilizer that can be directly loaded into compound in addition to bioash.

The fatty acids affect the hydrophilicity of the bioash and so improve the formation of small bioash grains. The best quantity of stearic acid is resulted to be 3% by weight of bioash (STD15-RAW AS3) and the reaction is mainly mechanical since the ball mill is used.

There is not an improvement on the storage modulus and on the Young modulus compared to raw bioash, and so the deformation at break is very high but there is an improvement on the compound strength since the main size of agglomerates is quite close the value of the standard compound case (STD0).

To increase the elasticity, or in other words, to promote higher grade of crosslinking, another fatty acid is used: the oleic acid. The reaction happens in a solution with toluene since the oleic acid consistence is like a gel, and so it is difficult to disperse by ball milling. The best amount of oleic acid results to be 5% by weight of bioash (STD15-RAW AO5).

The oleic acid has a double bond along its organic chain that improves its reactivity and so induced higher grade of cross-linking, but its shape is bulky and so less acid is linked to bioash. In fact, the storage modulus value is improved, the acceleration effect of bioash is lost (the cure time is longer probably since higher number of reactions that occur), and the size of agglomerates is small but there is not a substantial difference in stress-strain curve compared to bioash treated by lower amount of stearic acid.

The cost of fatty acids used in above functionalization is negligible.

From literature, it is know that fatty acid reacts with calcite that is the main component of the bioash but the small presence of silicon in the bioash also suggests the usage of a silane: the Bis(triethoxysilylpropyl)tetrasulfide (TESPT). The reaction occurs with 7% by weight of bioash in a solution with toluene and catalyst (STD15-RAW TESPT). The silane has a great effect on the value of modulus that is the higher achieved, it decreases the deformation that becomes comparable to untreated filled.

Despite the mean size of agglomerate is low, the value of rubber stiffness is worsened. Moreover, TESPT is an expensive material.

Instead of acting on the bioash, the effect of the loading in compounding of a compatibilizer has also been investigated. The literature suggests the usage of 30 phr of polyisoprene-graft-maleic anhydride (gMAH) for 15 phr of bioash (STD15-gMAH).

The modified compound has a very low modulus that reflects the very high deformability of final product. The rubber stiffness is quite high, but it is not comparable to standard compound, even if the dispersion is good.

The high quantity of cheap gMAH in the compound permits a great decrease of presence of other materials, and so the cost of final compound is almost halved.

The last option is the use of 5 phr of epoxidized natural rubber 50 (ENR) for 15 phr of bioash. The resulting compound (STD15-ENR) shows the properties closer to untreated compound. The main differences are the higher optimum cure time and the higher value of stress at the break point. It means that STD15-ENR is a compound more stiffness than STD0.

To sum up, with only 5 phr of ENR and with the recycle of 15 phr of the bioash, it is possible to obtain a compound with mechanical properties higher than standard.

The cost of this compound is almost the same of standard compound but the bioash is recycled and the properties of compound are increased.

4.2. Future developments

4.2.1. Further analysis on modified bioash

The study can be deepened by further analysis.

To verify the effective quantity of functionalizer that has reacted with the bioash found by the Thermal Gravimetric Analysis (TGA), the extraction by Kumagawa, done on bioash modified by stearic acid, can be extended to the other functionalization methods.

Moreover, the optical contact angle measure (OCA) of a water drop on the bioash modified by stearic acid turns out to be a good method to analyse the grade of hydrophobicity of filler that is appeared to be a key property to obtain the compatibility of bioash with the rubber, ad so also this analysis can be extended to all samples.

Furthermore, to better understand mechanism of reaction, Differential Scanning Calorimetry (DSC) and Scanning Electron Microscope (SEM) can be performed on modified bioash.

4.2.2. Further analysis on modified compound

The compound with bioash as filler can be further analysed.

Other properties of rubber can be investigated base on the final application: rubber for tyre in the case of this study.

First of all, it is recommendable repeating the measure of vulcanization time by a rheometer such as Rubber Process Analyser (RPA), instead of dynamic mechanical analysis (DMA), since RPA is the instrument industrially used to measure optimum cure time with an appropriate sensibility of the measure and its resulted data include also the scorch time, the time within which the rubber can be moulded, that has not been discussed in this work.

Also transition temperature (Tg) can be find from this test, by the cross of storage and loss modulus curves. Transition temperature gives information about the rolling resistance of final product.

Other properties to investigate are the Mooney viscosity, the hardness and the abrasion resistance of the compound.

Moreover, in addition to tensile test, compression test can be performed.

Another important data, to know the effect of functionalization on compound is the measure of the cross-linking density that can be estimated according to ASTM D6814.

On the other hand, to understand the grade of functionalization, the extraction on final rubber compound can be performed, following the ISO1407, ISO 1795 and ISO 4661-2.

To find the optimum amount of functionalizer, the Fourier-Transform Infrared Spectroscopy (FT-IR) on compound can be performed. In this way, it is possible to detect the quantity of unreacted agent.

4.2.3. Future developments of functionalization

The discussed functionalization methods can be improved.

For example, the bioash modification by stearic acid can be performed in water (wet method). The immersion of bioash, main composed by calcite, in distilled de-ionized water result in high dissociation of calcium carbonate (CaCO3) that produces higher surface activity that promote the physical adsorption of the acid.

Moreover, a combination of the two functionalization processes can be explored.

A first modification of bioash by TESPT creates a silica filler that can use in rubber compound modified by ENR. It is the green tyre concept introduced by Michelin in early nineties. Silica-filled ENR compound provides low rolling resistance together with high wet grip which gives fuel benefit to consumer.

This is possible due to the similar polarity of ENR and silica that turns out to strong interaction that confers these unique properties to final compound.

The higher presence of functionalizer leads to less of accelerators but other compounding ingredients interact with silanol group of silica and results in the fast cure of the compound.

Finally, a good dispersion of fillers is obtained for this compound [76].

Appendix

Results of preliminary studies on functionalizers

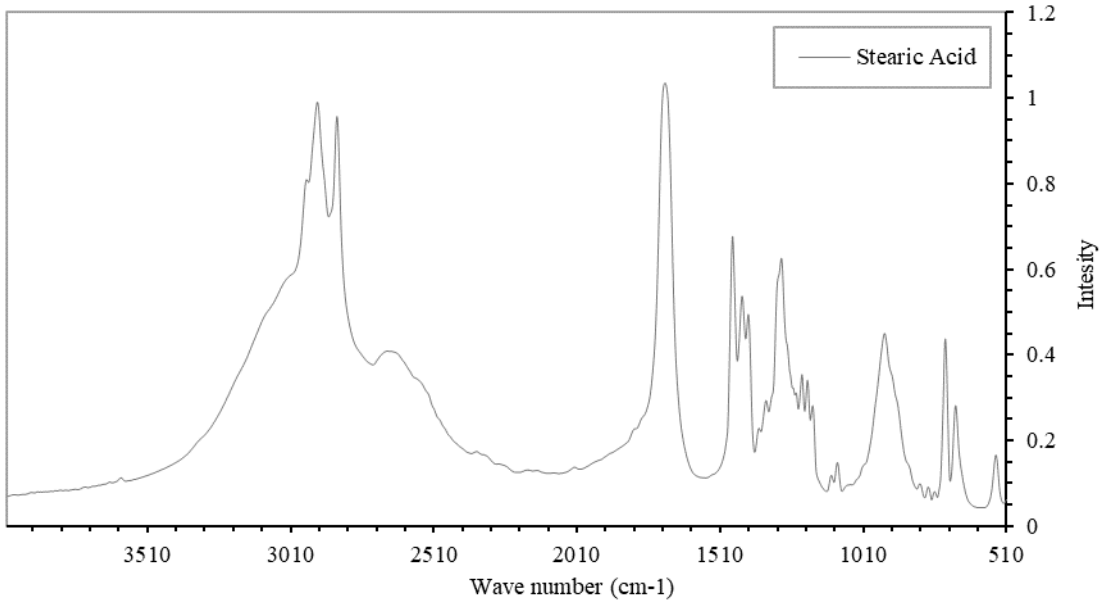

Figure A.1 FT-IR spectra of Stearic Acid

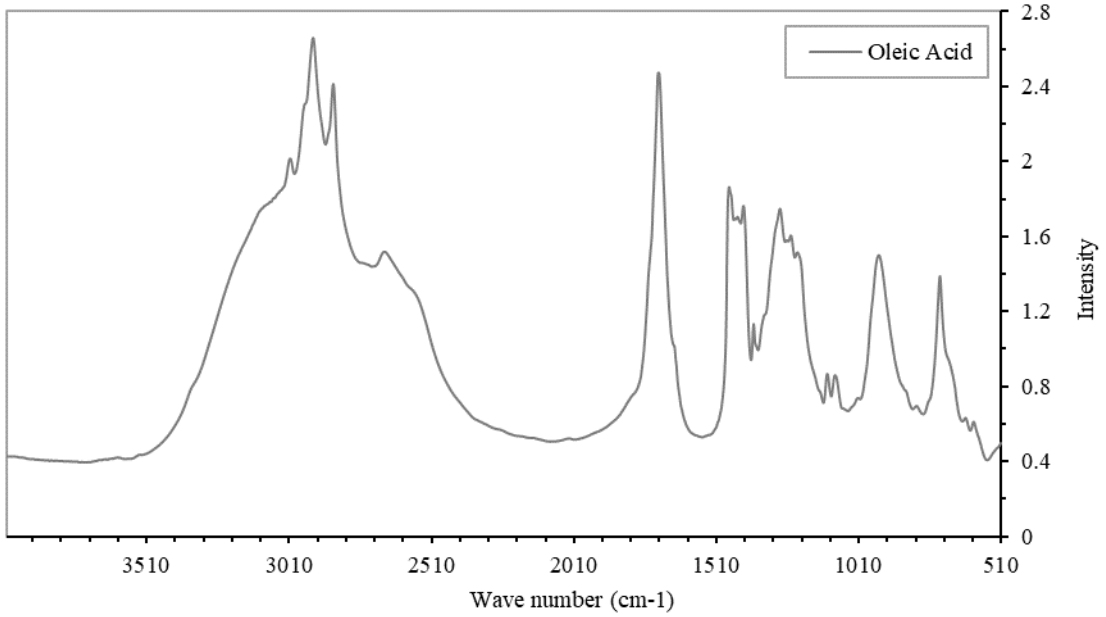

Figure A.2 FT-IR spectra of Oleic Acid

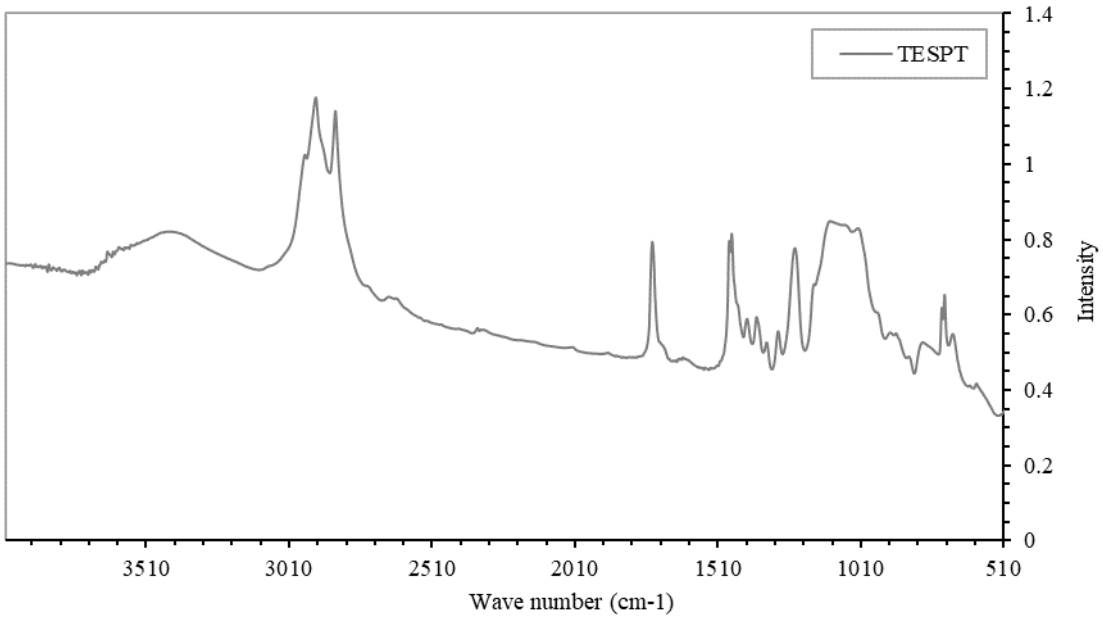

Figure A.3 FT-IR spectra of TESPT

Bibliography

[1] Bothello, Joel, and Marie-Laure Salles-Djelic. "Evolving conceptualizations of organizational environmentalism: A path generation account." Organization Studies 39, no. 1 (2018): 93-119.

[2] Wautelet, T. "The Concept of Circular Economy: its Origins and its Evolution." Research Gate. DOI 10 (2018).

[3] MacArthur, Ellen. "Towards the circular economy." Journal of Industrial Ecology 2 (2013): 23-44.

[4] UNIDO United Nations Industrial Development Organization. "Circular Economy." Report (2018).

[5] Ghisellini, Patrizia, and Sergio Ulgiati. "Circular economy transition in Italy. Achievements, perspectives and constraints." Journal of Cleaner Production 243 (2020): 118360.

[6] European Commission, "Communication from the commission to the European Parliament, the Council, the European Economic and Social Committee and the Committee of the Regions, on a monitoring framework for the circular economy." Report (2018).

[7] World Economic Forum, and Accenture "Driving the Sustainability of Production System with Fourth Industrial Revolution Innovation." Report (2018).

[8] European Environment Agency - EEA, "Robust monitoring and targets are key in shifting Europe to a more circular economy." Report (2020).

[9] Rault, J., J. Marchal, P. Judeinstein, and P. A. Albouy. "Chain orientation in natural rubber, Part II: 2 H-NMR study." The European Physical Journal E 21, no. 3 (2006): 243-261.

[10] Schaefer, Ronald J. "Mechanical properties of rubber." Harris' Shock and Vibration Handbook, Sixth edition, A. Piersol, T. Paez (Eds), McGraw-Hill Companies Inc (2010): 33-1.

[11] A. Y. Coran "Vulcanization." The Science and Technology of Rubber - Fourth Edition (2013): 337-381.

[12] ASTM International D2084-17 "Standard Test Method for Rubber Property - Vulcanization Using Oscillating Disk Cure Meter." Standard (2017).

[13] Kruželák, Ján, Richard Sýkora, and Ivan Hudec. "Sulphur and peroxide vulcanisation of rubber compounds–overview." Chemical Papers 70, no. 12 (2016): 1533-1555.

[14] Kohls, D. J., and G. Beaucage. "Rational design of reinforced rubber." Current Opinion in Solid State and Materials Science 6, no. 3 (2002): 183-194.

[15] Paul C. Hiemenz, and Timothy P. Lodge "Networks, Gels, and Rubber Elasticity." Polymer Chemistry - Second Edition (2007): 381-418.

[16] Sina Ebnesajjad, and Cyrus Ebnesajjad "Surface and Material Characterization Techniques." Surface Treatment of Materials for Adhesive Bonding - Second Edition (2014): 39-75.

[17] André, M., and P. Wriggers. "Thermo-mechanical behaviour of rubber materials during vulcanization." International journal of solids and structures 42, no. 16-17 (2005): 4758-4778.

[18] Toki, Shigeyuki, and Benjamin S. Hsiao. "Nature of strain-induced structures in natural and synthetic rubbers under stretching." Macromolecules 36, no. 16 (2003): 5915-5917.

[19] Wang, Fenfen, Shengli Chen, Qiang Wu, Rongchun Zhang, and Pingchuan Sun. "Strain-induced structural and dynamic changes in segmented polyurethane elastomers." Polymer 163 (2019): 154-161.

[20] Yang, Ruiquan, Yihu Song, and Qiang Zheng. "Payne effect of silica-filled styrene-butadiene rubber." Polymer 116 (2017): 304-313.

[21] Chen, Yukun, Yanpeng Wang, and Chuanhui Xu. "Study of viscoelastic properties of EPDM filled with zinc dimethacrylate prepared in situ by using a rubber process analyzer." Journal of Macromolecular Science, Part B 51, no. 10 (2012): 1921-1933.

[22] ASTM International D412-16 "Standard Test Methods for Vulcanized Rubber and Thermoplastic Elastomers - Tension." Standard (2016).

[23] Wisojodharmo, L. A., R. Fidyaningsih, D. A. Fitriani, D. K. Arti, and H. Susanto. "The influence of natural rubber–butadiene rubber and carbon black type on the mechanical properties of tread compound." In IOP Conference

Series: Materials Science and Engineering, vol. 223, no. 1, p. 012013. IOP Publishing, 2017.

[24] Saowapark, Thanunya, Narongrit Sombatsompop, and Chakrit Sirisinha. "Viscoelastic properties of fly ash-filled natural rubber compounds: Effect of fly ash loading." Journal of applied polymer science 112, no. 4 (2009): 2552-2558.

[25] Ismail, H., R. Nordin, and A. M. Noor. "The effect of filler loading on curing and mechanical properties of natural rubber/recycled rubber powder blends." International Journal of Polymeric Materials 54, no. 1 (2005): 9-20.

[26] Sarkkinen, M., T. Luukkonen, and K. Kemppainen. "A wasterock and bioash mixture as a road stabilization product." In Selected papers from the 3rd Edition of the International Conference on Wastes: Solution, Treatments and Opportunities, Viana do Castelo, pp. 283-288. 2015.

[27] Shimpi, N. G., and S. Mishra. "Synthesis of nanoparticles and its effect on properties of elastomeric nanocomposites." Journal of Nanoparticle Research 12, no. 6 (2010): 2093-2099.

[28] Fu, Shao-Yun, Xi-Qiao Feng, Bernd Lauke, and Yiu-Wing Mai. "Effects of particle size, particle/matrix interface adhesion and particle loading on mechanical properties of particulate–polymer composites." Composites Part B: Engineering 39, no. 6 (2008): 933-961.

[29] R. B. Simpson "Rubber Compounding - Section 4" Rubber Basics (2002): 125-165.

[30] Choi, Sung-Seen, and Chae Eun Son. "Influence of silane coupling agent on bound rubber formation of NR/SBR blend compounds reinforced with carbon black." Polymer Bulletin 73, no. 12 (2016): 3453-3464.

[31] Tavakoli, Mitra, Ali Asghar Katbab, and Hossein Nazockdast. "Effectiveness of maleic anhydride grafted EPDM rubber (EPDM-g-MAH) as compatibilizer in NR/organoclay nanocomposites prepared by melt compounding." Journal of Macromolecular Science, Part B 50, no. 7 (2011): 1270-1284.

[32] Wongsorat, Wittawat, Nitinat Suppakarn, and Kasama Jarukumjorn. "Effects of compatibilizer type and fiber loading on mechanical properties and cure

characteristics of sisal fiber/natural rubber composites." Journal of Composite Materials 48, no. 19 (2014): 2401-2411.

[33] Ismail, Hanafi, R. Nordin, and Ahmad Md Noor. "The comparison properties of recycle rubber powder, carbon black, and calcium carbonate filled natural rubber compounds." Polymer-Plastics Technology and Engineering 41, no. 5 (2002): 847-862.

[34] Khimi, S. Raa, and Kim L. Pickering. "A new method to predict optimum cure time of rubber compound using dynamic mechanical analysis." Journal of Applied Polymer Science 131, no. 6 (2014).

[35] Barbara H. Stuart. "Infrared Spectroscopy: Fundamentals and Applications – first edition." John Wiley & sons Ltd (2004).

[36] Heryanto, Rudi, Masitah Hasan, Ezzat Chan Abdullah, and Andri Cahyo Kumoro. "Solubility of stearic acid in various organic solvents and its prediction using non-ideal solution models." ScienceAsia 33 (2007): 469-472.

[37] Li, Ming-Guo, Chang-Jung Sun, Sue-Huai Gau, and Chia-Jung Chuang. "Effects of wet ball milling on lead stabilization and particle size variation in municipal solid waste incinerator fly ash." Journal of hazardous materials 174, no. 1-3 (2010): 586-591

[38] Noor, Ahmad-Fauzi Mohd, Yanny-Marliana Baba Ismail, Masakazu Kawashita, Aye Aye Thant, and Myat Myat-Htun. "Effects of Milling Speed and Sintering on the Formation of Akermanite (Ca2MgSi2O7) Bioceramics." In Journal of Physics: Conference Series, vol. 1082, no. 1, p. 012074. IOP Publishing, 2018.

[39] Al-Busaidi, Intisar K., Rashid S. Al-Maamari, Mahvash Karimi, and Jamil Naser. "Effect of different polar organic compounds on wettability of calcite surfaces." Journal of Petroleum Science and Engineering 180 (2019): 569-583.

[40] Mihajlović, Slavica R., Dušica R. Vučinić, Živko T. Sekulić, Sonja Z. Milićević, and Božo M. Kolonja. "Mechanism of stearic acid adsorption to calcite." Powder technology 245 (2013): 208-216.

[41] Mahmood, Nasir, Mohammad Sohail Khan, Asad Ullah Khan, Klaus Werner Stöckelhuber, and Gert Heinrich. "Purification, surface modification of coal ash

silica and its potential application in rubber composites." Journal of applied polymer science 117, no. 3 (2010): 1493-1501.

[42] Ali, Zulfiqar, Hai Hong Le, Sybill Ilisch, Thomas Thurn-Albrecht, and Hans-Joachim Radusch. "Morphology development and compatibilization effect in nanoclay filled rubber blends." Polymer 51, no. 20 (2010): 4580-4588.

[43] Radhakrishnan, C. K., Prajitha Kumari, A. Sujith, and G. Unnikrishnan. "Dynamic mechanical properties of styrene butadiene rubber and poly (ethylene-co-vinyl acetate) blends." Journal of Polymer Research 15, no. 2 (2008): 161-171.

[44] Ente Italiano di Normazione UNI EN 15309:2007 "Caratterizzazione dei rifiuti e dei suoli - Determinazione della composizione elementare mediante fluorescenza a raggi X." Standard (2007).

[45] Yang, Yu, Tao Ji, Xujian Lin, Caiyi Chen, and Zhengxian Yang. "Biogenic sulfuric acid corrosion resistance of new artificial reef concrete." Construction and Building Materials 158 (2018): 33-41.

[46] Karimi, Mahvash, Rashid S. Al-Maamari, Shahab Ayatollahi, and Nasir Mehranbod. "Mechanistic study of wettability alteration of oil-wet calcite: The effect of magnesium ions in the presence and absence of cationic surfactant." Colloids and Surfaces A: Physicochemical and Engineering Aspects 482 (2015): 403-415.

[47] Prime, R. Bruce, Harvey E. Bair, Sergey Vyazovkin, Patrick K. Gallagher, and Alan Riga. "Thermogravimetric analysis (TGA)." Thermal analysis of polymers: Fundamentals and applications (2009): 241-317.

[48] Karimi, Mahvash, Rashid S. Al-Maamari, Shahab Ayatollahi, and Nasir Mehranbod. "Impact of sulfate ions on wettability alteration of oil-wet calcite in the absence and presence of cationic surfactant." Energy & Fuels 30, no. 2 (2016): 819-829.

[49] Ismail, Hanafi, M. N. Nasaruddin, and H. D. Rozman. "The effect of multifunctional additive in white rice husk ash filled natural rubber compounds." European Polymer Journal 35, no. 8 (1999): 1429-1437.

[50] Lacey, Jeffrey A., Rachel M. Emerson, David N. Thompson, and Tyler L. Westover. "Ash reduction strategies in corn stover facilitated by anatomical and size fractionation." Biomass and Bioenergy 90 (2016): 173-180.

[51] Paul, K. Thomas, S. K. Satpathy, I. Manna, K. K. Chakraborty, and G. B. Nando. "Preparation and characterization of nano structured materials from fly ash: a waste from thermal power stations, by high energy ball milling." Nanoscale Research Letters 2, no. 8 (2007): 397.

[52] Kato, A., Y. Kokubo, R. Tsushi, and Y. Ikeda. "Hydrophobic and hydrophilic silica-filled cross-linked natural rubber (NR): structure and properties." In Chemistry, Manufacture and Applications of Natural Rubber, pp. 193-215. Woodhead Publishing, 2014.

[53] Mihajlović, Slavica, Živko Sekulić, Aleksandra Daković, Dušica Vučinić, Vladimir Jovanović, and Jovica Stojanović. "Surface properties of natural calcite filler treated with stearic acid." Ceramics–Silikáty 53, no. 4 (2009): 268-275.

[54] Cao, Zhi, Michael Daly, Lopez Clémence, Luke M. Geever, Ian Major, Clement L. Higginbotham, and Declan M. Devine. "Chemical surface modification of calcium carbonate particles with stearic acid using different treating methods." Applied Surface Science 378 (2016): 320-329.

[55] Liu, Peng, Chuanfa Feng, Fazhou Wang, Yining Gao, Jin Yang, Wenqin Zhang, and Lu Yang. "Hydrophobic and water-resisting behavior of Portland cement incorporated by oleic acid modified fly ash." Materials and Structures 51, no. 2 (2018): 38.

[56] Cao, Zhengfeng, and Yanqiu Xia. "Study on the preparation and tribological properties of fly ash as lubricant additive for steel/steel pair." Tribology Letters 65, no. 3 (2017): 104.

[57] Silverstein, Robert M., and G. Clayton Bassler. "Spectrometric identification of organic compounds." Journal of Chemical Education 39, no. 11 (1962): 546.

[58] Gomari, KA Rezaei, Renaud Denoyel, and A. A. Hamouda. "Wettability of calcite and mica modified by different long-chain fatty acids (C18 acids)." Journal of colloid and interface science 297, no. 2 (2006): 470-479.

[59] Osman, Maged A., and Ulrich W. Suter. "Surface treatment of calcite with fatty acids: structure and properties of the organic monolayer." Chemistry of materials 14, no. 10 (2002): 4408-4415.

[60] Thongsang, S., and N. Sombatsompop. "Dynamic rebound behavior of silica/natural rubber composites: fly ash particles and precipitated silica." Journal of Macromolecular Science, Part B: Physics 46, no. 4 (2007): 825-840.

[61] Zhou, Yonghui, and Mizi Fan. "Recycled tyre rubber-thermoplastic composites through interface optimisation." RSC advances 7, no. 47 (2017): 29263-29270.

[62] Marrone, Michelle, Tania Montanari, Guido Busca, Lucia Conzatti, Giovanna Costa, Maila Castellano, and Antonio Turturro. "A Fourier transform infrared (FTIR) study of the reaction of triethoxysilane (TES) and bis [3-triethoxysilylpropyl] tetrasulfane (TESPT) with the surface of amorphous silica." The Journal of Physical Chemistry B 108, no. 11 (2004): 3563-3572.

[63] Ismail, Hanafi. "The effects of filler loading and a silane coupling agent on the dynamic properties and swelling behaviour of bamboo filled natural rubber compounds." Journal of Elastomers & Plastics 35, no. 2 (2003): 149-159.

[64] Thongsang, S., N. Sombatsompop, and A. Ansarifar. "Effect of fly ash silica and precipitated silica fillers on the viscosity, cure, and viscoelastic properties of natural rubber." Polymers for Advanced Technologies 19, no. 9 (2008): 1296-1304.

[65] Thongsang, S., and N. Sombatsompop. "Effect of NaOH and Si69 treatments on the properties of fly ash/natural rubber composites." Polymer composites 27, no. 1 (2006): 30-40.

[66] Sengupta, R., S. Chakraborty, S. A. Bandyopadhyay, S. Dasgupta, R. Mukhopadhyay, K. Auddy, and A. S. Deuri. "A short review on rubber/clay nanocomposites with emphasis on mechanical properties." Polymer Engineering & Science 47, no. 11 (2007): 1956-1974.

[67] Nelson, P. A., and S. K. N. Kutty. "Studies on Maleic anhydride grafted reclaimed rubber/acrylonitrile butadiene rubber blends." Progress in Rubber Plastics and Recycling Technology 19, no. 3 (2003): 171-188.

[68] Khan, Muhammad J., Abdulhadi A. Al-Juhani, Reyad Shawabkeh, Anwar Ul-Hamid, and Ibnelwaleed A. Hussein. "Chemical modification of waste oil fly

ash for improved mechanical and thermal properties of low density polyethylene composites." Journal of Polymer Research 18, no. 6 (2011): 2275-2284.

[69] Teh, P. L., ZA Mohd Ishak, A. S. Hashim, J. Karger-Kocsis, and U. S. Ishiaku. "Effects of epoxidized natural rubber as a compatibilizer in melt compounded natural rubber–organoclay nanocomposites." European Polymer Journal 40, no. 11 (2004): 2513-2521.

[70] Ahmad, Hazwani Syaza, Hanafi Ismail, and Azura A. Rashid. "Tensile properties and morphology of epoxidized natural rubber/recycled acrylonitrile-butadiene rubber (ENR 50/NBRr) blends." Procedia Chemistry 19 (2016): 359-365.

[71] Arayapranee, Wanvimon, and Garry L. Rempel. "Effects of polarity on the filler-rubber interaction and properties of silica filled grafted natural rubber composites." Journal of Polymers 2013 (2013).

[72] Arroyo, M., M. A. Lopez-Manchado, J. L. Valentin, and J. Carretero. "Morphology/behaviour relationship of nanocomposites based on natural rubber/epoxidized natural rubber blends." Composites science and technology 67, no. 7-8 (2007): 1330-1339.

[73] Irez, A. B., E. Bayraktar, and I. Miskioglu. "Design and mechanical-physical properties of epoxy-rubber based composites reinforced with nanoparticles." Procedia engineering 184 (2017): 486-496.

[74] Saramolee, Prachid, Natinee Lopattananon, and Kannika Sahakaro. "Preparation and some properties of modified natural rubber bearing grafted poly (methyl methacrylate) and epoxide groups." European polymer journal 56 (2014): 1-10.

[75] Rajasekar, R., Gert Heinrich, Amit Das, and Chapal Kumar Das. "Development of SBR-nanoclay composites with epoxidized natural rubber as compatibilizer." Journal of Nanotechnology 2009 (2009).

[76] Sarkawi, Siti Salina, Ahmad Kifli Che Aziz, Rohaidah Abdul Rahim, Rassimi Abdul Ghani, and Ahmad Nazir Kamaruddin. "Properties of epoxidized natural rubber tread compound: the hybrid reinforcing effect of silica and silane system." Polymers and Polymer Composites 24, no. 9 (2016): 775-782.


NON MI ASPETTAVO ANDASSE A FINIRE COSÍ.
NON MI PARE SIA TUTTO FINITO, CAVALIERE...
VOI UMANI PENSATE CHE IL PRESENTE SIA SOLO DOVE TERMINA IL PASSATO...
MA DIMENTICATE CHE È SOPRATTUTTO DOVE COMINCIA IL FUTURO.
coma empirico